Behavioral and neural correlates of human visual processing as assessed by psychophysics and functional magnetic resonance imaging

PhD thesis

Lajos R. Kozák, MD

János Szentágothai PhD School of Neurosciences
Semmelweis University

Supervisor: György Karmos, MD, PhD (MTAPI, Budapest)
Consultant: Miguel Castelo-Branco, MD, PhD (IBILI, Coimbra)

Opponents: Imre Szirmai, MD, DSc
Gábor Jandó, MD, PhD

PhD Theoretical Exam Committee:
Chair: Anita Kamondi, MD, PhD
Members: Péter Barsi, MD, PhD
Róbert Bódizs, MD, PhD

Budapest
2009

TABLE OF CONTENTS

LIST OF ABBREVIATIONS

1D one dimensional

2D two dimensional

2-IFC two interval forced choice

4-AFC four alternatives forced choice

AM apparent motion

ANOVA analysis of variance

BOLD blood oxygenation level dependent

C/D cup-to-disc ratio

CCT Cambridge Color Test™ (Cambridge Research Systems Ltd., Rochester, UK)

CIE Commission Internationale de l'Éclairage (International Comission on Illumination)

CRS Cambridge Research Systems Ltd., Rochester, UK

cpd cycles per degree

CRT cathode ray tube

dps degrees per second

EEG electroencephalogram

EOG electrooculogram

ERG electroretinogram

FDR false discovery rate

FM-100 test Farnworth- Munsell color test

ggl ganglion

GLM general linear model

hMT$^+$ the human motion complex, analogue to monkey MT (V5) and MST

HLLC high luminance low contrast

HLHC high luminance high contrast

HRF hemodynamic response function

IBILI Institute of Biomedical Research on Light and Image – Faculty of Medicine, University of Coimbra, Portugal.

IOP intraocular pressure

ISI inter-stimulus interval

L-cone long wavelength sensitive or red cone (peak sensitivity at 560 nm)

LCD liquid crystal display

LGN lateral geniculate nucleus

LL low luminance

M-cell retinal parasol ganglion cell projecting to the magnocellular pathway

M-cone medium wavelength sensitive or green cone (peak sensitivity at 530 nm)

MAE motion aftereffect

MD mean deviation

MST primate middle supratemporal visual area (involved in motion processing)

MT primate middle temporal visual area (V5, involved in motion processing)

MTAPI Institute for Psychology of the Hungarian Academy of Sciences, Budapest, Hungary

ns non-significant

OHT ocular hypertension

P-cell retinal midget ganglion cell projecting to the parvocellular pathway

PLSD protected least significant difference, statistical test for post hoc comparisons

POAG primary open-angle glaucoma

RPE retinal pigment epithelium

RM real motion

S-cone short wavelength sensitive or blue cone (peak sensitivity at 400 nm)

SD standard deviation

SEM standard error of the mean

V1 primary visual cortex

V2,V3,V3a,V4,V5 higher order visual areas

VA visual acuity

VMD vitelliform macular dystrophy or Best disease

VSG 2/5 Visual Stimulus Generator 2/5™ (Cambridge Research Systems Ltd., Rochester, UK)

I. INTRODUCTION

1. General introduction

This thesis, like any other PhD thesis, is a summary of research done over years, and there are numerous ways to order and present someone's work. As my focus shifted from color vision to motion perception over the years, I decided to introduce the studies in chronological order. All of the studies included deal with different aspects of vision, thus the common background is set by the way visual information is processed in the brain from the retina to the cortex.

1.1. Structural overview

1.1.1. The retina

Humans have on average 128 million photoreceptor cells in the retina,[1] 120 million of them are rods representing a homogeneous cell population with photosensitivity peaking around 500 nm wavelength. The other 8 million receptor cells are three different types of cones, with differing photosensitivities (400 nm for blue, or S-cones; 530 nm for green, or M-cones; and 560 nm for red, or L-cones).[2] The photoreceptors are distributed in an intermingled mosaic fashion, with cones predominantly located around the fovea, and rods mainly being present at higher eccentricities.

The very first step of visual perception occurs when light is transformed into neural signals in these cells. Photoreceptor output is then transmitted via network or interneurons to the retinal ganglion cells that provide output towards higher order processing in the brain.

Retinal processing represents a major processing stage in the central visual system, involving about 80 morphologically and physiologically distinct cell populations,[3] and providing output for about 20 visual pathways.[4-6] Each of the pathways originates from distinct cell populations and underlying circuitry, and connects to distinct targets in the thalamus and the midbrain.

Table 1. Properties of retinal ganglion cells in the parvocellular, magnocellular, and koniocellular streams
Modified from Frishman LJ. Basic visual processes. In: Goldstein EB (ed), *Blackwell handbook of perception*[8]

Processing streams	Parvocellular	Koniocellular	Magnocellular
Morphology			
Retinal ggl. cell class	Midget	Small bistratified	Parasol
% of ggl. cell population	70%	10%	10%
Cell body (soma) area	Small	Small	Large
Dendritic field area	Small	Large	Large
Axon diameter	Thin	Very thin	Thin
Response properties			
Axonal cond. velocity	Slow	Very slow	Fast
Receptive field configuration	Center/Surround (Surround > Center)	Center/Surround (Surround > Center)	Center/Surround (Surround > Center)
Spatial resolution	High	Low	Low
Temporal resolution	Low	Low	High
Contrast gain	Low	Low	High
Spectral selectivity	L vs M wavelengths	S vs LM wavelengths	No (broadband)
Linearity of spatial summation	Linear	?	75% Linear 25% Nonlinear
Circuitry			
Bipolar cell input	Midget	Short wavelength (blue) Bipolar	Diffuse
LGN layers	Parvocellular (P) layers (2-6)	Intercalated koniocellular (K) layers between P layers	Magnocellular (M) layers (1-2)
Projections to primary visual cortex (V1)	V1 layer 4Cβ, 6 (upper half)	V1 layers 2/3 (blobs)	V1 layer 4Cα, 6 (lower half)

Although the distribution of the different cell types varies across the retina, the majority of the ganglion cells are parasol and midget cells (see **Table 1**) projecting to the magnocellular and parvocellular layers of the lateral geniculate nucleus (LGN), respectively.[2, 7] Based on their projection targets midget ganglion cells are often called as P-cells, and parasol ganglion cells as M-cells.

Midget cells are the most numerous, contributing to about 70% of the retinal ganglion cells in the central fovea, where there are two midget ganglion cells for every cone.[9] Since it is the density of the cones in the central retina that limits the

spatial resolution, the midget ganglion cells might have a crucial role of preserving and transmitting high spatial resolution information to the brain.[10] On the other hand, these cells are shown to be involved in color vision by comparing inputs from L-cones and M-cones, and projecting L- vs. M-cone signal to the LGN.[11] Whether the midget pathway does double duty, being specialized both for color vision and achromatic spatial vision is still controversial.[7]

Parasol cells have larger dendritic field and lower density than midgets. Their input originates from multiple cone bipolar cells that receive synergistic input from L- and M-cones. As a result, these cells respond strongly to achromatic stimuli. Moreover, these cells are more sensitive to low contrast stimuli, they respond with burst discharges, and conduct action potential faster to the optic nerve than midget cells.[2] Based on their response properties and their projections to the magnocellular pathway, parasol ganglion cells are implicated to create direction sensitivity in the primary visual cortex thus reflecting the first step of the motion processing pathway.[12]

Small bistratified cells represent a minority of the retinal ganglion cells (~10%),[8] nevertheless they play a crucial role in color vision by providing the S vs. L+M cone opponency signal.[7, 13] The S-cone opponent response represents one of the major axes of color opponent space.[11]

1.1.2. The lateral geniculate nucleus

The LGN is the main relay between the retina and visual cortex. It has multilayer structure with 6 principal layers (four dorsal parvocellular and two ventral magnocellular layers). The P and M retinal ganglion cells project to the parvocellular and the magnocellular layers of the LGN, while small bistratified cells project to koniocellular cells localized between the principal layers. Cells in the principal layers receive input both from the ipsilateral (layers 2, 3, and 5) and the contralateral (layers 1, 4, and 6) eye. The output of LGN is similarly segregated as its input; cells in different layers project to distinct layers of the primary visual cortex (see **Figure 1**)

Almost all of the cells in the parvocellular and koniocellular layers of the LGN are color-opponent cells with either red-green or blue-yellow opponency, thus providing

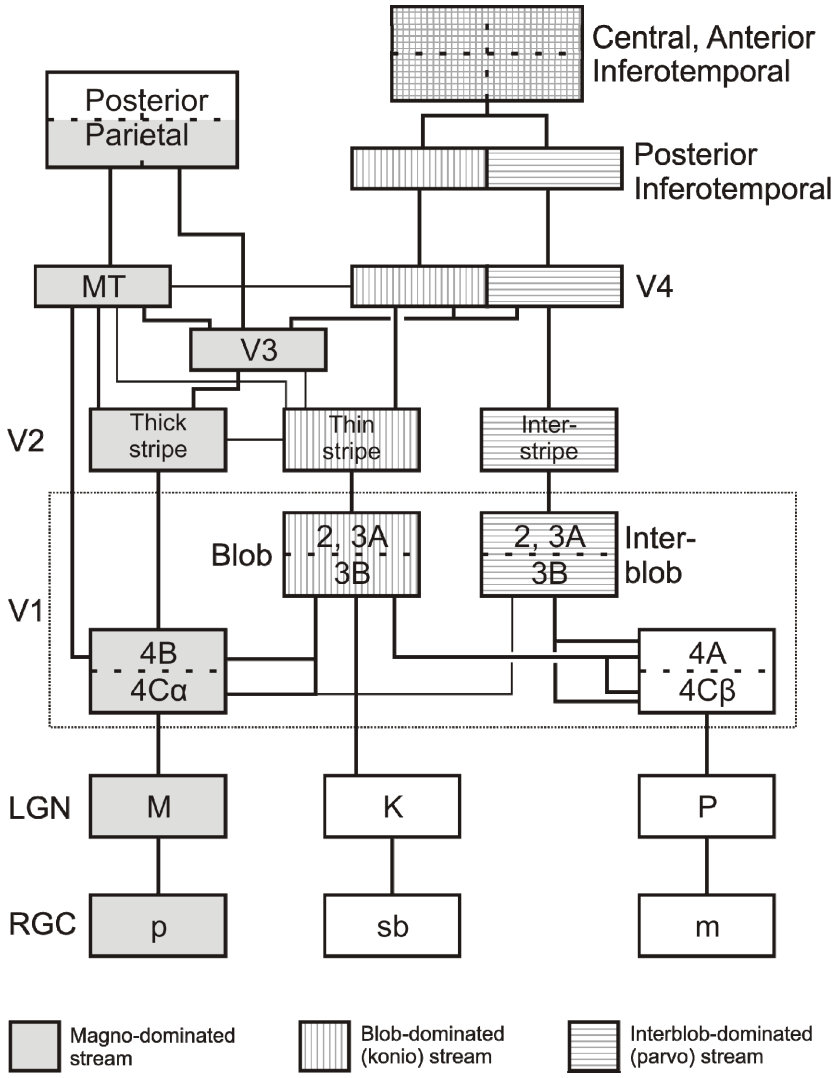

Figure 1 Hierarchical and compartmental organization of the visual pathways
This scheme illustrates subcortical and cortical visual information flow. Lines between boxes represent reciprocal pathways, and (except for the retino-geniculate projection) feedback connections are typically as robust as forward connections. Parallel processing is manifested at subcortical levels by the distinction among P, M, and K cells. RGC: retinal ganglion cells; LGN: lateral geniculate nucleus; p: parasol; sb: small bistratified; m: midget; M: magnocellular; K: koniocellular; P: parvocellular.
Modified from Van Essen DC, Anderson CH. Information processing strategies and pathways in the primate visual system. In: Zornetzer S, Davis JL, Lau C, McKenna T (eds), *An Introduction to Neural and Electronic Networks.*[15]

substrate for color vision.[11, 14] On the contrary, cells in the magnocellular layers are insensitive of color variations, but highly sensitive to quick changes of intensity, providing a substrate to visual motion perception.[1, 14]

1.1.3. The primary visual cortex (V1)

Both the magnocellular and the parvocellular axons from LGN project to layer 4C of V1, but their connections remain segregated (magnocellular axons terminate on

cells of layer 4Cα, parvocellular axons terminate on cells of layer 4Cβ). The konicellular axons terminate in layers 2 and 3 in the so called cytochrome oxidase blobs. These blobs receive input from V1 layer 4C, as well.[14, 16]

The receptive field structure of layer 4C cells are similar to those of LGN cells that project to them: they are in general small monocular center-surround receptive fields. These neurons are organized into ocular dominance columns based on the monocular input projected to them.[14, 16] This ocular dominance column structure can be visualized by autoradiography,[17] or optical imaging[18] as a fingerprint-like structure.

Cells in the interblob regions of layers 2 and 3 receive their input from the parvocellular pathway. These cells are not wavelength sensitive, but they are orientation selective simple and complex cells, having the smallest orientation selective receptive fields in the visual cortex, suggesting that they might be involved in the analysis of fine object shape.[14, 16]

Cells in the blobs of layers 2 and 3 have mixed input originating from direct koniocellular, and indirect parvocellular and magnocellular connections. These cells are usually monocular, center-surround and color opponent. The high wavelength sensitivity in the blobs suggests that these neurons are involved in color processing.[14, 16]

Cells in layer 4B receive their inputs from the magnocellular pathway. Most of these cells combine input from both eyes, thus having binocular receptive fields. These cells are orientation selective, and most of them are direction selective, suggesting their role in motion processing.[14, 16]

1.1.4. Extrastriate cortex

With slight exaggeration one could say that most of the extrastriate cortex is involved in visual processing to a given degree,[19] but the most important regions related to my thesis are V4 and hMT^+ (the human visual area analogue to primate MT and MST), therefore I focus on them.

Visual area V4 is part of the ventral processing stream or the “what” pathway; the pathway that deals with perception of the visual world and the recognition of objects.

Area V4 receives its input from the blob and interblob regions of V1 via V2 and partly V3, and projects to temporal regions. Neurons in V4 have larger receptive fields than those in V1, and many are orientation and color selective. The role of V4 in color and shape processing is proven by lesion studies.[14, 20, 21]

Visual area hMT^+ is part of the dorsal processing stream or the "where" pathway; the pathway that serves the analysis of visual motion and visual control of action. Area hMT^+ receives its inputs mainly from the magnocellular pathway via V1 layer 4B, V2, and V3, and projects towards parietal areas. Neurons in area hMT^+ have large receptive fields; they are direction selective either in a component or a pattern selective fashion.[22] The importance of hMT^+ in visual motion perception is supported by neuropsychology data.[23]

1.2. Functional overview

1.2.1. Color vision

Healthy humans have trichromatic vision just like primates, which means that any visible wavelength of light can be specified by mixtures of three suitably chosen colors. These color primaries were first standardized by the International Commission on Illumination (Commission Internationale de l'Éclairage, CIE) as 700 nm (red), 546.1 nm (green) and 435.8 nm (blue). For the representation of possible color mixtures the CIE 1931 (xy) standard was defined (see **Figure 2a**).[24] The weakness of this standard was that chromaticity discrimination thresholds were described in non-uniform distances depending on the reference color, as observed by MacAdam.[25] The CIE 1976 (u′v′) uniform color space (see **Figure 2b**) was defined as a nonlinear transformation of the CIE 1931 (xy) space that maps equal differences in color to equal distances. The MacAdam color discrimination ellipses become circles after this transformation if the observer has normal color vision.[24]

Color vision deficits may have different severity based on their causes. Anomalous trichromates (6% of males and 0.4% of females) have three cone pigments, however one of them has different wavelength sensitivity than in normals (trichromates). Dichromats have only two classes of photopigments, leading to more severe color vision deficits. In protanopia (1% of males) the obsever lacks the L-cone

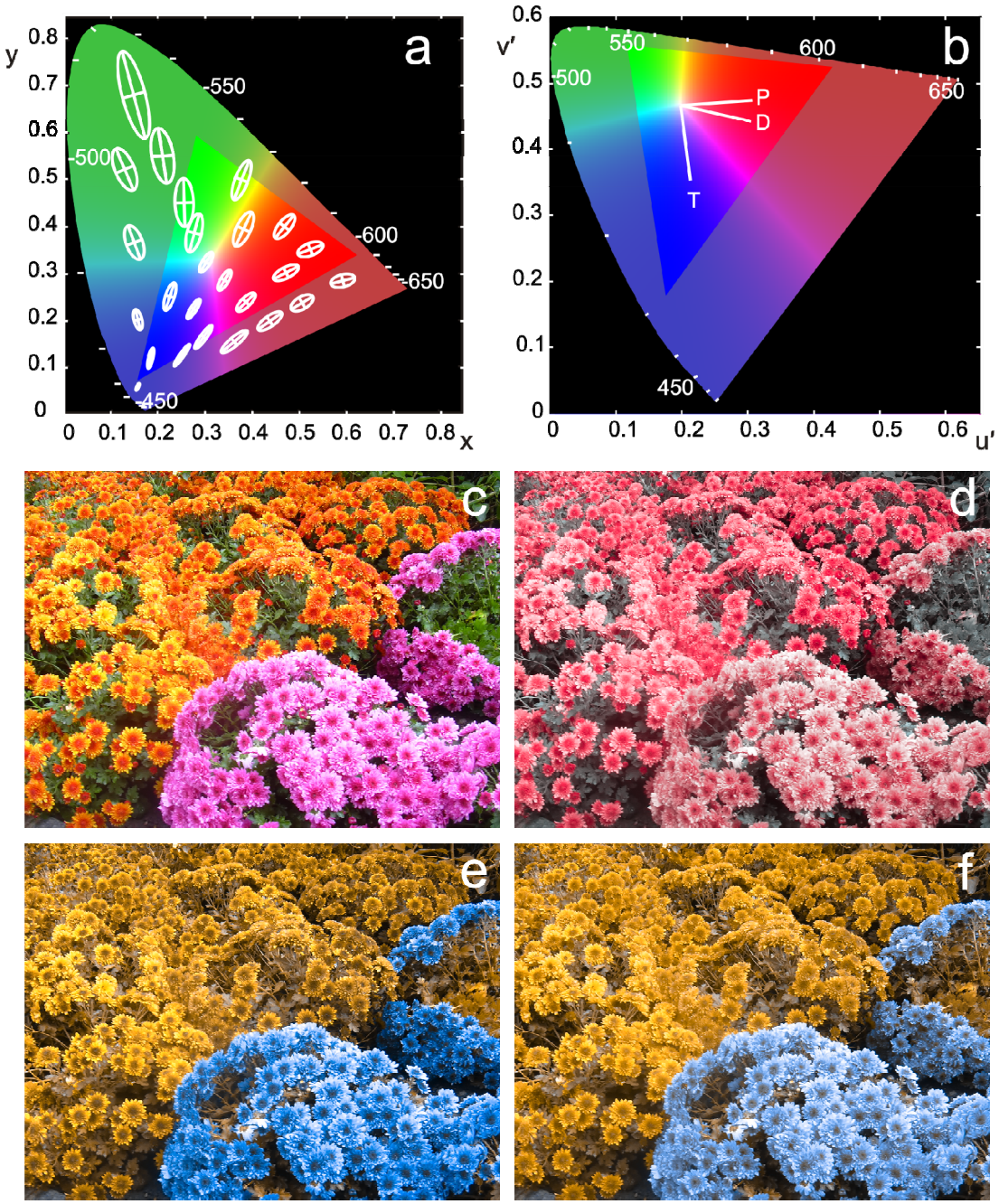

Figure 2 Normal and anomalous color vision
(a) MacAdam color dicrimintation ellipses overlaid on the CIE 1931 xy chromaticity diagram. **(b)** color confusion vectors used in our experiments overlaid on the CIE 1976 u′v′ chromaticity diagram. P: protan axis; D: deutan axis; T: tritan axis. Image of flowers as observed by **(c)** normals (trichromats); **(d)** tritanopes; **(e)** protanopes; **(f)** deuteranopes. Color rendering of chromaticity diagrams is based on the sRGB standard (IEC 1996-2.1); the triangles represent the gamut imposed by trinitron phosphors. Colorblind vision was simulated with Vischeck[26], on a stock image.[27]

pigment, in deuteranopia (1% of males) the observer lacks the M-cone pigment, and in tritanopia (very rare) the observer lacks the S-cone pigment. Simulated deficits can be seen on **Figure 2d-f**. Monochromats are extremely rare; they are totally color blind, having either one type of cones and rods, or only rods.

1.2.2. Motion processing

The role of area MT

Motion perception is possible via the direction selective tuning properties of neurons in the visual pathways. Direction selectivity first emerges in layer 4B of the primary visual cortex and then propagates through the dorsal stream.[14, 16] There are multiple motion sensitive areas in the dorsal stream, with specific subfunctions,[28-37] but area MT seems to be vital for motion processing.[21, 38]

While cells in V1 and V2 are selective for a single direction (component cells), cells in area MT can either be selective for a single direction or a combination of directions (pattern cells).[22] Component cells can be probed by 1D stimuli (with velocity perpendicular to orientation, such as drifting gratings), pattern cells can be probed with 2D stimuli (plaids, random dot fields, etc.)[22, 39]

Moving plaids are built from superimposed gratings moving in different directions (see **Figure 3**). Plaids may be perceived either as two surfaces, one being transparent and sliding on top of the other (transparent or component motion) or as a single coherent pattern whose direction of motion is intermediate to the component vectors (non-transparent or pattern motion). The degree of perceived transparency depends on the luminance of the grating intersections, the angle between movement directions, and the speed of the components.[39-41] Based on their bistability, plaid stimuli represent a perceptual paradigm that allows the investigation of switches between integration and segmentation of motion vectors.[22, 42-44]

There are biologically plausible models of global motion perception generated by

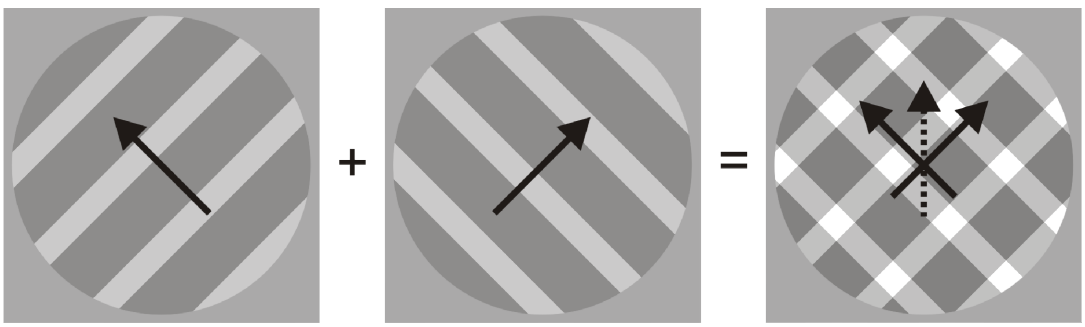

Figure 3 Drifting gratings and moving plaids
Component directions are represented by solid arrows; pattern direction is represented by dotted arrow.

neurophysiological research.[42-44] Area MT has been shown to contain a map for the direction of global motion,[28, 30, 35, 36, 41, 45-55] and is involved in the simultaneous representation of multiple global directions. [50, 52, 56-58] Moreover, it has been shown that changes in perceptual grouping go along with changes in neuronal synchrony,[43] and that perceptual switches are associated with activity changes in MT.[41] These findings represent converging evidence supporting the view that coding strategies in MT and medial superior temporal (MST) area may shift between vector averaging and a winner-take-all mode even when stimulus conditions are constant.[58]

Gestalt rules

Gestalt theory was developed by Wertheimer, Köhler and Koffka in the early 1900s; its main claim being that perceptual processes are holistic. Classical principles of Gestalt psychology postulate that the visual system uses information about local similarities to link and segment surfaces of visual scenes.[1, 59]

The *law of closure* states that the mind may experience non-perceived elements in order to complete a regular figure. The *law of good continuation* states that the mind connects elements of visual and kinetic patterns if they can be connected by straight lines. The *law of similarity* states that similar elements are grouped into collective entities or totalities based on similarity of their form, color, size, or brightness. The *law of proximity* states that elements in close spatial or temporal proximity are perceived as a collective or totality. The *law of common fate* states that elements with the same movement direction are perceived as a unit. The *law of symmetry* (figure ground relationships) states that symmetrical images are perceived collectively, even in spite of distance.[1, 59]

Based on these principles, collinear configurations, spatial proximity, and common fate are believed to impose grouping of moving contour segments into spatially extended objects through predominant feed-forward processing.[59-63] However, it still remains unclear into which extent local-global feedback mechanisms can modulate such bottom-up processes. In other words, it remains unclear how perceptual organization influences the dynamics of binding, and how the visual system partitions the visual scene into individuated entities such as surfaces and objects.

Motion aftereffect

Motion aftereffect (MAE) is an illusion of motion perceived on static test patterns upon prolonged directional motion adaptation[64, 65] generally in the opposite direction to the adapting movement.[66-68] The underlying neuronal process is generally considered to be an adaptation-induced imbalance in the activation of directional selective neurons in area hMT^+.[66-68] It is still an open question whether net blood oxygenation level dependent (BOLD) responses in area hMT^+ to MAE[69-74] reflect global motion adaptation-related responses or only non-specific shifts in arousal and/or specific attentional modulation of activity.[75]

Apparent motion

Apparent motion (AM) is an illusion of movement that can be induced when spatially segregated visual stimuli are presented in alternation. Subjects can then perceive a visual stimulus smoothly traversing the intervening space where no physical stimulus exists.[1, 76-78] It has been shown that area hMT^+ is the first within the dorsal processing stream to respond with a clear increase in signal intensity to AM stimuli.[35, 76-80]

Strictly speaking, the presentation of real motion, either surface motion (plaids, or moving random dots) or a smooth translocation of a moving patch on a computer screen is also an apparent motion stimulus, but since the critical fusion frequency of healthy subjects is usually well below 60 Hz[81] we can safely assume that they indeed perceived smooth real motion during our experiments.

1.3. Methodological overview

1.3.1. Psychophysics

Psychophysics is the study of relationship between physical stimuli and perceptual responses. It provides a relatively easy, consistent and reproducible means for non-invasive quantification of sensation. Its principles were first described in the mid-1800s by Gustave Fechner.[82]

Ophthalmology, in principle, is based on psychophysics since any patient examination consists of a series of psychophysical tests. In most cases, these tests are

used to determine thresholds, that are either the minimum value of a stimulus required to evoke a perceptual response (detection tasks for finding absolute threshold) or the minimum amount of change that is perceivable (discrimination tasks for finding difference threshold).[83] The same principles are valid for research purposes, as well.

There are different approaches to find the threshold. In the *method of constant stimuli* a set of fixed, predetermined stimuli is presented in random manner, and the threshold is determined as the stimulus value with 50% correct responses. In the *method of limits* predetermined stimuli are presented in sequential order to find transition points, and the average of these perceptual transition points are deemed as threshold. This approach is faster than the method of constant stimuli. *Staircase methods* are modifications of the method of limits, where the direction of presentation of stimulus values are reversed according to some pre-set criterion. These procedures provide balanced and efficient approach for the determination of transition points, and thus the thresholds.[83] *QUEST* is a fast adaptive staircase procedure that places each stimulus value at the current most probable Bayesian estimate of threshold.[84]

Psychophysical measurement of color vision

Basic evaluation of color vision deficits can be done by color plates such as Ishihara plates of Hardy-Rand-Rittler plates, however these methods can only detect severe disturbances of color vision.[24]

Detailed color psychophysics are usually done by means of color matching operations, such as the Farnsworth D-15 color test or the Farnsworth-Munsell 100-hue test, in which patients has to order color according to hues.[24, 85] However, the Farnsworth-Munsell 100-hue (FM-100) test has already been shown to be semi quantitative.[85] Indeed, Farnsworth himself considered that 30% changes in test-retest responses could occur, which has been repeatedly confirmed.[85] It is thus important to find novel approaches when quantifying and phenotyping chromatic damage e.g. in macular disorders and to reassess traditional clinical classifications using new quantitative criteria.[85-88]

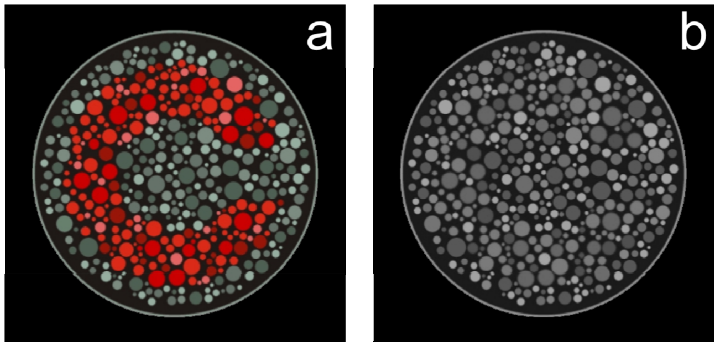

Figure 4 The stimulus used for our color psychophysics experiments
(a) Schematic illustration of the stimulus with chromatic contrast added **(b)** The same stimulus after removing the chromatic contrast (desaturation); the Landolt C shape is not visible

A recent article showed that computerized methods of studying color vision provide more information than the traditional approaches by modulating chromaticity along selected axes in color space.[86] The Cambridge Color Test (CCT, Cambridge Research Systems Ltd, Rochester, England) is a commercially available implementation of such computerized color vision tests.

During a CCT examination patients look monocularly at a screen with a pattern of disks of varying sizes and luminances with superimposed chromatic contrast defining a gap in a Landolt-like C-shaped ring (**Figure 4a**). Different luminance levels are randomly assigned to the patches forcing the subject to use specific color cues, because they could not use spatial or luminance cues (**Figure 4b**) to infer the embedded shape. Four-alternative forced choice staircase procedures are implemented for chromaticity threshold estimations.

The quantitative modulation of chromatic contrast allows for isolation of cone or color opponent-specific responses in the CIE 1976 u′v′ color space, e.g. the trivector version of the test assesses the three cone confusion axes simultaneously **(Figure 2b).** Color discrimination ellipses can also be estimated by measuring 8 or more confusion line vectors, also in an interleaved random manner, with independent staircases running at a given backgrounds (neutral background: 0.1977, 0.4689 u′v′).

Psychophysics used during visual motion experiments

Tasks during the evaluation of center-surround interactions and during estimation of neural correlates of illusory and real motion perception experiments were simple detection tasks. In the center-surround experiments subjects were required to

continuously report their observed percept of a moving central ambiguous plaid. In the functional magnetic resonance imaging (fMRI) study of real and illusory motion signals subject had to make color matching, orientation matching or speed tracking tasks using randomly presented pre-determined stimuli.

During the learning experiment QUEST adaptive staircases were used to determine motion coherence thresholds before and after the training period, and for the training session, as well.

1.3.2. Functional magnetic resonance imaging

Functional magnetic resonance imaging maps neuronal activations in the cerebral cortex in a non-invasive manner using the blood-oxygenation level dependent (BOLD) response. The BOLD response reflects complex hemodynamic interactions evoked by neuronal activity.[89] Such interactions include increases in regional blood flow and regional blood oxygenation. The latter can directly be measured using the difference between the magnetic properties of oxygenated and deoxygenated hemoglobin. As deoxy-hemoglobin is paramagnetic, it causes susceptibilities in the magnetic field leading to decreased signal intensity on T2* weighted gradient echo MR images.[90, 91]

Stimulus-related activations and deactivations can be localized either by fitting a model of the expected BOLD response using correlation methods, or general linear models,[92-95] or can be inferred by data-driven analysis methods, such as principal components analysis or independent component analysis.[96-99]

Functional MRI of the visual system can be performed either by using a back-projection system, where the stimuli are projected from outside the scanner room to a screen that is attached to the bore or head coil of the scanner, and visible through a mirror attached to the head-coil, or by using specialized LCD goggle systems. Behavioral data can be recorded using MR-compatible response boxes.

2. Study-specific introduction

2.1. Disease-related changes in color vision

2.1.1. Glaucoma study

Glaucoma is a chronic, degenerative optic neuropathy (most often associated with elevated intraocular pressure) that can be distinguished from most other forms of acquired optic neuropathy by the characteristic thinning of the neuroretinal rim of the optic nerve. This process leads to a phenomenon referred to as optic-disc cupping. The underlying pathology of these clinical symptoms is loss of retinal ganglion cells and their axons.[100-110] However, there is a current controversy in glaucoma research on the degree of relative damage across pathways, in particular regarding the parvo- and koniocellular (more recently identified and which processes blue-on signals[13, 111]) systems. The main reason lies in the difficulty of establishing the best method to promote equivalent activation of different pathways (see Pearson et al.[112]) which would be critical for the evaluation of loss of redundancy and pathophysiologic hypotheses regarding preferential damage. It is therefore crucial to assess how early each pathway is affected and to measure differential damage across different disease stages.

Regarding the specificity of damage within chromatic pathways, it is widely believed that glaucoma is predominantly associated with tritan-like defects.[113-148] Because photoreceptors seem not to be significantly damaged in glaucoma,[149] most studies imply a predominant involvement of the koniocellular pathway although important parvocellular dysfunction has also been reported.[122, 126, 134, 138, 140, 150] Few studies that try to compare the function of multiple pathways in early and late stages of glaucoma are available, however. Some studies including patients with ocular hypertension have emphasized the level of dysfunction at the visual periphery for the tritan axis[123, 134] but their results have not always been concordant.[141, 147] Substantial damage has been extensively reported for the magnocellular system[100, 101, 103, 151-154] (for a review see Shabana et al.[154]), partly from indirect evidence that large fibers are preferentially affected early on in this disease.[155-157] These findings have formed the basis for the so-called preferential damage hypothesis. There is, however, increased

awareness that detectable impairment in a visual pathway depends on its internal degree of redundancy (e.g., the amount of overlap between the receptive fields of its neurons). This hypothesis postulates that damage can be detected only if the degree of redundancy is not too high.[112, 128, 132, 139]

Effective redundancy may be influenced by effects such as stimulus size in patients with glaucoma. It is also known that the same stimulus size activates different numbers of midget, parasol, and bistratified cells at a given eccentricity, which creates further complications in assessing relative damage.[112] Moreover, the relative level of background luminance may also bias the relative adaptation state of different pathways. These facts may explain the wide discrepancies that can be found in the literature.

Unfortunately, primate models of glaucoma can only partially contribute to solve these issues, because IOP is artificially elevated to very high levels that tend to be associated with more advanced stages of glaucoma.[108-110, 150, 158, 159]

Early functional impairment of small bistratified cells would be consistent with the well-documented advantage of blue-on-yellow over standard white-on-white perimetry but the specificity of this effect remains questionable. [121, 127-129, 132, 135, 136, 139, 142]

Our design allowed good activation of both the parvocellular and koniocellular pathways and made it possible to investigate evidence for early and late concomitant damage. Earlier studies could not bring much insight into the question, because some did not include subjects with ocular hypertension,[140] and others have only described changes along the tritan axis in detail or included patient populations that were not age matched.[125] Also, strategies based on semi-quantitative testing have often been fairly unsuccessful in finding color vision abnormalities in glaucoma.[124] This has been emphasized by Falcao-Reis et al.[123, 125] and Yu et al.[126] who have championed the use of computerized color tests, as an advantage over more traditional semi-quantitative methods.

2.1.2. Best's vitelliform macular dystrophy (VMD) study

Best disease is an autosomal dominant disorder with variable expressivity[160-168] and is characterized by the accumulation of a yellowish lipofuscin-like material within and beneath the retinal pigment epithelium (RPE).[169-173] The "egg yolk" or vitelliform lesion is easily visible on fundus examination and evolves through several stages across many years. Lesions may be central or paracentral, single or, rarely, multifocal, with foci at different stages.[173]

The VMD gene was isolated several years ago,[174, 175] and many mutations have been identified since then.[176-180] It is likely that bestrophin (the VMD gene product) mutations lead to alterations in the RPE, although one cannot exclude a direct role in photoreceptors. Bestrophin defines a new family of chloride-channel proteins[181] and is in the signal transduction pathway that modulates the light peak of the electrooculogram (EOG).[182] In VMD, a possible decrement in Cl-conductance occurs across the basolateral membrane of the RPE. The notion that the primary defect is located in the RPE is also suggested by the considerably reduced light peak to dark-through in clinical EOGs in the presence of normal global electroretinographic (ERG) findings.[163, 183-187] Multifocal ERG techniques can be useful in further isolating macular deficits in VMD.[184-186] The multifocal ERG peak amplitudes of the central and pericentral responses are indeed significantly reduced in patients with VMD.[184]

It is believed that most hereditary forms of macular disease, such as VMD and Stargardt disease, exhibit the so-called type I red-green deficit. Roth and Lanthony[85] recently reviewed the current consensus on how dyschromatopsia evolves in different stages of Stargardt disease. They emphasized the difficulty in staging chromatic deficits even when using the FM-100 test, and they have mostly relied on colorimetric equations (such as the Raleigh equation) to describe that in the mentioned condition there occurs initially a stage of mild red-green deficit. At a later stage, a blue-yellow deficit is observed, as documented by the Moreland equation. In the final stage, functional achromatopsia may occur. However, colorimetric equations provide only indirect estimates of relative cone dysfunction.

Useful and repeatable measures of cone function might be clinically relevant for the diagnosis of this condition because patients having normal or near-normal Snellen visual acuity (VA) may already have abnormal flicker fusion threshold intensities.[188] Direct cone-probing measures can also be more easily related to other techniques used to measure macular damage.[189-191] It is crucial is to find better ways to detect and monitor disease progression in VMD because although EOG and ERG is helpful for diagnosis, it does not correlate well with other clinical measures, such as VA.[187] Quantitative color testing paradigms like the one presented in this thesis can thus be useful for measuring cone function in a more direct manner.

2.2. Experiments on visual motion perception

2.2.1. Center-surround interactions in visual motion integration and segmentation

The study of center-surround interactions in visual perception is of great relevance in health and disease, in particular for understanding different forms of visual impairment in which central and peripheral vision is differentially affected. This occurs in diseases such as macular degenerations[192, 193] as well as in patients with scotomas of cortical origin.[55] Previous literature has shown that what patients can see is not necessarily correctly anticipated from their visual fields or neurophysiological data.[55, 194, 195] Indeed, patients with acquired or neurodevelopmental disorders could integrate coherent motion representations in spite of the presence of local disruption of magnocellular information processing; such strategies need to involve integrating contextual information over space to solve for local ambiguity.[55, 194, 195]

In this study, we have explored the well known concept that visual context can influence the perception of local stimuli[63, 196-199] an effect that is observed even if the experimental subject is not aware of the presence of a modulatory stimulus.[200] The most commonly explored and discussed types of center-surround interactions are the contextual sensitivity of human contrast, orientation discrimination, and vernier thresholds, because they can be directly related to neurophysiological studies in monkey V1 and also because the role of primary visual cortex in contour integration is relatively well understood. It is known that contrast detection can be improved up

to 40% by suprathreshold contextual information, the effect being modulated by low level properties such as relative orientation and collinearity.[201] Moreover, it is well established that responses of visual neurons may be markedly modulated by stimuli outside the classical receptive field (i.e., stimuli that do not themselves evoke responses of such neurons), and such modulation is dependent on the relative orientation, direction of motion, and contrast of stimuli presented in surrounding regions.[47, 202-204] Accordingly, there is also evidence that relative-motion stimuli represent important contextual influences.[205] Most of these interactions can be explained by models that postulate contour integration mechanisms through long-range horizontal connections[61-63] or competition processes based on surround suppression and/or binocular rivalry.[206-208]

However, the rules governing peripheral contextual influences on the interpretation of ambiguous central motion stimuli remain largely unexplored. Gestalt psychology postulates that the visual system uses information about local similarities to link and segment surfaces of visual scenes. Collinear configurations, spatial proximity, and common fate are believed to impose grouping of contour segments into spatially extended objects through predominant feedforward processing.[59-63] However, it remains unclear into which extent local-global feedback mechanisms can modulate such bottom-up processes. In other words, it remains unclear how perceptual organization influences the dynamics of binding, and how the visual system partitions the visual scene into individuated entities such as surfaces and objects. It is possible that simple feedforward rules may be overridden by dynamical interactions among local-global contextual cues, and even local common fate, sometimes even leading to unexpected perceptual incongruence between center and surround percepts.

Phenomena of perceptual dissociation, in which global congruence fails to act as a binding cue, are particularly interesting in this respect, because they cannot be explained by traditional Gestalt, competition, or contour integration models.[61, 207, 208] Moreover, the effectiveness of the classical *good continuation* Gestalt rule will depend on the interaction of multiple local *common fate* processes. The outcome is then determined by the competition among these mechanisms. However, other processing mechanisms, such as causal contour capture[209] may also be involved in

the integration of globally coherent representations[205] based on common fate of local cues. Center-surround bi-stable moving stimuli such as plaids seem to be an optimal choice to investigate the interplay of these processes.

Comprehending the local/global rules that constrain the effects of visual context in solving visual integration problems is equally relevant in the understanding of normal and pathological vision since ambiguity in perception is a common denominator in diseases causing visual impairment. A better insight on these mechanisms can lead to an improved understanding of disease pathophysiology and also to the development of new rehabilitation strategies.

2.2.2. Neural correlates of real and illusory motion perception

It is well known that modulation of activity in area hMT^+ is related to the perception of global motion[28, 30, 35, 36, 41, 53-55] and that response levels also depend on attentional modulation.[210-213] However, it is still an open question whether net BOLD responses in area hMT^+ to MAE[69-74] reflect global motion adaptation-related responses or only non-specific shifts in arousal and/or specific attentional modulation of activity.[75]

It is worth noting in this context that even weak motion signals can be modulated by selective attention[214-216] or contextual influences[217]. Huk et al.[75] observed no net MAE-related increase of area hMT^+ activity in a task directed to near threshold stimulus motion, and interpreted this result as an indication that the observed BOLD response characteristics were explained by shifts in attention and/or non-specific effects of arousal. However, selective attention to concurrent motion may be confounded by interference due to the presence of dual motion processing.

Generalization to other selective attention conditions and most importantly also to motion-unrelated features is important, as well. In other words, the presence of a net MAE-related signal may require selective attention to features that do not compete for motion processing. This can be achieved by controlling attention using tasks either with concurrent motion or motion-unrelated stimuli. If modulation of hMT^+ activity during perception of MAEs is specifically present in the motion-unrelated attention tasks, then the presence of a net MAE signal in area hMT^+ requires the

absence of concomitant processing of competing motion cues. This would render the results of Huk et al.[75] not generalizable for concurrent attention directed to non-motion features.

We have therefore decided, in contrast with Huk et al.[75], to use concurrent illusory motion distinct from MAE in addition to real surface motion as attentional task. We chose apparent motion for this purpose since it has already been shown that hMT^{+} responds with a clear increase in signal intensity to AM stimuli.[35, 76-80]

2.2.3. Learning-induced changes in motion processing

Developing perceptual expertise is essential in many situations, from an air traffic controller monitoring complex video displays to a radiologist searching for a tumor on an x-ray. With practice, these complex tasks become much easier, a phenomenon referred to as *perceptual learning*. Previous functional neuroimaging research in humans has focused on the role of training in increasing neural sensitivity for task-relevant visual information; such plasticity in early sensory cortices is thought to support improved perceptual abilities.[218-227] However, in most complex natural scenes, an ideal observer should also attenuate task-irrelevant sensory information that interferes with the processing of task-relevant information.[228, 229] The implementation of this optimal strategy is supported by the observation that training leads to much stronger learning effects when the task-relevant information is displayed in a noisy, distractor rich environment compared to when no distractors are present[230-234] (for a review see Fine & Jacobs[235]). However, previous studies have not examined how training influences the neural representation of task-irrelevant information to facilitate learning.

Previous behavioral research addressing the effect of perceptual learning on the processing of task-irrelevant information showed that pairing a very weak task-irrelevant motion stimulus with a task-relevant stimulus during training actually increased perceptual sensitivity for the task-irrelevant stimulus.[236-238] Based on this result, they proposed that perceptual learning involves a diffuse reinforcement signal that improves information processing for all stimuli presented concurrently with the task-relevant information during training, even if the stimulus is a task-irrelevant distractor.[238, 239] However, in contrast to the weak task-irrelevant stimuli used by

Watanabe and coworkers, real world perception more often involves suppressing highly salient and spatially intermingled distractors. Accordingly, recent psychophysical studies suggest that salient stimulus features are suppressed when they are present as task-irrelevant distractors during the training phase of a perceptual learning task.[229, 240] These findings are also in line with the results of a previous neurophysiological study showing that neural responses to irrelevant masking patterns are suppressed in the monkey inferior temporal cortex as a result of training to recognize backward-masked objects.[241]

II. AIMS

1. Disease-related changes in color vision

1.1. Glaucoma study

To assess the relative vulnerability of color pathways during the course of glaucoma by using a novel psychophysical approach based on luminance noise. Also, to investigate the relationship between color vision deficits and standard clinical markers of disease progression.

1.2. Best disease study

To quantify chromatic dysfunction in Best disease by using a novel methodological approach based on luminance noise. Also, to reassess the classic categorization of chromatic damage by investigating correlations between color vision and standard clinical markers of disease progression.

2. Experiments on visual motion perception

2.1. Center-surround interactions in visual motion integration and segmentation

To study how visual context influences visual motion integration and segmentation in the center. Also, to assess the interaction of suppression and facilitation mechanisms related to congruence and incongruence between center and surround percepts.

2.2. Neural correlates of real and illusory motion perception

To study illusory and real motion processing in area hMT^+ using fMRI, with special focus on the effects of attention and the interactions between motion signals. Also, to investigate whether there is a genuine motion aftereffect signal in hMT^+.

2.3. Learning-induced changes in motion processing

To study how perceptual learning changes the processing of relevant and irrelevant visual motion signals.

III. METHODS

1. Disease-related changes in color vision

We followed a strategy of parallel interleaved stimulus presentation to evaluate the degree of differential impairment of parvocellular and koniocellular function in patients and compare them with those of normal age-matched subjects.

1.1. Patient selection and classification

1.1.1. Glaucoma study

One hundred ninety two subjects participated in this study. The individuals were divided into three different groups based on a complete ophthalmic examination: patients with primary open-angle glaucoma (POAG; $n = 51$ eyes) or ocular hypertension (OHT; $n = 95$ eyes) and control subjects ($n = 46$ eyes). The ophthalmic examination was performed in all individuals by two ophthalmologists at the Department of Ophthalmology, Faculty of Medicine, University of Coimbra, Portugal. The examination consisted of best corrected visual acuity (VA; Snellen chart), IOP measurement (Goldmann applanation tonometer), slit lamp examination of anterior chamber, angle, and fundus examination (Volk lens). Multiple perimetric examinations with Humphrey 30-2 (FASTPAC strategy; Carl Zeiss Meditec, Dublin, CA, USA) were also performed in all groups. Patients with POAG filled the following criteria: cup-to-disc ratio (C/D) vertical diameter of 0.4 or more, a mean deviation (MD) visual field global index less than –2 dB (or < 5% of confidence interval). Patients with OHT were selected according to the following criteria: IOP of 21 mm Hg or more (on at least two occasions), MD more than –2 dB (or > 5%, of confidence interval) and C/D less than 0.5. Control subjects were patients' spouses, age-matched hospital or university staff, or relatives, with normal or corrected to normal refraction. Similar to the other groups, they all underwent a full ophthalmic examination; subjects with complaints unrelated to ophthalmology were excluded from the study. Individuals in this group had IOP less than 21 mm Hg, C/D less than 0.5, and normal visual fields.

Exclusion criteria included the following: age (< 21 or > 80), pseudophakic and aphakic eyes, significant media opacification (corneal leucoma or cataract), retinal diseases, neuro-ophthalmic diseases, known color vision disorders, VA less than 0.6, and high ametropia (spherical diopters > 4 and cylindrical diopters > 2).

Our patient and control groups were age matched (control subjects: mean ± SD, 57.022 ± 7.603; ocular hypertension, 59.862 ± 7.283; glaucoma, 59.875 ± 9.849; ANOVA, *ns*). There was no sex-related significant difference among the groups for any of the psychophysical measures used. There was no difference in hypotensive medical treatment guidelines across glaucoma and ocular hypertension groups.

The research was conducted at the Institute of Biomedical Research on Light and Image – Faculty of Medicine, University of Coimbra, Portugal (IBILI). The procedure followed the tenets of the Declaration of Helsinki, and informed consent was obtained from all participants in strict accordance with the local ethical committee guidelines.

1.1.2. Best disease study

We included 17 patients (34 tested eyes) in this study whose diagnosis of Best disease was obtained based on the characteristic photographic appearance of the fundus and on changes in EOG findings (an Arden ratio < 1.8 was considered abnormal). No patient revealed any other ophthalmologic or systemic conditions. Most patients had a positive family history of dominant inheritance (15 of 17 patients in 5 families). Patients were diagnosed, evaluated and classified at the Department of Ophthalmology, Faculty of Medicine, University of Coimbra, Portugal. The classification was done in accordance with the Fishman criteria:[242] a fundus appearance develops from a normal fovea with abnormal EOG findings (stage 0); to minimal macular pigment mottling and hypopigmentation (stage I); to a typical egg-yolk vitelliform lesion, usually slightly elevated (stage II); which then can break through the RPE and accumulate in the subretinal space in a cyst with a fluid level formed that moves with head position changes called pseudohypopyon; and follows various stages of resorption of the vitelliform lesion (stage III); to resorption plus fibrotic- or gliotic-appearing scar formation with or without neovascular membranes (stage IV). Patient distributions across stages were as follows: stages 0/I, 6 eyes;

stages II/III, 14 eyes; and stage IV, 14 eyes. Visual acuity was determined using postcycloplegic manifest refraction on Snellen charts, in a masked manner. We used standard operational procedures for fundus photography following the guidelines of the Fundus Photograph Reading Center, Department of Ophthalmology and Visual Sciences, University of Wisconsin, Madison.

A population of 21 normal-sighted controls (41 eyes) was also selected for statistical comparisons. Patient and control populations were age matched (mean ± SD age, 29.558 ± 14.894 and 28.024 ± 9.940 years, respectively; ANOVA, *ns*).

The research was conducted at the IBILI. The procedure followed the tenets of the Declaration of Helsinki, and informed consent was obtained from all participants in strict accordance with the local ethical committee guidelines.

1.2. Psychophysical methods and data analysis

We used a slightly modified version of the Cambridge Color Test (Cambridge Research Systems Ltd, Rochester, UK) developed by Regan et al.[86] to modulate chromaticity along selected axes in color space.

Subjects looked monocularly, with the refraction corrected for viewing distance, at a screen with a pattern of disks of varying sizes and luminances with superimposed chromatic contrast defining a gap in a Landolt-like C-shaped ring (**Figure 4a**). Six different luminance levels were randomly assigned to the patches (8, 10, 12, 14, 16, and 18 $cd \cdot m^2$) forcing the subject to use specific color cues, because they could not use spatial or luminance cues (**Figure 4b**) to infer the embedded shape. A minimum excursion of 0.002 CIE 1976 u′v′ color space units was superimposed on such luminance noise levels to define the chromatic shape, but the chromaticity of the Landolt C-shape was adjusted according to a staircase procedure during the experiments (see below).

The subjects had to indicate one of four possible positions of the gap of the Landolt C. In the *glaucoma study* given the subjects' average age and also to exclude confounding motor errors, subjects performed an oral response, which was converted into a button press response by the experimenters. For further emphasis of accuracy

versus speed in this study group, subjects had up to 20 seconds to report their decisions. In the *Best disease study* participants had to respond themselves by means of button presses on a 4-button response box with a response time-out of 3 seconds).

Viewing conditions in both studies were such that all regions the subjects had to consider to perform chromatic comparisons were in the macular region of the retina (viewing distance: 1.8 m, gap size: 1.6°, outer diameter: 7.6°, inner diameter: 3.81°).

Quantitative modulation of chromatic contrast allowed for isolation of cone or color opponent-specific responses in the CIE 1976 u′v′ color space. Calibration procedures were performed using software and hardware provided by Cambridge Research Systems Ltd. (colorimeter, Minolta, Osaka, Japan; calibration software and VSG 2/5 graphics card, with 15-bit contrast resolution per pixel; Cambridge Research Systems Ltd.). Stimuli were displayed on a gamma corrected 21-inch CRT monitor (GDM-F520; Sony, New York, NY, USA).

Psychophysical thresholds were obtained through three parallel, randomly interleaved staircases, from the trivector version of the test, which assessed simultaneously the three cone confusion axes in color space **(Figure 2b)**. This ensured unbiased measurement of thresholds across different chromatic mechanisms. To determine discrimination ellipses 8 confusion line vectors were measured in an interleaved random manner, with independent staircases running at a neutral background (neutral point coordinates: 0.1977, 0.4689 u′v′; minimum excursion: 0.002 CIE 1976 u′v′ color space units in this space; protan confusion point: 0.678, 0.501 u′v′; deutan confusion point: –1.217, 0.782 u′v′; tritan confusion point: 0.257, 0.0 u′v′; maximum excursion for the Trivector version: 0.1100). To ensure unbiased color perception tinted contact lenses and spectacle lenses were replaced by trial lenses in a trial frame.

Our four alternative forced-choice (4AFC) staircases were interleaved in a random manner to ensure that all color axes were tested simultaneously, which made comparisons regarding relative damage of chromatic pathways reliable. On each axis, the separation between the background and target chromaticities was initially large and had been decreased after each correct response and increased after each error on that axis. The test terminated after 11 reversals of each of the three

individual staircases, and the mean of the last 7 reversals was taken as the threshold estimate for a given confusion line. The step size was computed in units of the CIE 1976 u′v′ uniform chromaticity space and was a function of the number of reversals completed and of the separation of test and background chromaticities. A small subset of random catch trials was included to detect malingering and to provide the subject clear cases when he or she was near threshold.

The ellipse-fitting method used[86] produces ellipses that are centered on the field point and that are obtained by minimizing the sum of squares of the log distances between the ellipse and the fitted point. We cross-validated this method using a custom procedure, which consisted of an equi-angled spline interpolation of the data points around the field point with the determination of the longest diameter (major confusion axis) of this spline curve and subsequent comparisons of the standard deviations of the data points parallel and perpendicular to this axis. We have extracted the following quantitative parameters from the color test results: confusion line length, ellipse length, and axis ratio. Further statistical analyses (factorial and repeated measures ANOVA, with the post hoc Fisher PLSD correction; multiple linear regression) were performed using Statview (SAS, Cary, NC, USA).

2. Experiments on visual motion perception

2.1. Center-surround interactions in visual motion integration and segmentation

2.1.1. Participants

Nine subjects (6 females) participated in Experiments 1 and 2, fifteen (11 females) in Experiment 3, and nine (6 females) in Experiment 4, all with normal or corrected-to-normal visual acuity, and good fixation abilities. All subjects were experienced observers and were selected on the basis of fixation ability on concurrent eye movement experiments. We have nevertheless run eye movement control experiments on a subset of our subjects, see below.

The experiments were conducted at the IBILI. The procedure followed the tenets of the Declaration of Helsinki, and informed consent was obtained from all participants in strict accordance to the local ethical committee guidelines.

2.1.2. Experimental setup and stimuli

Stimuli were generated in Matlab (MathWorks Inc, Natick, MA, USA) using the Cogent 2000 Software Toolbox and presented on a gamma corrected 21" SONY Trinitron monitor with 800×600 pixel resolution and a refresh rate of 60 Hz. The monitor was the only light source in the room during the experiment. The 60 cm viewing distance and the head position of observers were stabilized with a chin/forehead rest. Stimuli were presented under three distinct overall luminance/contrast sets: high luminance high contrast (HLHC), high luminance low contrast (HLLC), and low luminance (LL, see **Table 2**, for details on exact luminance parameters).

Table 2 Exact luminance values for the three overall luminance/contrast sets of the center-surround motion experiments
The three luminance sets differed in the luminance and contrast relations of their elements. Elements composing the stimuli could be gratings, grating intersections or dots. 'Pattern bias (G1 & G2)' refers to the luminance of the gratings leading to pattern biased stimuli, regardless of the presence of dots. These patterns are symmetrical; hence the '(G1 & G2)' indication. For component biased stimuli without dots grating luminance parameters differ, thus they are shown separately. HLHC, high luminance and high contrast; HLLC, high luminance and low contrast; LL, low luminance.

Element	Luminance ($cd \cdot m^{-2}$)		
	HLHC	HLLC	LL
Background	45	58.5	0.27
Gratings			
Baseline (G1 & G2)	75	61.5	0.71
Pattern bias (G1 & G2)	75	61.5	0.71
Component bias (G1)	80	63	0.71
Component bias (G2)	70	60	0.57
Intersections			
Pattern bias	37	50	0.4
Component bias	80	63	0.71
Lum_1	60	59.75	0.57
Lum_2	68	60.97	0.66
Lum_3	76	62.19	0.74
Lum_4	84	63.41	0.82
Lum_5	92	64.63	0.91
Lum_6	100	65.85	1
Dots	1.6	42	1.6
Average Michelson contrast of gratings	24.9%	2.48%	41.23%

Table 3 Stimulus parameters in the temporal domain of the center-surround motion experiments

		Center		Surround	
		Grating 1	Grating 2	Grating 1	Grating 2
	Velocity	1 dps	1 dps	1 dps	1 dps
Movement direction	No surround	30 deg	150 deg	NA	NA
	Surround up	30 deg	150 deg	30 deg	150 deg
	Surround right	30 deg	150 deg	30 deg	330 deg
	Surround down	30 deg	150 deg	210 deg	330 deg
	Surround left	30 deg	150 deg	210 deg	150 deg

Observers were asked to give continuous on-line report whether they perceived non-transparent or transparent plaid motion within the 5° central circular region of the 20° diameter plaid display (**Figure 7**). Behavioral responses (perceptual decisions) were continuously recorded during the motion period by means of mouse button presses. The recorded button-press data yielded the percentage of non-transparent, transparent and ambiguous (either no-response, or both buttons pressed simultaneously) perceptual states during the period of moving stimulus presentation.

A 0.15° diameter fixation dot was present throughout the experiments and center and surround regions were separated by a 0.25° wide red annulus of fixed size, so that they were not adjacent (**Figure 5**).

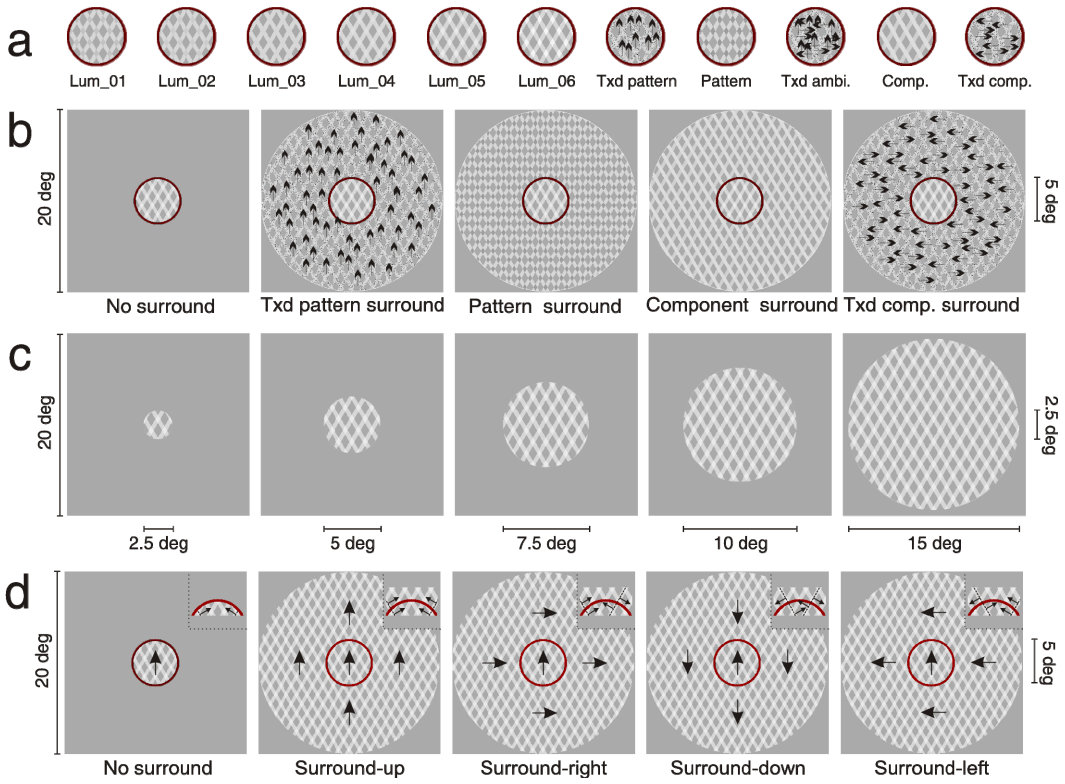

Figure 5 Stimulus conditions of the center-surround motion experiments
(a) Luminance defined and textured central plaid patches. *Pattern* and *component* labels describe stimuli biased for perceptual coherence (one perceived surface) or transparency (two perceived surfaces), respectively. **(b)** Surround conditions used for studying contextual modulations caused by luminance defined and textured plaids. **(c)** Stimuli used to examine the dependence of perceived perceptual transparency on stimulus size. **(d)** Stimuli used to examine the effect of dissimilar center an surround directions.
All of the schemes are representative of the "high luminance high contrast" (HLHC, see **Table 2**) stimulus set, "Lum" indices represent different intersection luminances. Arrows on (a) depict direction of motion of dots forming textures; arrows on (b) depict patter movement direction. Txd: textured; Txd Ambi.: textured ambiguous; comp: component.

Defining regions of maximal perceptual ambiguity

Prior to Experiment 1 we searched for regions of perceptual ambiguity for the different stimulus conditions, to determine the best parameter range for contextual modulations. We have observed the previously described inverted u-shaped curve[40] (the peak corresponding to frequently perceived transparency) for all overall luminance and contrast sets for stimuli in which no modulatory surround was present (see **Figure 6**). This procedure was replicated prior to Experiment 3, see below.

Selection of contextual surround stimuli

For providing reliable surround modulation we needed to select contextual modulatory stimuli with stable perceptual effects and, possibly, with low ambiguity. Therefore, we decided to use textured stimuli alongside with luminance defined stimuli. Textured surrounds indeed proved to be more stable (0% transparency for *Textured Pattern* and 90% transparency for *Textured Component* stimuli) than luminance defined surrounds (~0% transparency for *Pattern* an ~45% transparency

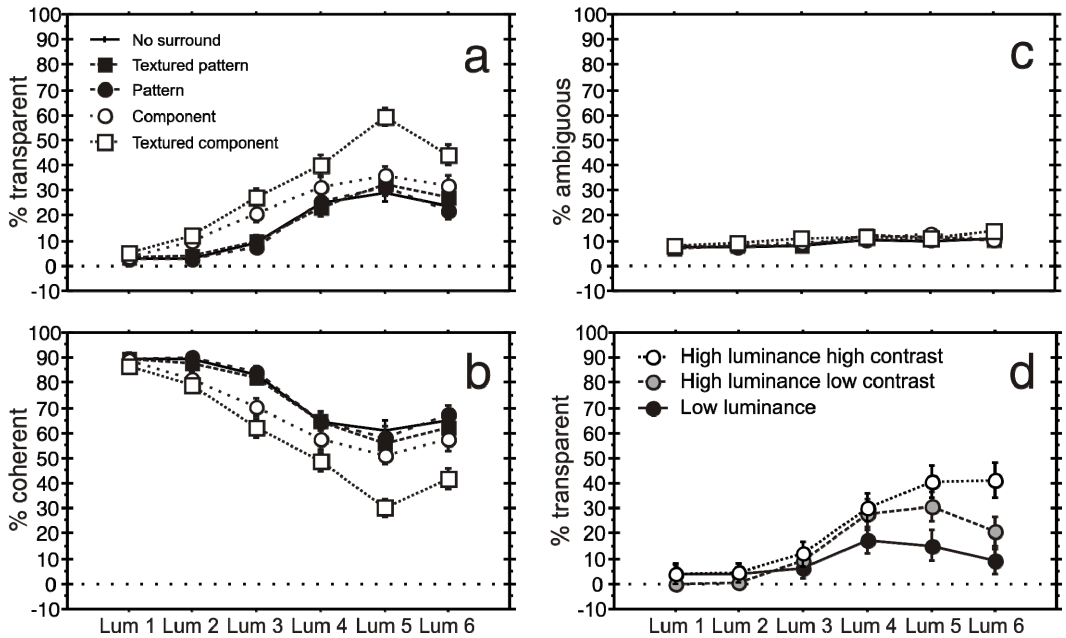

Figure 6 Perceptual response patterns are not influenced by the level of subject uncertainty.
The percentage of transparent percepts **(a)** mirror the percentage of non-transparent responses **(b)**, while the percentage of ambiguous responses **(c)** are low and stable across conditions. The perceived transparency of center only conditions **(d)** shows similar characteristics across the three distinct global luminance/contrast sets.
Results obtained on luminance defined centers, for texture defined centers see **Figure 22a**. Data collapsed across the three global luminance/contrast sets on panels a-c. HLLC: high luminance low contrast; HLHC: high luminance high contrast; LL: low luminance; Tx^d: textured. Error bars represent 1 SEM.

for *Component* stimuli), regardless of the overall luminance/contrast conditions. The reason for the perceptual stability of textured stimuli is their local (single dot) and global (populations of dots moving vertical for *pattern* and horizontally for *component*) unambiguity. In sum, textured surrounds and luminance defined *Pattern* stimuli showed the most stable perceptual effects and efficacy for contextual modulation (see details in Results), and an intermediate stability/efficacy was observed for luminance defined *Component* (transparent) stimuli. The observed low level of ambiguity and strong perceptual stability of textured surround stimuli, confirms the prediction that local dot motion provides physical disambiguation and reduces uncertainty[243].

Experiment 1: Modulatory effects under short viewing times

Stimuli were presented in subject-initiated 12-second blocks containing 2 seconds fixation and 10 seconds plaid movement (**Figure 7a**). We have defined eleven center conditions for all luminance/contrast sets with graded levels of perceptual coherence: eight were obtained by varying the luminance of grating intersections (for details see **Table 2**) and three by applying local dynamic texture on the gratings (**Figure 5a**). Surround conditions were defined as either no surround (in order to establish perceptual ambiguity of the central stimuli per se), or as a 20-degree diameter moving plaid patch surrounding the central patch, having similar spatio-temporal properties as the central stimulus, thus differing only in terms of intersection luminance and/or local texture (**Figure 5b**), yielding categories of surround stimuli biased either towards non-transparent or transparent motion.

The spatiotemporal parameters of plaid movement were kept constant throughout the experiment: 30% duty-cycle gratings, 1 cpd spatial resolution, 1 dps movement velocity, and 120° difference in movement direction with upward coherent motion direction (**Table 3**, 'No surround' and 'Surround up' conditions) Only luminance parameters, texture, and the presence or absence of the surround patch were varied across conditions.

Direction of motion of dots forming the textures was the following (when referring to the upward motion used in this experiment): 3 directions (1 vertical, 2 horizontal) for ambiguous textures (*Textured Ambiguous*), 2 directions (both

horizontal) for textures unambiguously biased for transparency (*Textured Component*) and 1 direction (vertical) for textures unambiguously biased for coherence (*Textured Pattern*). Note, that ambiguous textures were constructed such that 50-50% of the superimposed dots provided a bias either towards transparency or non-transparency, respectively.

Experimental blocks were organized into 3 repeated runs for each of the 3 luminance conditions, each run containing 66 blocks in randomized presentation order.

Experiment 2: Ruling out patch size as the explanation of the main effect

In the second experiment we have analyzed the effect of stimulus size on coherency decisions by varying the size of plaid stimuli (**Figure 5c**). We have included 5 luminance and/or texture defined plaid conditions (*Lum_3*, *Lum_4*, *Lum_5*, *Lum_6*, and *Textured Ambiguous,* see **Table 2**) from Experiment 1 in all of the previously described three overall luminance and contrast sets while varying the size of the moving plaid patches in five steps. The spatiotemporal characteristics of plaid movement and the perceptual task were the same as in Experiment 1, described

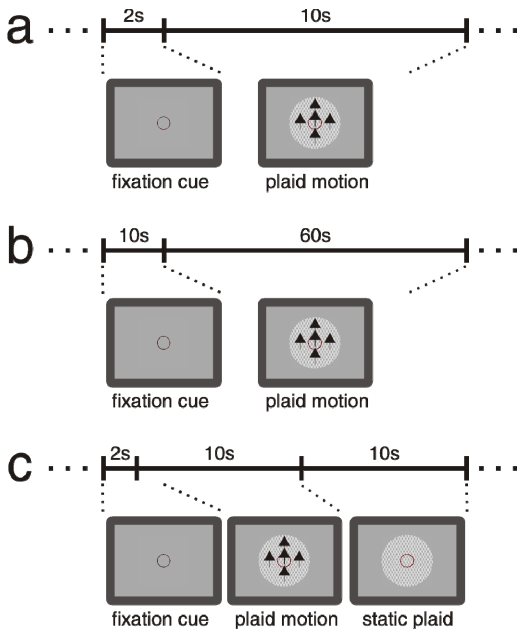

Figure 7 Scheme of basic experimental design of the center-surround motion experiments
Timing of Experiments 1 & 2 **(a)**; Experiment 3 **(b)**; and Experiment 4 **(c)**.

above.

Experiment 3: Modulatiory effects under longer viewing times

In the third experiment we have investigated the modulation of highly ambiguous center stimuli during relatively long stimulus presentation periods. Since the three overall luminance and contrast sets defined in Experiment 1 yielded similar results (**Figure 6**), we only used stimuli from the HLHC set for this follow-up investigation. The stimulus arrangement and spatiotemporal characteristics were similar to that of the first two experiments; however, stimulus blocks were presented for 72 seconds, with 12 seconds static fixation and 60 seconds plaid movement (**Figure 7b**).

Every subject underwent two sessions of experimental runs. In the first session we presented center-only stimuli with varying luminance of intersections, in order to minimize possible floor and ceiling effects by finding the region of highest ambiguity of each subject. In the second session we presented the central patch found to be the most ambiguous either with no contextual surround or with textured component and pattern biased surrounds.

We decided to present textured unambiguous surrounds only because this way we could prevent any possible bias induced by switches in the surround percepts. In addition, coherent plaid motion directions were randomized across the four cardinal directions in order to further generalize our results for long exposure times[244].

Experiment 4: Modulatory effects of different surround directions

In this experiment pattern motion of the central patch was always kept vertical whilst the pattern movement in the surround could follow any of the four cardinal directions (**Figure 5d**). There were also control conditions without any moving surround. The stimuli were presented in two sessions using subject initiated 22-second blocks (2 seconds period for fixation, 10 seconds plaid motion period and 10 seconds intermixed static plaid rest period; **Figure 7c**) The static rest periods were included to allow for directional motion adaptation to return to baseline levels.

In the first session of the experiment each stimulus condition was presented using *'Baseline'* gratings with *'Lum_4'* intersections five times from the HLHC and five times from the HLLC stimulus set (**Table 2**), in a randomized manner. It is important

to point out that, except for motion direction, center and surround stimuli were physically identical preventing confounding saliency pop-out effects and ensuring that relative motion of collinear contours was the only critical variable during this experiment (see insets in **Figure 5d**). Center stimuli were designed to elicit ~70% coherent pattern motion percept (**Figure 6d**), ensuring a dominant single direction pattern bias whilst still being in the range of ambiguity, and therefore prone to contextual effects. This baseline center coherent bias rose to ~95% when the same stimulus was located in surround locations, rendering surround modulations very stable.

In the second session we compared the surround modulation induced by the previously described symmetric surround plaids with that induced by a set of asymmetric surround plaids (*'Component bias'* gratings with *'Component bias'* intersection) under HLHC stimulus conditions, to exclude that the perceived relative contrast of the surround plaid components would be the determining factor of perceived central plaid transparency. Experimental conditions, subject instructions, and stimulus timing were similar to session 1.

2.1.3. Data analysis

Statistical methods

The continuous recording of responses allowed to estimate the overall duration of single percept types (transparent or nontransparent), the relative ratio of these perceptual states during the presentation periods, and the number of perceptual switches as a possible measure of percept stability. Note, that the total amount of time in a given state is dependent both on the number of switches to that state and single state durations.

In the description of the overall perceptual state duration during the presentation period we present statistics based on the percentage of "transparent" responses because these statistics complement those based on the percentage of "non-transparent" responses (taking into account that % transparent + % non-tranparent + % unsure = 100%), and the percentage of "unsure" responses, in which subjects pressed either both buttons or none of them due to their uncertainty in describing the

percepts, was low and stable across all conditions (see **Figure 6a, b, and c**). The latter observation proved that the perceptual response patterns were indeed not influenced by the level of subject uncertainty. We have applied ANOVA statistics (except otherwise stated, see below) after excluding potential violations of its statistical assumptions (including Kolmogorov-Smirnov normality verification, and Levene homogeneity tests).

In Experiment 3, we have performed GLM (General Linear Model) / ANOVA repeated measures as well as random effects analyses (given a relatively large number of subjects), using 'subjects' as a random variable. Effects were tested both using between-subjects (with 'subjects' entered as random effects) and within-subjects comparisons. In all analyses Bonferroni correction for posthoc comparisons was applied. The same dichotomy of contextual influence was found using within-subjects GLM and non-parametric statistical models (Friedman and Wilcoxon tests, for within subject comparisons), thereby proving the robustness of our results, and their independence of the statistical model used. In the special case of assessment of the number of percept switches as an indicator of perceptual stability we have used the Kruskal-Wallis test given the gross violations of ANOVA assumptions even after variable transformations.

In experiment 4, we used the non-parametric Friedman test for a distribution free repeated measures analysis because the distribution of the data was not normal and the variances across stimulus conditions differed significantly. Multiple comparisons were performed using Wilcoxon's signed rank test with Bonferroni's post hoc correction.

Assessment of single-percept stability

Although our main analyses focused on the overall time spent in each perceptual state, it is also important to specifically analyze how stable a single percept is. We have therefore departed in this part of the analysis from considering the total amount of time spent in a given perceptual state and used the duration of single perceptual states. This approach helps differentiating between the inherent perceptual bias and the ambiguity of a given stimulus, thus providing an independent measure of percept stability or stimulus ambiguity. Note that a highly ambiguous stimulus with a given

perceptual bias can solely differ from a similarly biased but less ambiguous stimulus in the number of perceptual switches. Accordingly, a given surround type may lengthen specific single percept durations even without a change in the overall summed duration depending on the number of switches during that condition. This notion may also be clinically relevant in the study of visual impairment and ageing processes.

Moreover, response type (pattern or component) ordering of single percept durations provides a means for describing the effects of surround modulation in terms of enhancement or suppression depending on perceptual congruency and incongruency between centers and surrounds compared to the no surround condition. In this kind of analysis there is a signature of enhancement of congruent percepts if the average single percept duration for the perceptually congruent surround condition is longer than that of the no surround condition. Similarly, active suppression is verified if the average single percept duration for the perceptually incongruent surround condition is shorter than that of the no surround condition.

2.1.4. Eye movement control experiments

All subjects were experienced observers and were selected on the basis of fixation ability on concurrent eye movement experiments. We have nevertheless run further control eye movements experiments using plaid stimuli in 8 subjects, with an iView X^{TM} HI-Speed eye tracker (Sensomotoric Instruments, Berlin, Germany) which allowed for data collection at 240 Hz. The eye tracker also served as a head rest during these experiments that fixed the viewing distance at 60 cm. Data time series were searched for fixation, blinks and saccadic events with an interactive computer program (Begaze, SMI, Germany), and subsequently exported to standard statistical packages (SPSS and StatView). Analysis of the recorded data showed that fixation could be stably held across all conditions, with very rare saccades, and reduced number and duration of blinks, which was similar across conditions. Under the conditions of the experiment, we could therefore ascertain that the subjects did not foveate the surround region.

2.2. Neural correlates of real and illusory motion perception

2.2.1. Participants and data acquisition

The experiments followed the tenets of the Declaration of Helsinki, and informed consent was obtained from all participants in strict accordance to the respective local ethical committee guidelines.

Experiment 1

The first set of functional magnetic resonance imaging (fMRI) experiments was performed at the Department of Neuroradiology, University Hospital Maastricht, The Netherlands on 4 subjects at 1.5 T in a Philips ACS-NT scanner (Philips Healthcare, Best, The Netherlands) by using the standard head coil and a gradient echo echo-planar imaging (EPI) sequence (TR = 2083 ms, TE = 40 ms, FOV = 224 × 224 mm^2, 22 slices, voxel size: 3.5 × 3.5 × 5 mm^3). A T1-weighted 3D magnetization prepared rapid acquisition gradient echo or fast field echo scan was recorded in the same session as the functional measurements (voxel size: 1.0 × 1.0 × 1.0 mm^3).

Experiment 2a

The second set of functional imaging experiments was performed at Ginoeco S.A, Porto, Portugal on 4 participants (only one of which had participated in Experiment 1) at 1.5T in a Philips Gyroscan Intera scanner (Philips Healthcare, Best, The Netherlands) by using the standard head coil and a gradient echo EPI sequence (TR=3000ms, TE = 50 ms, FOV=230 × 230 mm^2, 30 slices, voxel size: 3.5 × 3.5 × 4 mm^3) A T1-weighted 3D magnetization prepared rapid acquisition gradient echo scan was recorded in the same session as the functional measurements (voxel size: 1.0 × 1.0 × 1.0 mm^3).

Experiment 2b

The third set of functional imaging experiments was performed at the Maastricht Brain Imaging Center, Maastricht, the Netherlands on 8 participants (only two of which had participated in Experiment 1 and none in Experiment 2) at 3T in a Siemens Allegra scanner (Siemens AG, Erlangen, Germany) by using the standard head coil and a gradient echo EPI sequence (TR=2000ms, TE = 30 ms, 33 slices,

voxel size: 2.97 × 2.97 × 3 mm^3) A T1-weighted 3D Tfl.ADNI anatomical sequence was recorded in the same session as the functional measurements (voxel size: 1.0 × 1.0 × 1.0 mm^3).

2.2.1. Visual stimuli and paradigms

Experiment 1

Plaid stimuli were constructed by superimposing square-wave gratings with 0.3 average duty cycle and angles of approximately ±75° in a 12º circular aperture (**Figure 8**). We have used plaids with opposite contrast polarity of dark and light stripes (~12 and 36 $cd \cdot m^{-2}$) on intermediate background luminance (~24 $cd \cdot m^{-2}$). Typical intersection luminances were 10 or 30 $cd \cdot m^{-2}$. Plaid velocities were either 8 or 16 $deg \cdot s^{-1}$.

Subjects viewed moving plaids (8 volumes, 16 seconds) separated by rest conditions. Any given rest condition was either a fixation baseline (6 volumes) or a stationary plaid (8 volumes), which evoked a salient unidirectional motion aftereffect. Subjects performed either an angle or a color task.

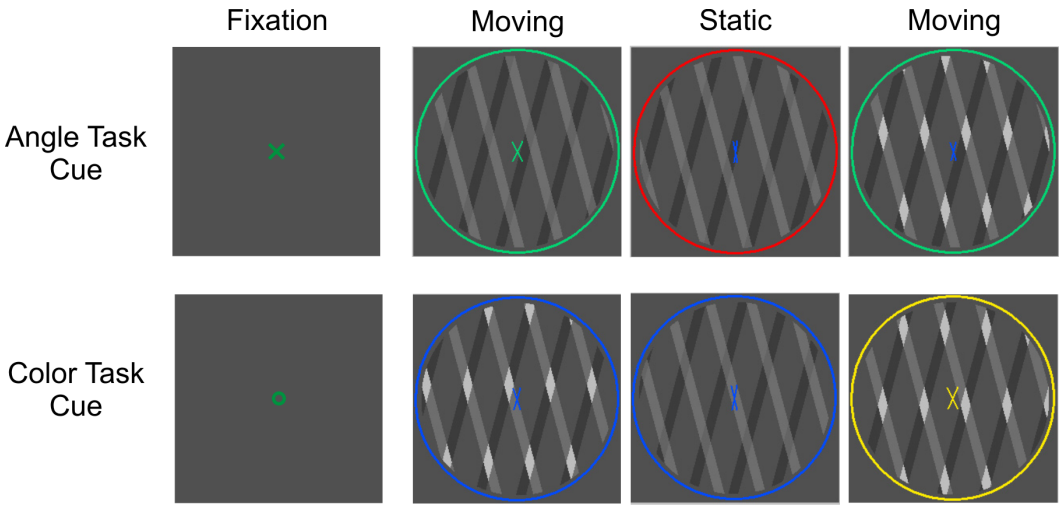

Figure 8 Full cycle of stimulus conditions in Experiment 1 within a block.
Subjects performed either an angle or a color task. In the angle task, subjects had to report whether the angle of the fixation cross (changing every 2 s) was larger or smaller than the plaid angle (note that fixation crosses had variable angles). In the color task, subjects had to report whether the fixation cross (changing every 2 s) had the same or different color from the curve outlining the stimulus aperture (note that fixation crosses had variable color in addition to the angle). During the fixation blocks only the fixation stimulus (crosses or circles cueing angle or color task, respectively) were present. Experiments included eight blocks per run (which were balanced for the 2 runs). Each block started with a fixation condition, followed by moving plaids, static plaids, moving plaids, and the fixation condition of the ensuing block.

In the *angle task*, subjects had to report whether the angle of the fixation cross (changing every 2 s) was larger or smaller than the plaid angle (see **Figure 8 top**). This task required direct stable attention to plaid stimuli, but the subjects still had to report on a motion-unrelated feature (angle between grating stripes).

In the *color task*, stable attention was required on features not directly related to plaid stimuli. In this task, subjects had to report whether the fixation-cross (changing every 2 s) had the same or different color from the curve outlining the stimulus aperture (**Figure 8 bottom**).

Each task was repeated in eight blocks per run interleaved in a balanced manner (concerning plaid luminance types) across the 2 experimental runs. Each block started with a fixation condition, followed by moving plaids, static plaids, moving plaids, and a fixation condition again (that started a new cycle). The shape of the fixation stimulus (cross or circle) cued whether subjects had to perform the *color* or the *angle comparison task* during the following motion and static period, since there was no difference in the moving and static plaid displays between the two attentional task conditions. Tasks were performed continuously, both during inspection of moving and stationary stimuli, to ensure stable control of selective attention, and to avoid confounding task-related contrasts.

Additional flow-field experiments were performed to localize motion-sensitive areas in single subjects for ROI definition (in addition to plaid motion contrast). During these measurements, two stationary stimuli (fixation cross and stationary dot pattern, repeated 4 and 10 times) and a motion condition (flow-fields, 30º wide by 23º high, 400 dots, size 0.06 × 0.06°, velocity 3.6-14.4 deg·s^{-1}, repeated 5 times for 16 s) were alternated.

Experiment 2a

Sixteen second epochs of plaid motion and static plaids were combined and presented in a block design manner. Motion blocks had either constant direction of motion (adapting *fixed motion conditions*) or the direction changed in every two seconds (non-adapting *mixed motion conditions*). There were motion and static blocks with and without overlaid apparent motion, as well as intervening fixation periods which were used to compute baseline activity (**Figure 9**). Subjects had to

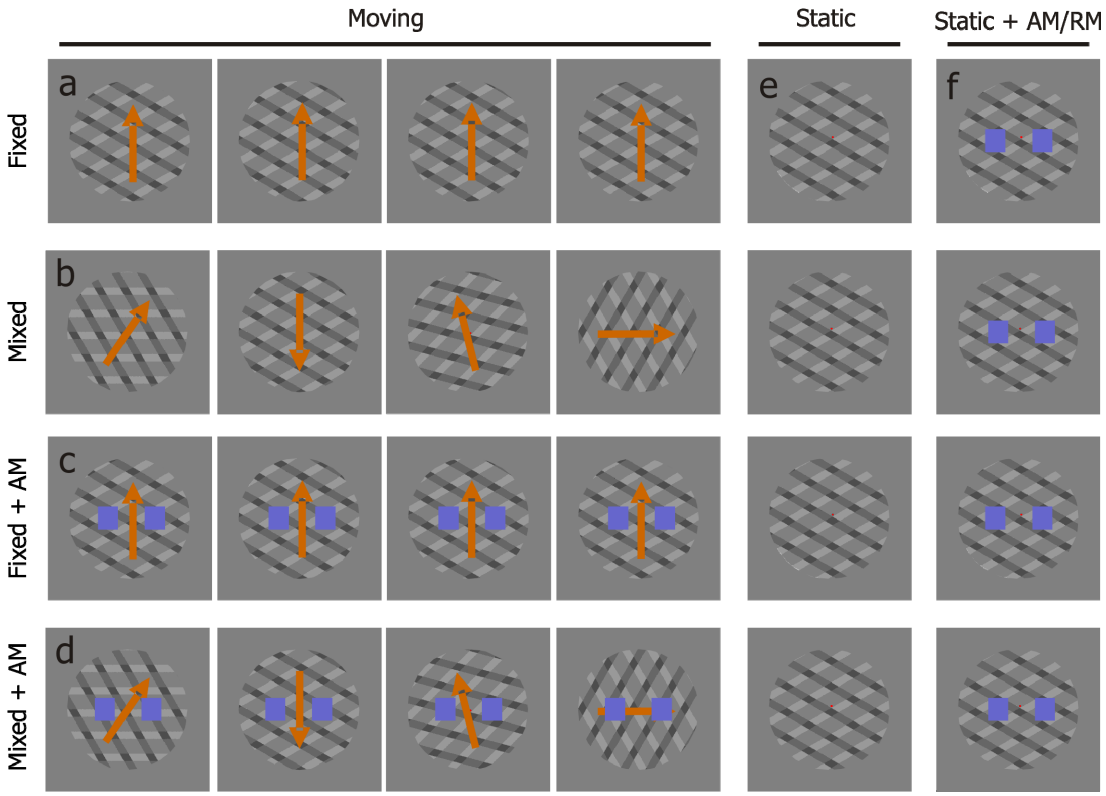

Figure 9 Experimental design for Experiments 2a and 2b (n=4 and n=8, respectively). Sixteen second blocks of plaid motion and static plaids were combined and presented in a block design manner in these experiments. Motion blocks had either constant direction of motion (fixed; **a,c**) or the direction changed in every two seconds (mixed; **b,d**). There were motion periods with and without overlaid apparent motion. Static blocks were also presented with **(f)** and without **(e)** overlaid apparent or real motion tasks (the speed judgment of moving squares RM task was only applied in experiment 2b). Note that there are no contrast transients between moving and static plaids. AM: apparent motion; RM: real motion.

track speed changes of the apparent motion stimulus superimposed on the moving and static plaids, as an attentional task. All subjects performed this behavioral task above 80% accuracy.

Plaid stimuli were constructed by superimposing square-wave gratings with 0.25 average duty cycle and angles of approximately ± 60° (directions ± 30º) in a 4° circular aperture with 1.5 cpd spatial resolution. Luminance of the background was ~10 cd·m^{-2}, for the gratings it was ~7.5 and ~25 cd·m^{-2}, with the intersection being ~ 4 cd·m^{-2}. The luminance of the blue AM stimulus was ~4 cd·m^{-2}. Plaid pattern velocity was 1.54 deg·s^{-1}.

Epochs of plaid motion (16 s), static plaids (16 s), and fixation (8 s) were combined and presented in a block design manner. Data were collected in 4 runs, containing 32 balanced blocks altogether (8 with adapting *fixed motion* without AM,

8 with adapting *fixed motion* with AM, 8 with non-adapting *mixed motion* without AM, 8 with non-adapting *mixed motion* with AM, each block containing a MAE test period with overlaid AM in half of the cases and a fixation period afterwards). This means that 4 blocks of MAE test periods were included that did contain the AM task and 4 that did not, which allowed for direct comparison of responses to static plaids with and without MAE perception.

Motion direction changed (only under *mixed-motion conditions*) in every 2 seconds (8 evenly distributed directions in a range of 360º) with and without overlaid AM. The overlaid apparent motion stimulus consisted of 2 squares of 0.4º size, separated by 1.6º oscillating horizontally back and forth (velocity was constant and the square was moving back and forth), such that they were orthogonal to the adapting plaid pattern motion direction. No stimuli were placed in intervening positions across frames, which ensured that no real motion was present. The speed of AM stimuli changed every 4 seconds; possible speeds were as follows: 3.33, 4.44, 6.66, and 13.33 $deg \cdot s^{-1}$.

Experiment 2b

Stimulus properties were similar to Experiment 2a, except for the inclusion of a real motion condition using similar stimuli as in the AM condition overlaid on top of the MAE period (**Figure 9a,b,e, and f**). Furthermore, AM and RM stimuli were only superimposed on the MAE test period. Accordingly, the experimental paradigm was built from 16-second blocks of *fixed-* or *mixed-direction* moving plaid and static plaid displays with and without an overlaid apparent or real motion task after the motion adaptation period.

Data were collected in 2 runs, containing 18 balanced blocks (9 with adapting fixed motion and 9 with non-adapting mixed motion, and each containing a fixation period, adapting period and MAE test period, with or without AM/RM superimposed during the MAE period). Subjects had to track speed changes of the apparent motion or real motion stimulus superimposed on the static plaids as an attentional task. All subjects performed this behavioral task above 80% accuracy. Real motion stimuli were identical to the AM stimuli, except that they moved horizontally back and forth with smooth motion, with speed matched to that of the AM condition.

It is important to mention here, that the presentation of real motion, either surface motion (plaids, or random dot kinematograms) or a smooth translocation of a moving patch (our RM stimulus) on a computer screen is also an apparent motion like stimulus. However, since the critical fusion frequency of healthy subjects is usually well below 60 Hz[81] we can safely assume that they indeed perceived smooth real motion during our experiments.

2.2.1. Eye movement control experiments

Eye movements were measured with an iViewX High-speed Eye-Tracker (Sensomotoric Instruments, Berlin, Germany) which allowed for data collection at 240 Hz. Data were collected outside the scanner in 8 subjects, using the exact same stimulus protocols as in Experiment 2b. Data time series were searched for fixation, blinks, and saccadic events with Begaze Software (SMI, Germany), and subsequently exported to standard statistical packages (SPSS and Statview).

Analysis of the externally recorded eye tracking data showed that fixation could be stably held across all conditions, with very rare saccades and reduced number and duration of blinks, which was similar across conditions. Analysis of variance did not show any interaction between conditions and fixation patterns.

2.2.2. Data Analysis

Data processing

Data analysis included preprocessing (slice scan time correction, 3D motion correction, and spatial and temporal filtering), coregistration and Tailarach transformation of scans. These steps were performed by using BrainVoyager 2000 and BrainVoyager QX (Brain Innovation B.V., Maastricht, The Netherlands) software. For multiple regression analysis, a general linear model (GLM) was fitted with predictors for each experimental condition. The time courses of individual predictors were obtained by using a linear model of the hemodynamic response.[245] The overall model fit was assessed by using F statistics. Significant differences between the experimental conditions were assessed by using contrast maps (t-maps). Conjunction analyses of experimental conditions were also performed (using a logical AND criterion for all contrasts). The obtained p values were corrected for

multiple comparisons by using a Bonferroni adjustment. Clusters were accepted only as significant when $p_{corr} < 0.001$.

Region of interest selection

A GLM with a boxcar regressor marking temporal epochs of plaid motion was applied to the BOLD time series data from the concatenated series of individual runs in every single subject. The regressor was then convolved with a prototypical hemodynamic response function (HRF) function. Area hMT^+ was defined as a contiguous group of voxels lateral to the parietal-occipital sulcus that exhibited a significant response during epochs of plaid motion compared with epochs of static plaids.

In experiment 1 an additional localizer run was included using flow-field stimuli for providing the motion contrast for hMT^+ selection. As the above-described plaid motion contrast yielded similar results as the flow-field localizer, the latter had been omitted from the further experiments.

Region of interest analysis

Percent signal change was calculated for each condition separately, based on the average activation level of the immediately preceding fixation period, taking into account the hemodynamic delay. For further analysis, data from subjects and runs were pooled according to stimulus conditions. In Experiments 2a and 2b ANOVA statistics with Fisher's post hoc comparisons were calculated on the pooled data of the first, second, third, and fourth 8 second epochs of the whole stimulation cycle. For presentation purposes we show the activation levels at data-points corresponding to the acquisition volumes.

2.3. Learning-induced changes in motion processing

2.3.1. Subjects

Fourteen subjects (6 females) participated in the main experiment and four additional subjects (1 female) participated in the control experiment. All had normal or corrected to normal visual acuity and reported no history of neurological problems. Subjects gave informed consent to participate in the study, which was approved by the local ethics committee of Semmelweis University. Functional MRI data of four observers were excluded due to excessive head movement in the scanner.

2.3.2. Stimuli and apparatus

Stimuli were programmed in Matlab (MathWorks Inc, Natick, MA, USA) using the Cogent 2000 Software Toolbox and were presented on generic PCs. All visual stimuli were rendered in white on a black background. The luminance of the background and the moving dots was < 2 $cd \cdot m^{-2}$ and 32.2 $cd \cdot m^{-2}$, respectively. In all experiments subjects were instructed to maintain gaze on a central fixation square subtending 0.25° visual angle present for the entire duration of each experiment. In all experiments, moving dots (N=200) were presented within a 20° (diameter) circular field centered on the fixation square, with a 1.6° (diameter) circular blank region around the fixation point. Dots subtended 0.15° in diameter, and had a limited lifetime of seven frames. Behavioral responses were collected by means of mouse button presses.

During the psychophysical experiments visual stimuli were presented at 75Hz on a 21” Syncmaster 1100mb CRT monitor (Samsung Electronics, Seoul, Korea); the monitor was the only light source in the room. Eye movements were recorded in these sessions using an iView X^{TM} HI-Speed eye tracker (Sensomotoric Instruments, Berlin, Germany) at a sampling rate of 240 Hz. The eye tracker also served as a head rest that fixed the viewing distance at 50 cm.

During the fMRI experiment visual stimuli were projected onto a translucent screen located at the back of the scanner bore using a Panasonic PT-D3500E DLP

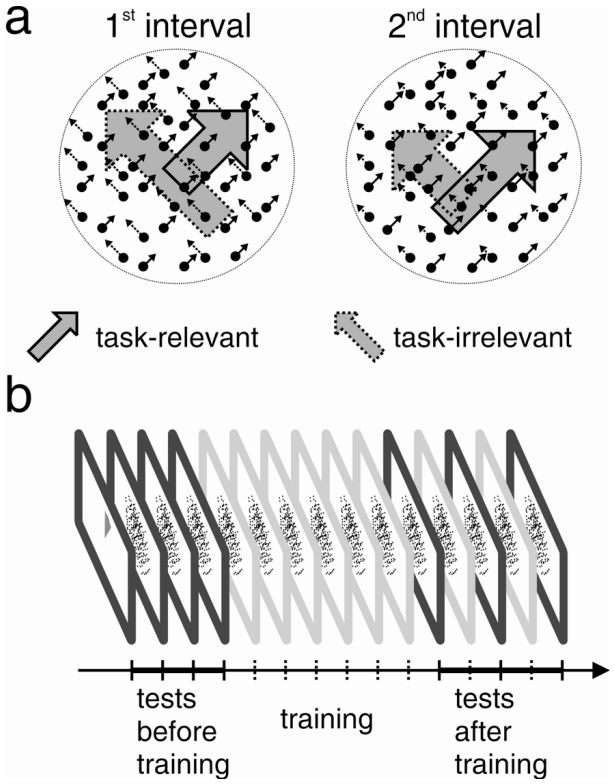

Figure 10 Schematic representation of the stimuli during training and the experimental procedure.
(a) Transparent random dot motion display used for training on the speed discrimination task. One of the motion directions was task-relevant and the other direction was task-irrelevant throughout training. The different length of the arrows indicate that dot speed was different in the two intervals both in the case of task-relevant and task-irrelavant direction. **(b)** The experimental protocol consisted of a training phase and two testing phases, one before and another after training. Training comprised six one-hour sessions of psychophysics during which subjects performed a speed discrimination task. Before training, the test phase included: (1) an fMRI retinotopic mapping session to localize the retinotopic visual cortical areas; (2) psychophysical measurement of motion coherence detection thresholds; (3) ERP recording session; and (4) an fMRI scanning session. In the test phase after training there was no retinotopic mapping and the psychophysical, fMRI and EEG measurements were separated by a top-up training session.

projector (Matsushita Electric Industrial Co., Osaka, Japan) at a refresh rate of 75 Hz. Stimuli were viewed from inside the magnet through a mirror attached to the head coil with a viewing distance of 58 cm. Head motion was minimized using foam padding.

2.3.3. General procedure

The experiment protocol consisted of a training phase and two testing phases, one before and another after training (**Figure 10b**). Training comprised six one-hour sessions of psychophysical testing during which subjects performed the speed discrimination task. Each observer underwent four different testing steps before

training: a retinotopic mapping scanning session to identify the boundaries of retinotopically organized regions of visual cortex, a psychophysical testing session to estimate motion coherence detection thresholds, an EEG session, and an fMRI scanning session. EEG data are not presented in this thesis. The same set of experiments (with the exception of retinotopic mapping) were repeated after training to evaluate training induced changes in performance and brain activity. The post-training sessions were separated by two additional 'top-up' learning sessions to ensure that learning was maintained. Each test session was performed on a different day and their order was randomized across subjects. Each psychophysical testing session and training sessions lasted for 1 hour, while fMRI experiments lasted for 1.5 hours.

2.3.4. Training

On each training day, subjects performed a series of 2-interval forced choice speed discrimination tasks. In each trial the two 500 ms stimulus presentation intervals were separated by a 200 ms inter-stimulus interval. The next trial was initiated by the subject's response button press with an inter-trial interval jittered between 300-500 ms. Each interval contained two populations of spatially superimposed dots moving in a direction either +45° or -45° tilted from the upward direction (**Figure 10a**). Subjects were instructed to attend to dots moving in one of the directions (task-relevant direction) while simultaneously ignoring dots that moved in the orthogonal direction (task-irrelevant direction). They were asked to indicate which of the two intervals contained faster motion in the task-relevant direction. The speed of the task-relevant direction was fixed for one of the two intervals (at 6 $deg \cdot s^{-1}$), while that of the other interval was varied using a QUEST adaptive staircase procedure[84] arriving at a value providing 75% correct performance. The speed of the task-irrelevant motion also differed between the first and second trial (a random speed jitter between 6 and 7 $deg \cdot s^{-1}$). Every training session consisted of 8 experimental blocks of 80 trials each. Task-relevant and irrelevant directions were randomized across subjects, but kept constant across training sessions.

2.3.5. Testing motion coherence detection thresholds

Motion coherence thresholds were acquired for three motion directions within the same block, two directions similar to those of the training (±45° from the upward direction) and a third, downward (180°) control direction. A single trial consisted of two 250 ms stimulus presentation intervals, separated by a 250 ms inter-stimulus interval (ISI). The next trial was initiated by the subject's response button press with an inter-trial interval jittered between 200-300 ms. The order of the intervals was randomized across trials and motion coherence for each direction was varied independently by using the QUEST adaptive staircase procedures to converge at 75% correct performance in 60 steps. Two staircases (one starting at 0% and the other starting at 100% coherence) were randomly interleaved within an experimental block for each motion direction. Data were analyzed with repeated measures ANOVA with factors of test session (before training, after training), and task relevance (task-relevant, task-irrelevant) for each experiment.

2.3.6. fMRI experiments

Subjects performed a 2-interval forced choice speed discrimination task during scanning. A single trial lasted 1875 ms and consisted of two 300 ms intervals of moving dots (separated by 300 ms ISI) and followed by a 950 ms period for response. Subjects were instructed to indicate which of the two intervals contained faster motion. The speed was fixed for one of the intervals at 6 $deg \cdot s^{-1}$ while for the other it was adjusted (based on pilot testing) so that subject's performance was around 75% correct during scanning. Trials were organized into blocks. During a single block of 8 trials the direction of motion of the dots was kept constant, either +45° or -45°. One run comprised a pseudo-randomized and balanced presentation of four 15 s blocks of each motion direction, interleaved with thirteen 15 s blocks of static dot display as rest periods. 6 runs were performed in an experimental session.

fMRI data acquisition and analysis

MRI scanning was performed at the MR Research Center, Szentágothai Knowledge Center, Semmelweis University, Budapest, Hungary on a 3 Tesla Philips Achieva scanner (Philips Healthcare, Best, The Netherlands) equipped with an eight-

channel SENSE head coil. High resolution anatomical images were acquired in all of the imaging session using a T1 weighted 3D TFE sequence yielding images with 1 × 1 × 1 mm resolution. During the retinotopic mapping session T2*-weighted functional images were acquired using an echo-planar imaging sequence, with 23 slices oriented parallel to the calcarine sulcus (64 × 64 image matrix, 3.4 × 3.4 × 3 mm resolution, TR = 1200 ms, TE = 30, FA = 75°, FOV = 220 mm, ascending non-interleaved acquisition order). During the main experimental session, 46 transverse slices were acquired with an EPI sequence (80 × 80 image matrix, 2.75 × 2.75 × 2.75 mm resolution, TR = 3000 ms, TE = 30, FA = 75°, FOV = 220 mm, ascending interleaved acquisition order).

Data analysis was performed using BrainVoyager QX (Brain Innovation B.V., Maastricht, The Netherlands) and custom time series analysis routines written in Matlab (MathWorks Inc., Natick, MA, USA). The three anatomicals were homogeneity corrected, coregistered and then averaged to provide a better grey and white matter contrast. Images were then normalized to Talairach coordinates and then segmented, and inflated to provide a 3D reconstruction of the grey and white matter boundary. All of the processing steps were done using BrainVoyager QX.

Region of interest selection: retinotopic mapping and hMT$^+$ functional localizer task

Retinotopic mapping was implemented using the standard traveling wave method.[246-249] Polar angle was mapped with a slowly rotating (8.3 deg·s^{-1}) phase reversing wedge stimulus (30° wide) extending from the center of gaze to 10° in the periphery. Eccentricity was mapped in a similar fashion by estimating the phase of the response to a slowly expanding or contracting (0.35 deg·s^{-1}) stimulus annulus with a width of 1.25° (**Figure 11**). Based on the activation maps 5 retinotopic visual areas were delineated for the ROI based analysis: V1, V2, V3, V4v, V3a.

The fMRI sessions before and after training included a localizer scan based on which hMT$^+$ was identified. Subjects viewed a stimulus consisting of twelve 15 s intervals of moving dots interleaved with eleven 15 s epochs of randomly plotted dots. The reference stimulus was windowed by the aperture in which the stimuli appeared in the experimental scans and contained either uncorrelated motion or a

correlated motion flow field with the direction of motion changing every 3 s. The speed of the moving dots was 6 deg·s^{-1}.

A general linear model (GLM) with two boxcar regressors was applied to the BOLD time series data from the functional localizer scans; the regressors marked temporal epochs of coherent motion and incoherent motion. Each of the boxcar regressors was then convolved with a prototypical hemodynamic response function (HRF) function (mixture of two gamma functions with an initial peak at 6 s and a later undershoot peaked at 16 s, with a 6:1 ratio between the early and the late γ functions). Area hMT$^+$ was defined as a contiguous group of voxels lateral to the parietal-occipital sulcus and beyond the retinotopically organized visual areas that exhibited a larger response during epochs of motion compared with epochs of static dots.

Region of interest analysis

To evaluate the fMRI responses obtained in the main experiment – in each subject – we extracted time course data locked to stimulus onset and averaged over blocks from each ROI and for each condition. A canonical HRF (described above) was convolved with boxcar regressors - reflecting the onset of the trials - to model the hemodynamic response for prolonged (block-type) stimulation. With a single free parameter this function was fitted to the averaged fMRI responses for each subject and condition separately. The free parameter was a scaling factor and was taken as the measure of response magnitude for each condition for all subsequent analyses.

In order to be able to compare activations between different scanning sessions (before and after training) we derived normalizing factors for each area and scanning session. The normalizing constants were calculated from the data acquired during the independent functional hMT$^+$ localizer scans in a similar way as the response magnitudes for the main experiment. Thus, the normalizing constants for a given ROI represent the average response magnitudes to coherent and incoherent motion in that region. We were able to estimate these values for 8 subjects, because data acquired during the reference scans of 2 subjects after training were not reliable due to excessive head motion. To increase the reliability of the estimates (the calculation of the constants are based on single scans), the normalizing values were averaged across the subjects.

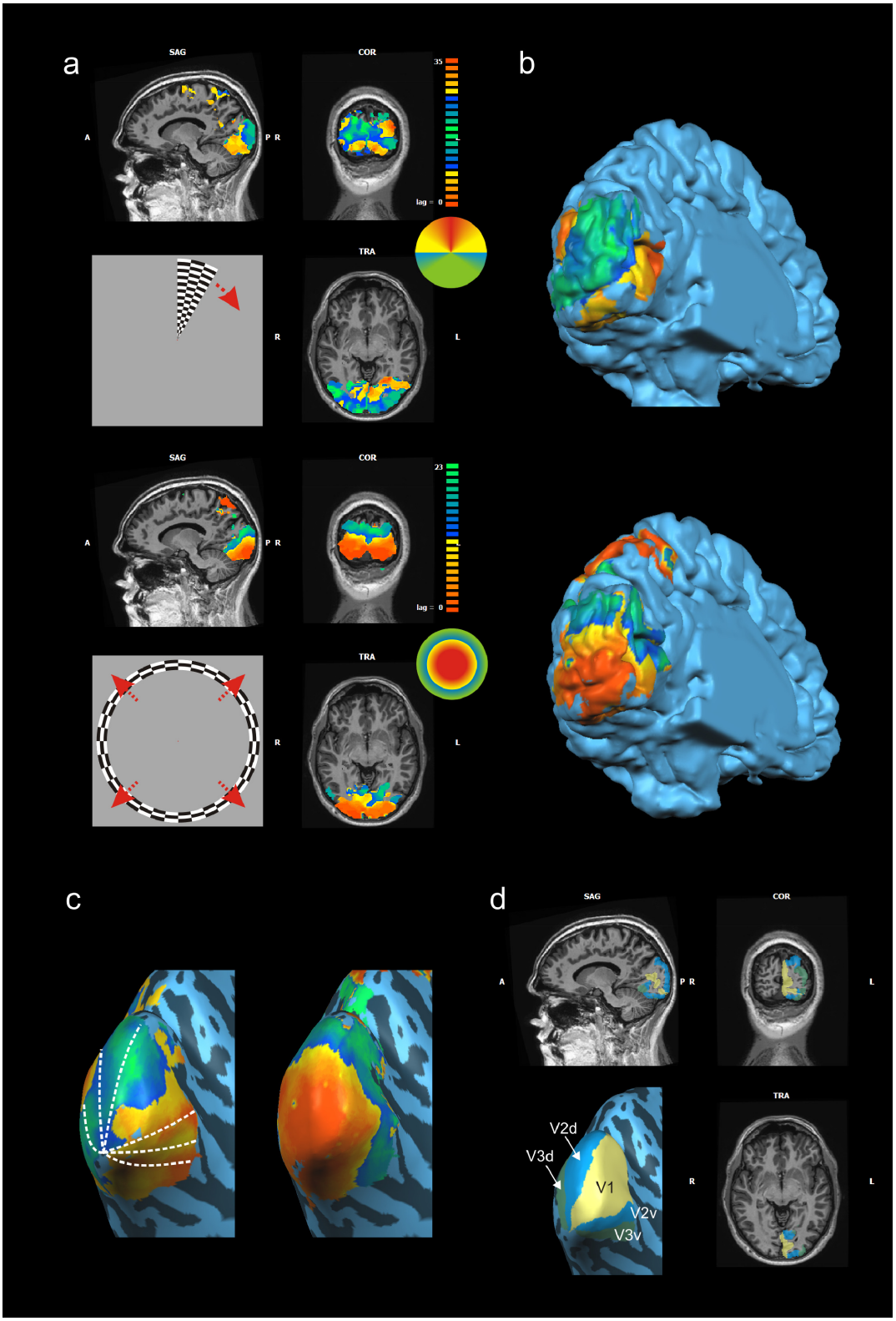

Figure 11 Retinotopic mapping and visual ROI definition
(a) Polar mapping (top) and eccentricity mapping (bottom) stimuli and their respective maps projected to anatomy. **(b)** Polar and eccentricity maps on the surface of the brain. **(c)** Polar and eccentricity maps on the inflated gray and white matter border. **(d)** Visual areas on the GM/WM border and projected to anatomy. Lines on panel C represent borders of visual areas. For description of visual area labeling see text.

The normalized magnitude $RN_{session}^{area}$ is calculated according to the formula:

$$RN_{session}^{area} = \left(R_{session}^{area} / N_{session}^{area}\right)\overline{N}^{area},$$

where $R_{session}^{area}$ is the uncorrected response magnitude for each condition, scanning session, subject and region, $N_{session}^{area}$ is the normalization factor for each region and scanning session and $\overline{N}^{area}$ is an average normalization constant for each region (averaged across the scanning sessions before and after training).

For statistical analysis of the difference between response magnitudes in different conditions we used repeated-measures ANOVA with test session (before training and after training), task relevance (task-relevant and task-irrelevant), and ROI (V1, V2, V3, V4v, V3a, and hMT^{+}) as factors. We also performed planned contrasts to evaluate pairwise differences between conditions.

2.3.7. Eye movement data analysis

We calculated the mean eye position, saccade frequency and cumulative saccade amplitudes using an interactive computer program. Saccade detection was performed by a velocity threshold algorithm (velocity threshold 50 $deg \cdot s^{-1}$). The algorithm detected saccades greater than 0.2°. Artifacts like drifts or blinks were identified by visual analysis and removed. The program yielded estimates of amplitude of each saccade. We calculated the frequency (ratio between number of saccades and total number of trials), and cumulative amplitude of gaze shifts[250] which occurred during the visual stimulus presentation separately for the different motion directions. We compared these values between the different conditions using repeated measures ANOVA and Student's t-test.

IV. RESULTS

1. Disease-related changes in color vision

1.1. Glaucoma study

1.1.1. Color discrimination deteriorates during the course of disease

We found robust evidence for early chromatic dysfunction in glaucoma under our testing conditions.

Figure 12a shows a significant and global increase in the mean ellipse axis length as revealed by repeated measures ANOVA, this increase is significant across groups ($p < 0.0001$ as a whole, with $p < 0.0001$ both for post hoc comparisons between patients with ocular hypertension and those with glaucoma and between the control and glaucoma groups; $p = 0.0578$ for comparisons between normal control subjects and patients with ocular hypertension)

Figure 12b shows independent evidence of the same finding, through the

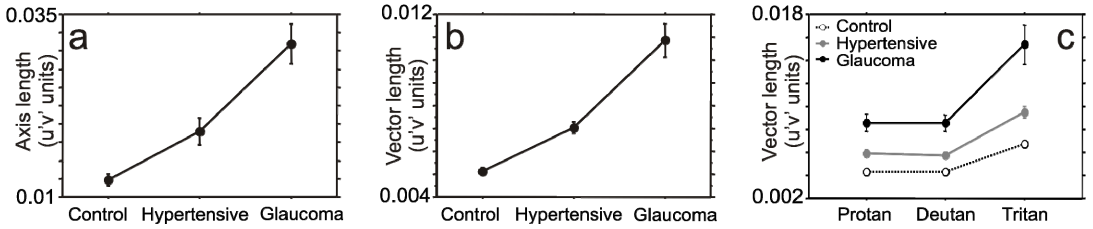

Figure 12 Length of discrimination ellipses and confusion vectors
(a) The length of the discrimination ellipses was significantly increased in glaucoma ($P < 0.0001$ as a whole, with $p < 0.0001$ both for post hoc comparisons between hypertension and glaucoma groups and between control and glaucoma groups; $p = 0.0578$ for comparisons between control and hypertension groups). **(b)** Mean length of confusion vectors (protan, deutan, tritan) is significantly increased in glaucoma and ocular hypertension, as revealed by repeated measures ANOVA ($p < 0.0001$ as a whole; with $p < 0.0001$ both for post hoc comparisons between the hypertension and glaucoma groups and between the control and glaucoma groups; $p = 0.0045$, for comparisons between control and hypertension groups). **(c)** Separate analyses of changes in confusion vector length across groups for protan, deutan, and tritan axes. All comparisons were significant across groups: protan: $p = 0.0118$ for comparisons between the control and hypertension groups, $p < 0.0001$ for comparisons between hypertension and glaucoma groups and control and glaucoma groups; deutan: $p = 0.0122$ for comparisons between control subjects and hypertension, $p < 0.0001$ for comparisons between hypertension and glaucoma and control subjects and glaucoma; tritan: $p = 0.0224$ for comparisons between control subjects and hypertension, $p < 0.0001$ for comparisons between hypertension and glaucoma and control subjects and glaucoma. A significant interaction was shown between groups and type of confusion vector ($p < 0.0001$). All vector units are in CIE 1976 u′,v′ color space coordinates, in all figures. Note that in some cases variability was so low that the SE bars are barely visible. The same applies to subsequent figures.

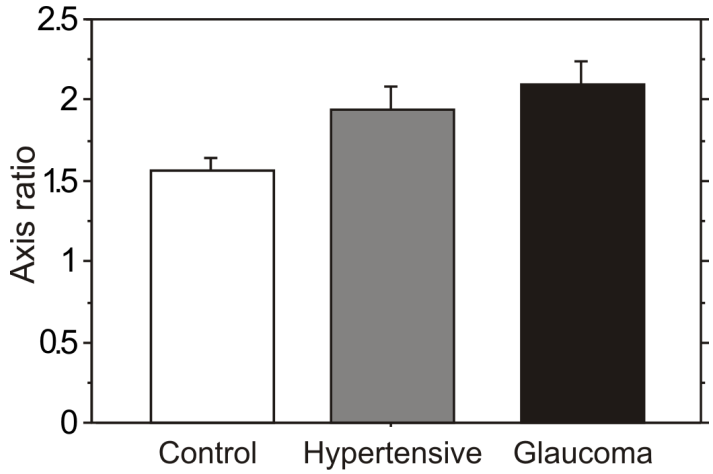

Figure 13 Axis ratios of discrimination ellipses are only significantly different between control and glaucoma groups
(p=0.0076, Fisher PLSD ANOVA).

measurements of the mean length of the three main confusion vectors (the trivector test) obtained from the three groups. This increase is significant across all study groups ($p < 0.0001$ as a whole; with $p < 0.0001$ both for post hoc comparisons between patients with ocular hypertension and those with glaucoma and between control subjects and patients with glaucoma; $p = 0.0045$, for comparisons between normal control subjects and patients with ocular hypertension). These values suggest that color confusion vectors are better measures than the length of discrimination ellipses in differentiating control subjects from patients with ocular hypertension, but care must be taken in this interpretation, because ellipses were fitted in fewer eyes ($n = 91$).

Figure 12c shows a separate analysis of changes in confusion vector length across stages for protan, deutan, and tritan axes. All increased significantly (see legend for details), albeit with a slight tendency for the tritan axis length to show a steeper increase. This global increase across all axes shows that concomitant early damage is already present in patients with ocular hypertension, regarding the konio- and parvocellular systems.

The global involvement of chromatic pathways is further suggested by the measurement of axis ratios of discrimination ellipses. These show a modest increase that can differentiate significance only between control and glaucoma groups ($p = 0.0076$), suggesting that damage may be preferential to the blue-yellow axis but not at all specific. This result becomes more obvious by inspection of **Figure 13**,

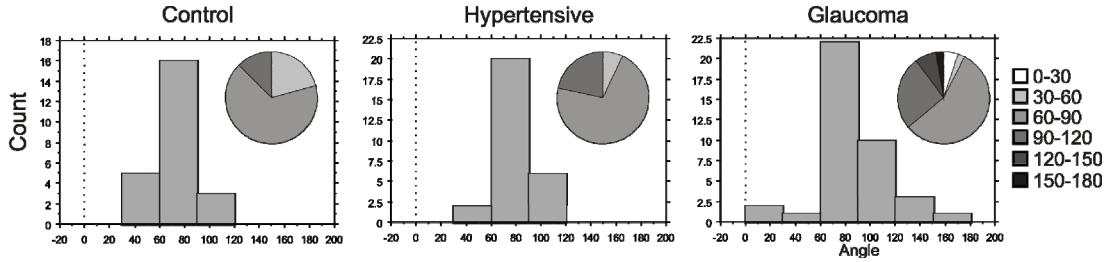

Figure 14 Distributions of discrimination ellipse angles (in degrees) across the control, hypertension, and glaucoma groups.

which shows that the axis ratio of chromatic discrimination ellipses is less prominently augmented than the elevation of length across stages (**Figure 12a**).

We next examined whether chromatic deficits in glaucoma follow any particular preferred axis. This could best be analyzed by inspection of population distributions of the angles of the discrimination ellipses. **Figure 14** shows that the distributions of angles of ellipses were similar (mean, ~80°) in the control, ocular hypertension, and glaucoma groups. In other words, the tendency for worse performance along the blue-yellow axis seen physiologically in normal control subjects was preserved in glaucoma and is evident on inspection of the pie chart inserts in **Figure 14**. Deviations from this pattern of disadvantage were not seen in ocular hypertension, but only in a small subset of patients with advanced glaucoma.

The observed exaggeration of the physiological disadvantage was subtle but significant. Indeed, repeated-measures ANOVA revealed a significant interaction between groups and type of confusion vector ($p < 0.0001$; see slopes of **Figure 12c**, showing steeper tritan loss).

1.1.2. Deterioration of chromatic function correlates well with C/D and MD measures

An important goal of this study was to compare our chromatic discrimination measures with clinical parameters used to classify patients with glaucoma, such as C/D ratio and visual field perimetry measures. Our evidence of chromatic dysfunction in patients with ocular hypertension contrasted quite strikingly with the lack of sensitivity of traditional perimetry measures such as MD. **Figure 15** shows representative graphs depicting individual raw data in u′v′ space, as well as fitted ellipses taken from the three study groups. The pattern of progressive deterioration is

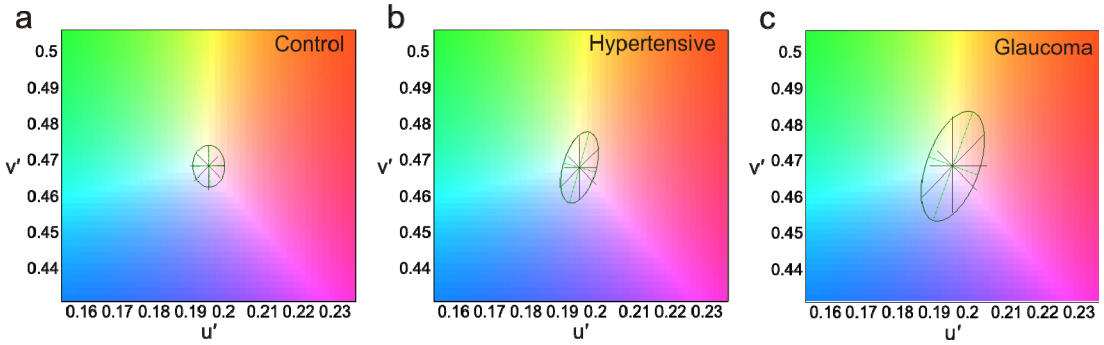

Figure 15 Representative examples of chromatic discrimination ellipses (raw discrimination vectors and fitted ellipses) in individual subjects in the three study groups of the glaucoma study
(a) control, **(c)** ocular hypertension, **(c)** glaucoma. *Solid straight lines*: measured color axes. *Curved solid line*: fitted ellipse; *dotted lines*: fitted ellipse axes. Color rendering is based on the sRGB (IEC1996 2.1) standard; the white point set to the white point of the test and the monitor gamut set to the gamut of our Trinitron monitor. The rendered colors are gamma corrected and the gamut of the monitor is outside the graphs. Parameters extracted from fitted ellipses were as follows (length, axis ratio, and angle, respectively): (a) 0.0116, 1.316, 92°; (b) 0.0203, 2.199, 74.2°; (c) 0.0319, 2.183, 69.9°.

further documented in **Figure 16**, which shows percentile distributions of ellipse length. The slight overlap between control and glaucoma groups is remarkable, with the hypertension group showing an intermediate pattern.

A significant deterioration of chromatic function over time was most prominent in patients with hypertension. The deterioration was analyzed by measuring time elapsed since diagnosis and correlating this measure with chromatic performance (length of discrimination ellipses). There was a significant correlation only in the group of patients with hypertension ($r = 0.493$, $p = 0.0095$, global $r = 0.206$, *ns*).

Regarding the analysis of C/D ratio, this value correlated significantly with almost all our measures of chromatic performance (protan, $r = 0.352$; deutan $r = 0.403$; tritan $r = 0.326$; ellipse length, $r = 0.400$; $p < 0.0001$ for all these correlation

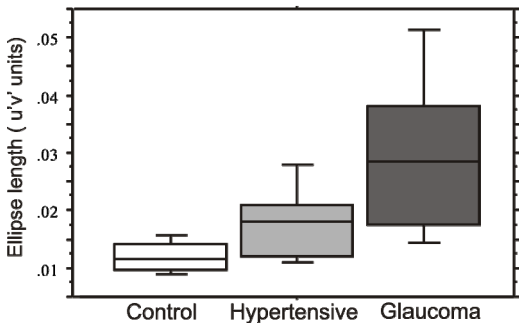

Figure 16 Percentile box plots measured for the three study groups of the glaucoma study
Bars depict 10th and 90th percentiles, the *top* and *bottom borders* of the boxes represent the 25th and 75th percentiles, and the *line* segment *inside* the boxes depicts the median

coefficients taken for the whole population of subjects). The ellipse axis ratio did not show any significant correlation with the C/D ratio, which is not surprising, given the lack of damage specificity that is evident in our data.

Regarding perimetric assessment: we found strong and significant correlations. Indeed, when psychophysical parameters were compared with parameters such as MD, strong global correlations were found (MD 30-2: protan, $r = -0.278$, $p = 0.0009$; deutan, $r = -0.391$ $p < 0.0001$; ellipse length, $r = -0.440$, $p = 0.0015$; axis ratio, *ns*). Not surprisingly, this correlation is mostly explained by the pattern of loss within the glaucoma group (MD 30-2: protan, $r = -0.545$, $p = 0.0027$; deutan, $r = -0.631$ $p = 0.0003$; ellipse length, $r = -0.479$, $p = 0.0231$; axis ratio, *ns*). No significant correlation was found with tritan axis length, suggesting that in spite of more prominent tritan loss, this measure is less correlated with field loss, once glaucoma is established.

Taken together we found that a concomitant involvement of multiple chromatic pathways within the central retina is present in the natural history of glaucoma earlier than previously believed. Moreover, this involvement is not restricted to the blue-yellow pathway, but includes the red-green processing stream. Furthermore, the deterioration of color vision correlated well with clinical measures (C/D ratio and MD).

1.2. Best disease study

1.2.1. Color discrimination deteriorates substantially in all cone pathways during the course of disease

Determination of chromatic discrimination ellipses allowed for detailed, unbiased assessment of chromatic function because in our procedure, thresholds were obtained simultaneously along multiple, evenly spaced axes in color space. Representative examples of deterioration of chromatic function during different stages of Best disease, as assessed by discrimination ellipses obtained from individual participants, are illustrated in **Figure 17**. These examples illustrate a steady elongation of the major axis of discrimination ellipses across the stages. It is also noticeable that the angle (orientation) of the ellipses, which is an indicator of the major axis of chromatic dysfunction, jittered markedly in patients in stages I and II, and a predominant tilt toward the red-green axis became obvious only for patients in stages III and IV.

Because none of the axes used for determination of discrimination ellipses

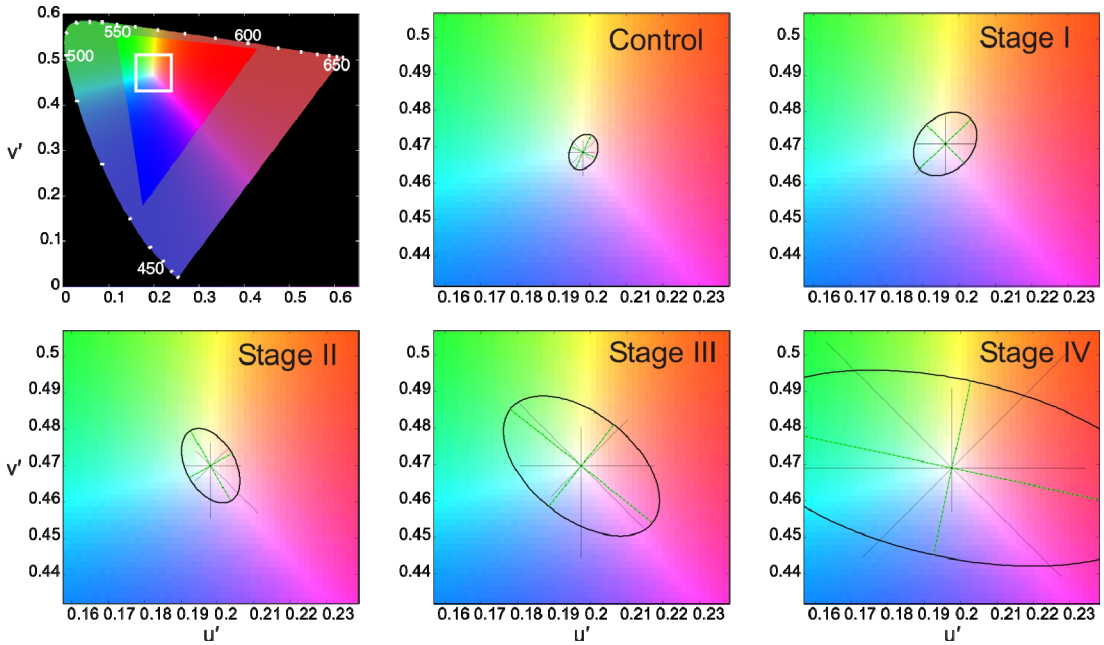

Figure 17 Representative examples of deterioration of chromatic discrimination ellipses in different stages of Best disease.
Black straight solid lines indicate measured color axes; curved solid lines: fitted ellipses; green dotted lines: fitted ellipse axes; panel labels: Fishman stages; color space units are CIE 1976 u′v′. For details on color rendering, see **Figure 15**.

coincided with cone confusion lines (protan, deutan, and tritan, which are more direct measures of cone function), we also measured chromatic thresholds along these lines, which are related to short-, medium-, and long-wavelength selective cones, respectively.

Comparison of chromatic loss along the 3 main confusion lines revealed a pattern of substantial functional impairment in Best disease (repeated-measures ANOVA, with a significant group effect: $p < 0.001$, **Figure 18**). All axes were significantly longer in the patient population than in the age-matched control population ($p < 0.001$ for the protan, deutan, and tritan axes, Fisher PLSD). The effects remained significant when the analysis was conducted separately for patients' right eyes ($p < 0.001$, ANOVA group effect) and left eyes ($p = 0.001$; even for individual eyes, comparisons split by axes remained in general with $p < 0.01$). The degree of protan and deutan loss was, on average, more prominent than the degree of tritan loss, but this effect was not significant on post hoc analyses, suggesting that the classic notion of a predominant red-green deficit has to be revised or, alternatively, that other factors, such as clinical staging, have to be considered (see **Figure 17**).

The specificity of damage can be better judged by analyzing the length, axis ratio, and orientation (angle) of chromatic discrimination ellipses. We found a significant increase in mean ellipse length in the patient population ($p < 0.001$, ANOVA group effect, **Figure 19a**), which was accompanied by a significant enlargement of the major ellipse axis compared with the minor axis (axis ratio: $p < 0.001$, **Figure 19b**). Stage had a significant effect on the deterioration of both measures ($p < 0.001$ for

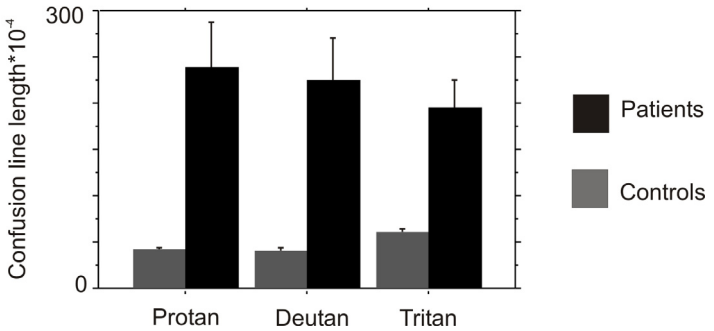

Figure 18 All three main confusion lines were significantly longer in Best disease patients than in the control population.
All effects remained significant when the analysis was conducted separately for participants' eyes (see text). Error bars represent SD.

both analyses **Figure 19c&d**). Post hoc analysis of such stage effect (Fisher PLSD) was significant not only between stages I and IV but also between controls and stages II/III and between stages II/III and IV. Regarding the axis ratio, comparisons were significant between all groups and stage IV.

The increased axis ratio suggests that although all axes are affected, there is some pattern of preferential damage. Such a finding does not necessarily mean that preferential damage occurs along specific axes in the early stages of Best disease. Indeed, although deviation of ellipse angles across stages shows a significant group effect ($p = 0.01$ by ANOVA, **Figure 17**), this effect could potentially be explained by late-stage patients. This notion is supported by the observation that the average peak at 87.13° that is measured in the distribution of the control group becomes significantly deviated only in the stage IV group (Fisher PLSD: $p = 0.04$ for

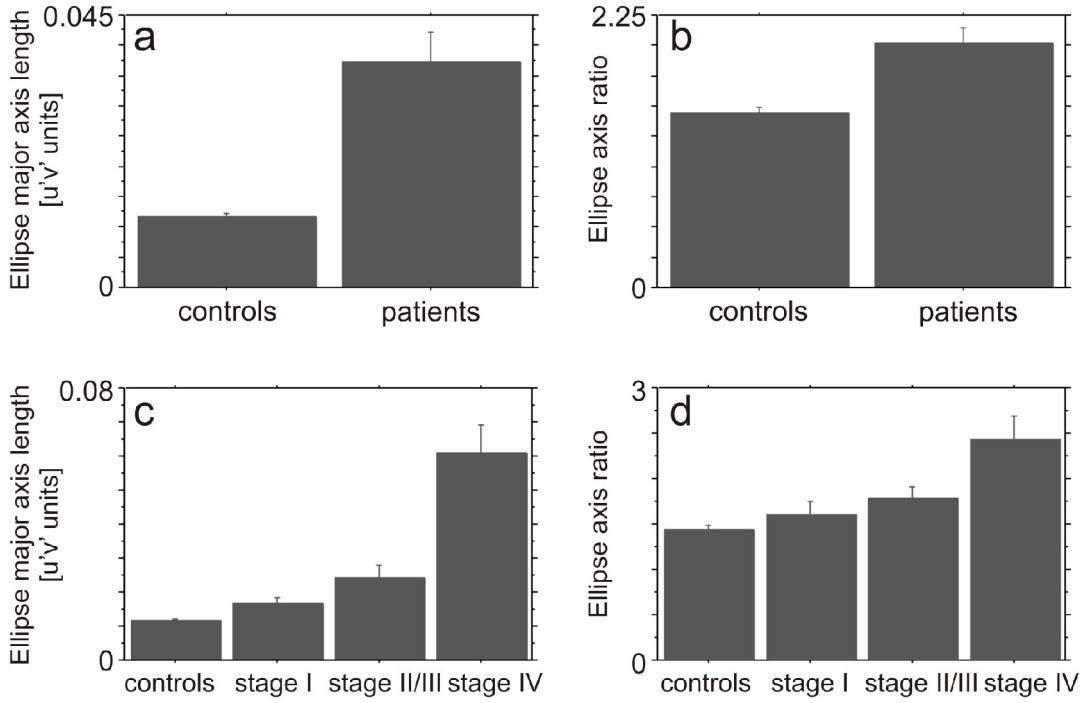

Figure 19 Length and axis ratio of discrimination ellipses increases according to disease stage
(a) Mean chromatic discrimination ellipse length is increased in the patient population compared with the control population ($p < 0.001$). **(b)** This increase is accompanied by a significant enlargement of ellipse axis ratios in the patient population ($p < 0.001$). **(c)** The length and **(d)** the axis ratio of discrimination ellipses increase significantly according to disease stage ($p < 0.001$ for both analyses) The Fisher PLSD was significant between stages I and IV between controls and stages II/III and between stages II/III and IV (see the "Results" section). Axis ratio comparisons were significant between all groups and stage IV. Data are presented in CIE 1976 u′v′ space. Error bars represent SD.

comparisons between stages II/III and IV; $p = 0.03$ for comparisons between controls and stage IV). Taken together, these analyses suggest that the specificity of damage may tilt in multiple directions of color space until stage III and that the horizontal orientation becomes prominent only in stage IV, suggesting that protan and deutan losses are more important only in the late stages of this macular disorder.

Although we favor ellipse measurements to quantify relative patterns of damage across stages, the same analyses for protan, deutan, and tritan measures reveal a clear-cut monotonic deterioration of chromatic function from early to late disease stages ($p < 0.001$, by ANOVA). The post hoc analysis showed that the tritan measure was the only one being significantly elevated between controls and stages II/III ($p = 0.02$), unlike protan and deutan measures, which became significant only for comparisons that included stage IV ($p < 0.001$). In other words, deficits are definitely not type I red-green in the early disease stages.

1.2.2. Deterioration of chromatic function correlates well with clinical parameters

We examined the correlation between our psychophysical measures and clinical criteria. Strong and significant negative correlations were found between chromatic variables and visual acuity (VA protan: $r = -0.654$; VA deutan: $r = -0.736$; VA tritan: $r = -0.708$; $p < 0.001$ for all correlations). Despite the strong correlations, it is likely that some of these measures convey redundant information. Partial correlation analysis was performed to assess the degree of redundancy across measures. In other words, we wanted to measure the independent value of each correlation with VA. It turned out that deutan and protan measures are highly correlated and that they are basically conveying the same information. Therefore, for clinical application, it is sufficient to obtain only one of these measures. Tritan loss, however, revealed a substantial independent correlation ($r = -0.320$), which suggests that it provides important additional information.

Ellipse variables were also strongly and significantly correlated with VA (length: $r = -0.691$; $p < 0.001$, for the total population of controls and patients; and $r = -0.534$; $p = 0.001$ for the patient population). The VA was better correlated with ellipse length than with the axis ratio, which proved to be significant only in the total

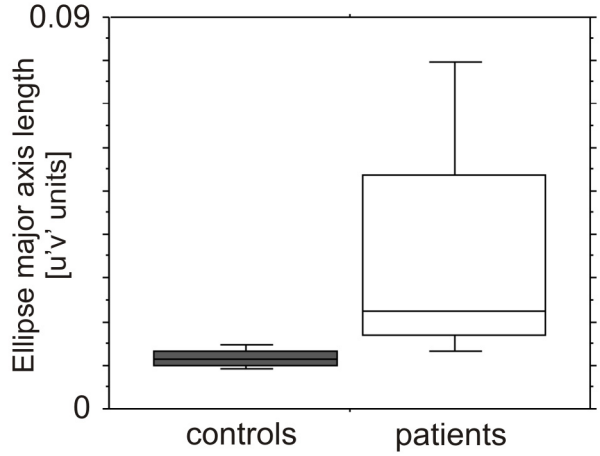

Figure 20 Percentile distributions of ellipse lengths in the control and Best disease populations
Box borders correspond to the 25th and 75th percentiles. Data are presented in CIE 1976 u′v′ space. Error bars represent the 10th and 90th percentiles.

population (r = -0.426; $p < 0.001$). However, despite those correlations, substantial chromatic dysfunction can occur with relatively preserved VA. Indeed, a subset of patients with good VA (0.8-1.0 [20/25-20/20 OU]) showed a manifold increase in confusion line or ellipse lengths.

Next we compared our measures with the size of retinal lesions as measured in units of optic disc. A significant correlation was also found between lesion size and chromatic dysfunction (disc area: protan, $r = 0.761$; $p < 0.001$; deutan, $r = 0.767$; $p < 0.001$; and tritan, $r = 0.545$; $p = 0.04$). Furthermore, ellipse length was also significantly correlated with lesion size ($r = 0.847$; $p < 0.001$) and the presence of foveal involvement ($p = 0.01$, by ANOVA with Fisher post hoc comparison between foveal and non-foveal involvement for ellipse length).

Given the clinical potential revealed by our procedure, we performed an analysis of percentile distributions of quantitative ellipse length scores in the control and patient populations (**Figure 20**). A relatively good separation between the values from both groups seems to be promising regarding the future establishment of procedures that can yield efficient clinical cutoff values.

Taken together, we found that a concomitant involvement of multiple chromatic pathways within the central retina is present in VMD. Moreover, the deterioration of color vision correlates well with disease progression, and also with standard clinical parameters used to evaluate performance in this disease.

2. Experiments on visual motion perception

2.1. Center-surround interactions in visual motion integration and segmentation

2.1.1. Transparent surrounds impose stronger modulation on central percepts than non-transparent surrounds

We found that reported central percepts significantly depended on the types of contextual surrounds used (one-way ANOVA, $p < 0.0001$ for the main effect of surround, for posthoc analyses see below). It is worth pointing out that we explored contextual surround modulations using both luminance defined and textured defined moving plaids (for details on stimulus parameters see **Table 2**), since it was critical that the chosen modulatory surrounds yielded perceptually stable reports across all luminance and contrast sets. Note, that *Textured Pattern* and *Textured Component* stimuli are best suited as efficient surround conditions (being perceived either with 0% or ~90% probability as transparent or non-transparent, respectively). Still, all of the utilized surrounds yielded stable percepts across all pre-defined luminance/contrast sets (**Figure 21a**).

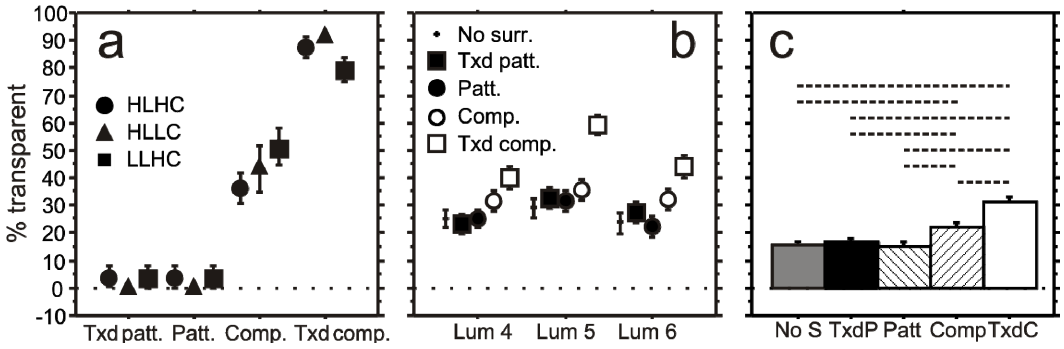

Figure 21 Patterns of center-surrond modulations
(a) Stimuli applied as surround modulation yield perceptually consistent reports across luminance and contrast conditions (for details see **Table 2**) Note, that textured pattern and component stimuli show a very low level of ambiguity (either close to 0% or near 90%). **(b)** Results of center-surround manipulations collapsed across the three distinct overall luminance/contrast sets (main effect of center-surround manipulations shown for stimuli with strongest baseline ambiguity). Component surrounds evoke significant effects as compared to pattern surrounds, while textured component surrounds yield significantly stronger modulation than luminance-defined component surrounds. **(c)** The similar pattern of modulation is observed on data collapsed across different center condition. Significant differences between surround modulation surviving correction for multiple comparisons are marked by dashed horizontal lines. Tx^d: textured; error bars represent 1 SEM

We observed a clear and statistically significant surround modulation of perceptual decisions of luminance defined (non-textured) central plaid patches, regardless of their inherent perceptual ambiguity; however, stronger modulations were observed for more ambiguous centers. **Figure 21b** shows data concerning the modulation effects for only the three most ambiguous center conditions; while **Figure 21c** shows data pooled across all investigated luminance defined central plaid patches. Note, that the inclusion of less ambiguous center conditions (putatively more prone to ceiling/floor effects) does not change the pattern of results.

Post hoc analyses of contextual effects, with data being split across the most ambiguous center conditions, showed that component surrounds yielded the most powerful modulations, with *Textured Component* surrounds having the biggest impact (**Figure 21b**). The following significant effects were observed on paired comparisons between surround conditions: *No Surround* vs. luminance defined *Component*, *Textured Component* vs. *No Surround*, *Textured Component* vs. *Textured Pattern*, *Component* vs. luminance defined *Pattern*, *Textured Component* vs. *Pattern, Textured Component* vs. *Component* (*underlined*: $p < 0.0001$, otherwise $p < 0.05$).

One way ANOVA showed significant modulation even on data collapsed across all center conditions ($p < 0.0001$) with the following significant post hoc effects on paired comparisons: *Component* vs. *No Surround* ($p = 0.0006$); *Textured Component* vs. *No Surround* ($p < 0.0001$); *Component* vs. *Textured Pattern* ($p = 0.0055$); *Textured Component* vs. *Textured Pattern* ($p < 0.0001$); *Component* vs. *Pattern* ($p = 0.0005$); *Textured Component* vs. Pattern ($p < 0.0001$); *Textured Component* vs. *Component* $p < 0.0001$ (significant post hoc differences are shown on **Figure 21c**)

In summary, comparison of context types revealed asymmetric dependence on the type of surround perceptual bias: component surrounds (transparent) being either textured or luminance defined evoked significant modulatory effects, while pattern (non-transparent) surrounds did not yield significant effects when compared to absent surrounds. This effect was present across all center conditions on all of the luminance and contrast sets. It is also important to note, that textured component surrounds yielded a stronger effect than luminance-defined component surrounds.

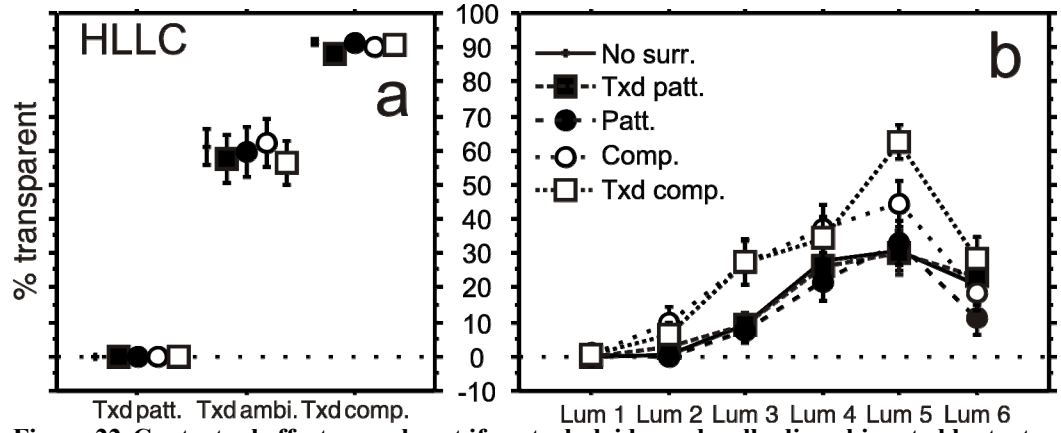

Figure 22 Contextual effects are absent if central plaids are locally disambiguated by texture. **(a)** Textured center stimuli are not susceptible to significant surround modulation being perceptually stable regardless of the type of surround applied, as expected from the disambiguation provided by dots. This is true regardless their inherent global ambiguity level. **(b)** Luminance defined center stimuli are prone to significant shifts in perceived transparency induced by component-surrounds, in contrast with the textured defined center stimuli. Effects are shown for the high luminance low contrast stimulus set (HLLC) but are also consistent for the high luminance high contrast, and the low luminance sets (HLHC, LL, not shown). Tx^d: textured. Error bars represent 1 SEM.

The stronger modulations evoked by textured component surrounds were likely due to the fact that they were inherently more biased for transparent motion because of the disambiguation provided by local dots, also resulting in higher perceptual stability. A complete disambiguation by local texture would predict that these stimuli should not be themselves be prone to be modulated by surround. This is indeed what we observed for central *Textured Component* and *Textured Pattern* stimuli (**Figure 22a**).

The absence of a modulatory effect is probably due to low uncertainty levels: *Textured Pattern* stimuli are virtually always perceived as one surface with (~100% probability) and *Textured Component* stimuli are most of the time perceived as two surfaces (~90% probability). We predicted that the generation of *Textured Ambiguous* stimuli – that have identical probability of being perceived as pattern or component (by having 50% of the dots moving vertically and 50% horizontally) – would render this type of stimulus more susceptible to contextual modulation. Surprisingly, no contextual effects were observed even in presence of global ambiguity. This finding suggests that local disambiguation by texture is sufficient to prevent contextual modulation.

In other words, textured stimuli had a strong contextual modulatory influence on other stimuli, but were in contrast, not susceptible to significant surround

modulation by themselves and were perceptually stable regardless of the type of surround applied (ANOVA, *ns*). This novel and intriguing finding suggests that if local motion becomes fully disambiguated by local texture, this is sufficient to render contextual modulation non-effective.

Indeed, the amount of perceived transparency of textured centers was quite stable over time even for the *Textured Ambiguous* plaids where texture lead to a locally disambiguated (bimodal motion directions) but globally ambiguous (due to the bimodality) interpretation. This global ambiguity was, as stated above, due to the fact that in the case of ambiguous textures, 50-50% of the dots provided bias towards transparency/non-transparency, respectively. **Figure 22a** shows that the overall level of perceived transparency was constant for central textured stimuli, regardless of surround manipulations. In contrast to textured centers, as stated above, luminance manipulated centers showed a significant dependence on surround manipulations (**Figure 22b**, data plotted for the HLHC stimulus set; see **Figure 21c** for statistics).

In summary, the above-described data suggests that transparent surrounds have a more powerful modulatory effect than non-transparent surrounds, with added local texture enhancing the effect. However, given the relatively short viewing time and a slight non-transparency bias for most baseline conditions, there remained a slight possibility for an explanation of the observed surround asymmetry based on floor effects.[251] Still, we found this interpretation unlikely because there were conditions clearly unaffected by floor effects while still showing a prominent modulatory influence (e.g. 40% transparency for the no surround condition of the high luminance high contrast set). In fact, the effect was strongest for the most ambiguous conditions (**Figure 21**). Nevertheless, to fully exclude the possibility of floor effects confounding the asymmetry of pattern/component contextual modulations we have performed a follow-up experiment with more ambiguous stimuli on longer viewing times and (see Experiment 3, below).

2.1.2. Patch size do not explain the observed modulation

By assessing the effect of size on perceived stimulus transparency as a control we have replicated previous findings suggesting that an increase in the size of the moving plaids augments perceptual coherence (pattern percepts) by increasing the

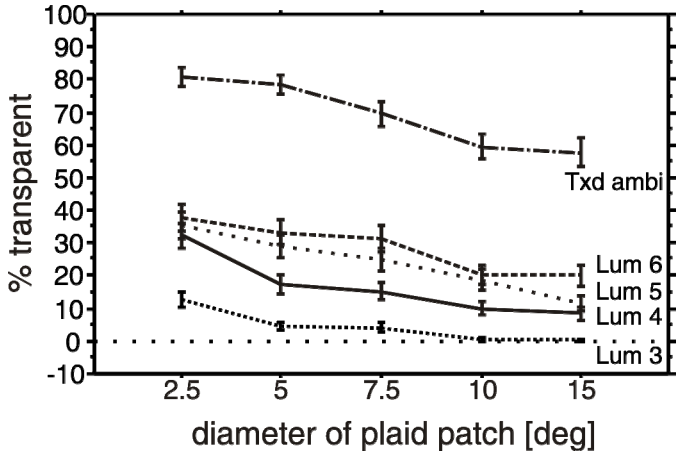

Figure 23 Perceived transparency decreases with increased stimulus size regardless of the plaid parameters.
The slope of the curve relating both parameters is approximately similar across conditions. Data collapsed across the three global luminance/contrast sets, Tx^d: textured, error bars represent 1 SEM.

number or visible intersections or blobs.[252] Slopes of the curves relating perceived % transparency with stimulus size were approximately constant across all investigated conditions implying that size does not interact with any particular condition or baseline perceptual bias of the stimuli (**Figure 23**). Furthermore, since increasing the size consistently decreased the transparency of the presented moving plaids, size effects cannot explain the surround modulations induced by component stimuli.

2.1.3. The pattern of modulation is consistent across viewing times

Our previous findings showing that shifts in the central percept are heavily influenced by the type of the perceptual bias of the modulatory surround are further supported by the results obtained using longer presentation times and center plaids closer to the point of maximal ambiguity (see **Figure 24** for all 15 subjects' data, collapsed across multiple plaid directions).

These results generalize the finding obtained under short viewing conditions and further substantiate the observation that transparent and non-transparent biased surrounds act differently: component surrounds had a highly effective and congruent modulatory effect across all 15 subjects in contrast to pattern (non-transparent) surrounds which, in general, had a more variable effect (ANOVA/GLM with 'Subjects' entered as random factor, $p < 0.001$ for component surrounds; *ns* for pattern surrounds, after correction for multiple comparisons, summary data shown on

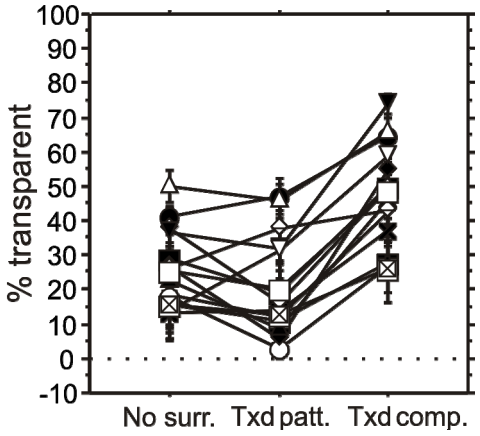

Figure 24 The pattern of center-surround interactions is replicated for longer presentation times.
Individual data from Experiment 3, interaction bar plots depict single subject (n = 15) data collapsed across subjects and all four cardinal plaid directions. Note, that component surrounds increase perceived central congruent percepts for all subjects, unlike pattern surrounds, which may even occasionally have an opposite paradoxical effect (e.g., increasing incongruent percepts.) Tx^{d}: textured; error bars represent 1 SEM.

Figure 25a). Moreover, we found that the described contextual effects are independent of the direction of the coherent plaid motion (data on **Figure 24** are collapsed across all directions). Non-transparent surrounds might nevertheless also have a significant effect at least in some subjects, which led us to study the subtle dynamics of single percept duration and perceptual switch frequency. We therefore also investigated the effect of context on stability of single percepts.

Transparent-biased surrounds induced more switches and coherent-biased surrounds induced fewer switches than what was observed without surround modulation ($p < 0.0001$, Kruskal-Wallis test, **Figure 25b**, posthoc analysis showed more significant effect for pattern surrounds). This finding suggests that non-transparent surrounds may also induce strong contextual effects, but these effects are represented as changes in perceptual switch frequency.

In any case, the average contextual modulation effect was significantly stronger for component surrounds. This was confirmed by analyzing effects induced when stimuli with at least 25% baseline ambiguity were considered in the effect size calculations in order to prevent possible bias caused by floor effects (see effect size plot in **Figure 25c**). *Textured Component* surrounds have a significantly higher modulatory effect on % component motion duration than *Textured Pattern* surrounds ($p = 0.013$, ANOVA, repeated measures).

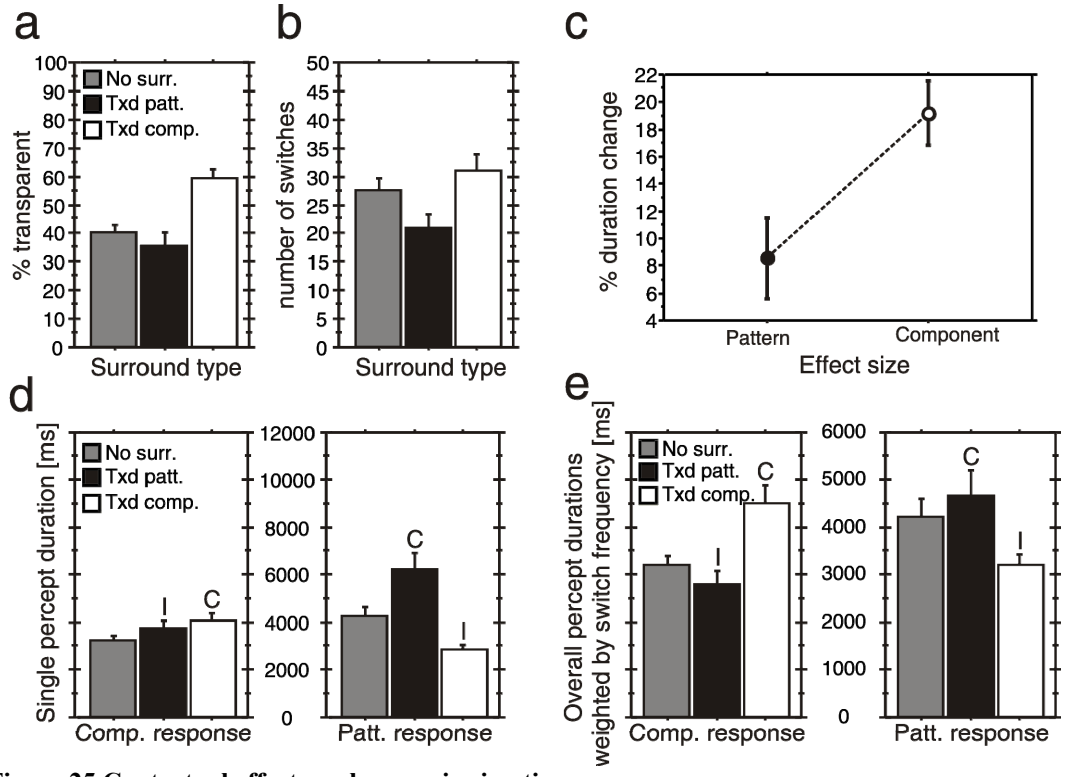

Figure 25 Contextual effects on longer viewing times.
(a) Component surrounds evoke significant overall contextual modulation effects as compared to pattern surrounds in the increased presentation time trials of Experiment 3. **(b)** Both pattern and component surrounds introduce significant modulation in switch frequency. **(c)** The effect size of component surrounds is higher than that of pattern surrounds. **(d)** Pattern and component surrounds cause differential modulation in single percept durations. **(e)** The overall impact of enhancement and suppression effects after weighting with the number of switches (i.e. percept stability). Data from upward moving plaids is shown on all plots. Tx^d: textured; C: congruent; I: Incongruent; error bars represent 1 SEM on all panels.

In order to find the mechanisms of contextual modulation at the single percept level, we have investigated whether the observed surround modulation is caused by the suppression of single incongruent center percepts or the enhancement of single congruent percepts. We found that both suppression and enhancement effects were present for component surrounds (ANOVA; $p < 0.0001$ and $p = 0.0005$ respectively) but only an enhancement effect was observed for pattern surrounds (ANOVA; facilitation effects, $p = 0.004$, suppression, *ns*), showing a clear facilitation of congruent percepts (see **Figure 25d**). In other words, while component surrounds enhance the duration of single congruent percepts and reduce the duration of incongruent percepts, pattern surrounds have a marked facilitatory effect on congruent percepts and no significant or even a slight facilitatory effect on incongruent percepts. The lack of a clear effect for incongruent states may be due to

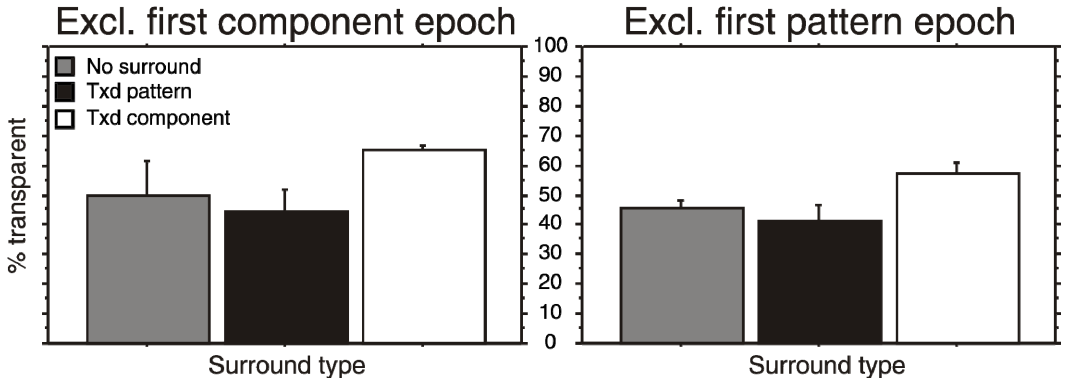

Figure 26 Excluding the first perceptual epoch in all trials does not change the pattern of surround effects.
Tx^d: textured, error bars represent 1 SEM

an overall stabilization of perceptual states (decreased switch frequency, thus increased percept stability) caused by the non-transparent surrounds.

It is indeed worth pointing out that the total percept stability, as indexed by the total number of switches between perceptual states in a given surround condition, and the durations of single percepts have to be treated independently in the estimation of overall perceptual effect. This is best achieved by weighting the single percept durations with the total number of perceptual switches (**Figure 25e**). The effect of component surrounds of increasing congruent transparency percepts in the center becomes even more evident with this weighting procedure. A phenomenologically distinct process is observed for pattern surrounds: facilitation of congruent effects is present, but the suppressive effects of incongruent pattern surrounds are still at an insignificant level after this transformation. The type of context thereby influences dominance and suppression durations in a distinct manner.

Taken together, average modulation effects were significantly stronger for component surrounds and invariably consistent across subjects.

To exclude that the initial perceptual bias influenced the observed pattern of results, we have performed and additional control analysis by excluding the first perceptual epochs from the data. The asymmetric modulatory effect of different surround types was still preserved after this manipulation (ANOVA, $p = 0.0042$ for component surrounds, *ns* for pattern surrounds, **Figure 26**). This result confirms that the initial perceptual bias is not relevant in the explanation of overall results.

2.1.4. The interactions between local and global context modulate observed transparency

Our 9 subjects were asked to report perceived coherence of a 5-degree central plaid patch moving upwards, which was surrounded by a perceptually identical 20-degree plaid patch that could move in any of the four cardinal directions (**Figure 5d**). As expected from the perceptual identity of center and surround regions the perceived transparency was, in general, similar when surround motion was in similar or in opposite direction to the center movement (**Figure 27a**).

This rule was, however, broken when surround patches moved either rightwards

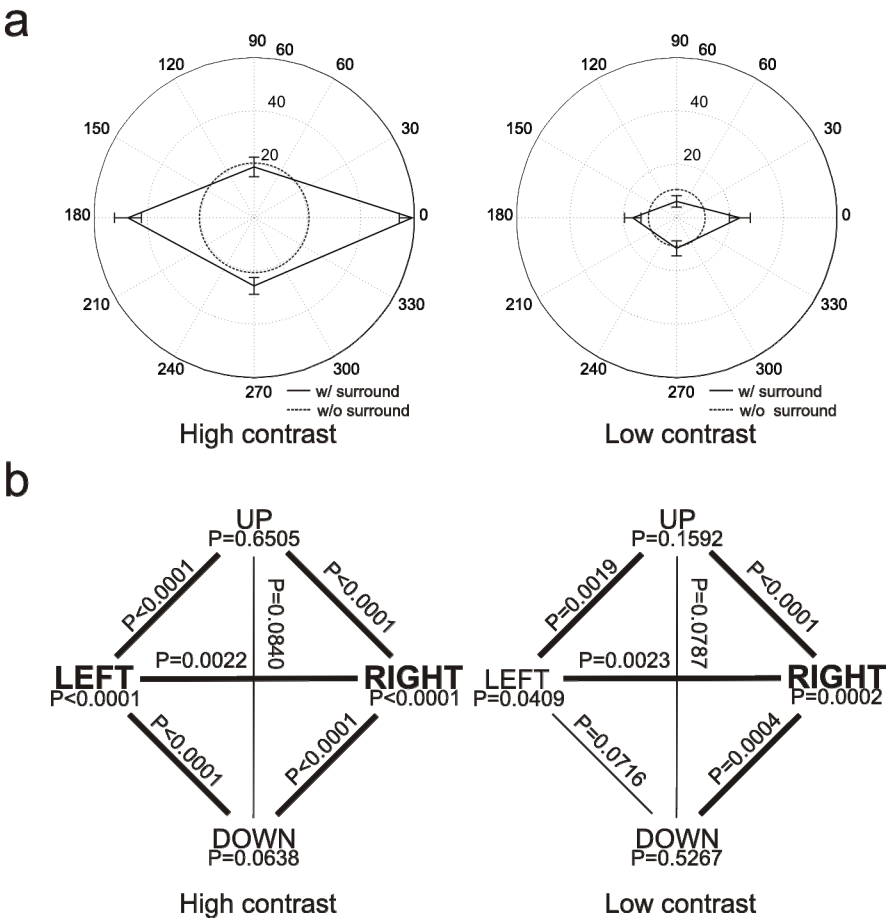

Figure 27 Effects of coherent surrounds
(a) Direction dependence of coherent surround effects. Axis length in polar plots depicts percentage of incoherent motion percepts; dashed circle represents no-surround baseline, and solid lines link the four different surround conditions. Note that left (180º) and right (0º) moving coherent surrounds paradoxically enhance center % incoherent motion perception. Error bars are SEM. B. **(b)** Post-hoc comparisons. Bold line connections represent $p < 0.005$ significance level on comparison between different surrounds, bold typeface represents the same significance level on comparisons between a given surround and a no-surround baseline Wilcoxon's signed rank significance level, with Bonferroni correction for 10 comparisons.

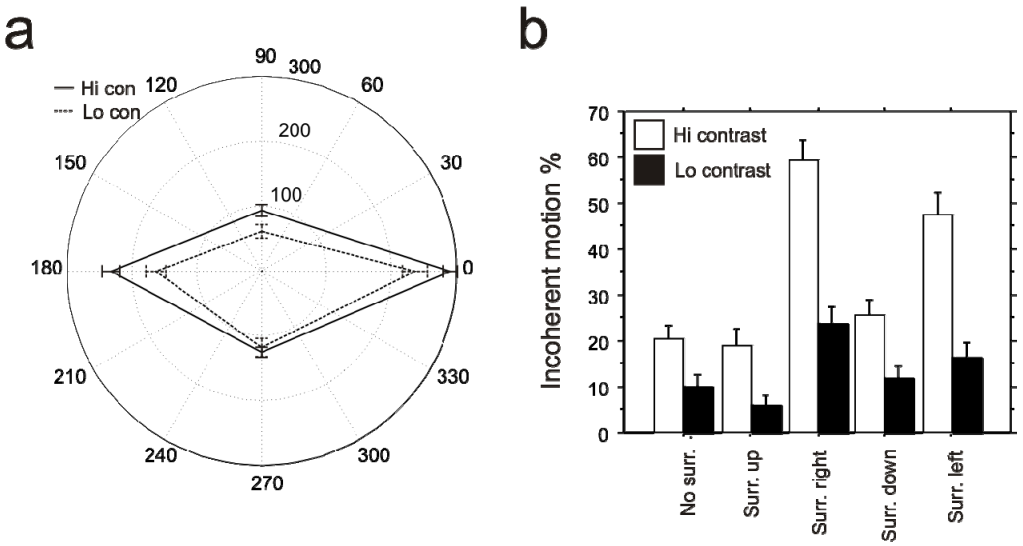

Figure 28 The effect of contextual incongruence is contrast independent
(a) Effects are independent of the baseline pattern vs. component bias. **(b)** Contextual incongruence has the same psychophysical profile under high contrast and low contrast conditions. White bars: high contrast, black bars: low contrast. Data are normalized for the respective baseline no-surround percentage of component percepts. Dashed line: low contrast conditions, solid line: high contrast conditions. Error bars in both plots are SEM.

or leftwards so that only one (not less and not more) set of the local moving grating contours of coherent surrounds was constantly collinear with one of the center component gratings (see arrows in top inset of **Figure 5d**, depicting local motion vectors in center and surround). Then, we observed an enhancement of transparent motion percepts in the central plaid patch, caused by the coherent pattern surrounds (*Surround left* and *right* conditions, as depicted in the directional polar plots of **Figure 27a**). The resulting percept was phenomenally striking due to the contrasting (incongruent) perceptual interpretations of center and surround regions.

This incongruence was highly significant and occurred under both high and low contrast conditions (Friedman test, $p < 0.0001$ and $p = 0.0011$, respectively; see **Figure 27b** for posthoc comparisons between conditions and baseline as well as across conditions). Interestingly, there was a statistically significant asymmetry concerning leftward and rightward surround motion. In fact, we have observed a threefold increase in the percentage of perceived transparent motion over the *No Surround* baseline for rightward motion under high contrast conditions as compared to a 2.3 fold increase for leftward motion. A similar asymmetry ratio was found under low contrast conditions (**see Figure 27a and b**).

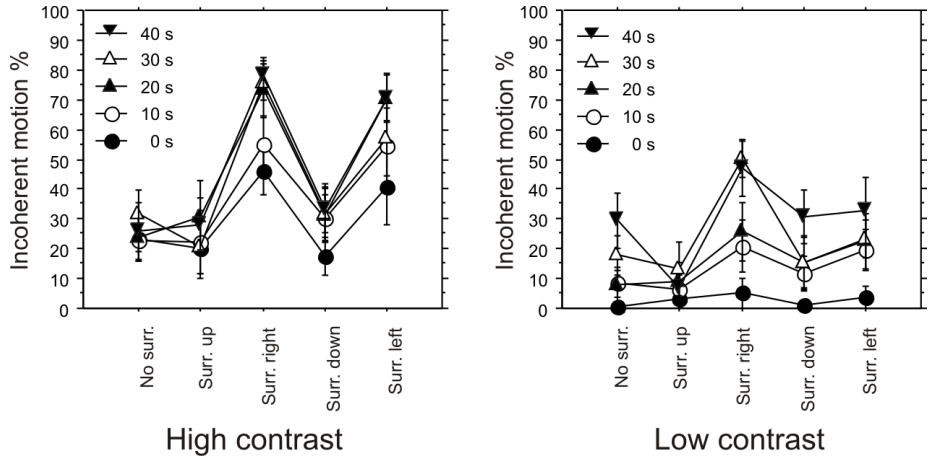

Figure 29 Incongruency effects are observed with different pre-adaptation periods, being enhanced with increased exposure time.
Data are split according to cumulative time of previous exposure to moving stimuli. Psychophysical curves are essentially unchanged, except for a general increase in offset. Error bars are SEM

The observed psychophysical effects were invariant under high and low contrast conditions (**Figure 28a**), irrespective of their distinct baseline transparency bias (19.02 vs. 9.99 %). After normalization for the respective baseline percentage of *No Surround* component percepts, the data can be described by distributions of nearly identical shape (**Figure 28b**).

The randomized stimulus presentation, and the intermediate static and fixation periods allowing for full decay of possible motion aftereffects minimized possible temporal order effects. Nevertheless, we tested the possibility of a storage bias induced by adaptation by re-plotting our data split by distinct cumulative time of previous stimulus exposure (from 0 to 40 seconds). We have found that cumulative exposure to moving stimuli enhanced the effect quantitatively, as represented by the predominant change in perceptual offset-bias (**Figure 29**), but did not change it qualitatively, as represented by the similar shape of the psychophysical curves.

Next, we compared surround modulation induced by symmetric surround plaids with that induced by a set of asymmetric surround plaids to exclude that the perceived relative contrast of the surround plaid components would be the determining factor of perceived central plaid transparency. We found no significant difference between the effect of symmetric and asymmetric surrounds.

In summary, coherent surrounds may even lead to segmentation, depending on the balance of local and global motion integration, and also on the presence of collinearity.

2.2. Neural correlates of real and illusory motion perception

2.2.1. MAE-related motion signal is present when attention is focused on motion independent features

In this experiment we have investigated neural responses to real motion and illusory motion after-effects, when attention is controlled for by motion-independent color and angle tasks. The hypothesis was that if a MAE-related net motion signal exists and is masked by interference with concurrent motion task (as possibly in Huk et al.[75]), this masking should not occur with motion independent tasks.

We have found strong hMT$^+$ responses to stationary plaids in comparison to baseline fixation stimuli (**Figure 30a**) in our group data. Analysis of variance of BOLD responses in these regions of interest showed highly significant differences across motion, stationary, and fixation conditions ($p < 0.001$, for all comparisons, with Bonferroni post hoc corrections).

BOLD responses to stationary plaids vs. fixation baseline showed a high degree of localization to hMT$^+$ (multi-subject cluster centers of gravity at $p_{corr} << 0.001$: X -48 Y -64 Z -1 and X +47 Y -66 Z +1). To assess whether hMT$^+$ was specifically

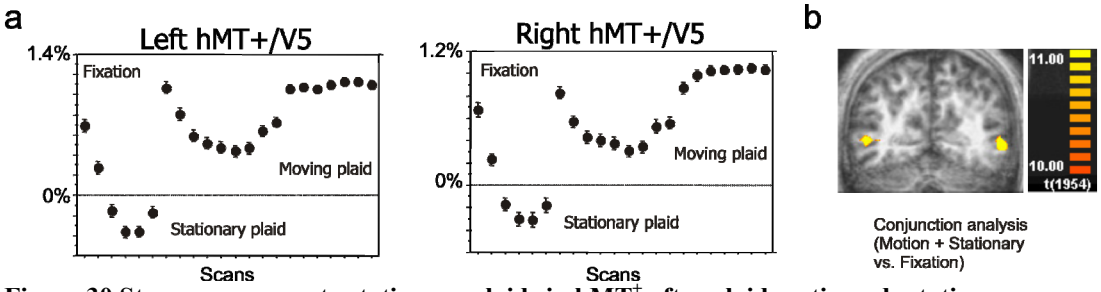

Figure 30 Strong responses to stationary plaids in hMT$^+$ after plaid motion adaptation
(a) activation data in left and right hMT$^+$. ROIs were defined by plaid motion contrast, which shows substantial overlap with flow-field mapping (see also Castelo-Branco et al.[41]) The temporal dynamics (per scan) of cortical responses to moving plaids, stationary plaids after adaptation to moving plaids and fixation baseline stimuli is shown (n = 4 for this experiment). Responses to stationary plaids are higher than responses evoked by fixation stimuli already within the first 2 scans suggesting a response to MAE (ANOVA, Fisher PLSD, $p < 0.0001$, for hMT$^+$, bilaterally), and both types of response decay significantly afterwards (ANOVA, $p < 0.0001$, for hMT$^+$, bilaterally). Note that order of conditions is variable and balanced (for details, see Methods). Error bars in this and subsequent figures depict 1 SEM. **(b)** GLM conjunction analysis (criterion being that all contrasts have to be significant for a voxel to be considered positive; for details see text) of BOLD responses to moving and stationary plaids upon motion adaptation shows a quite specific degree of localization to hMT$^+$ (multi-subject, multi-study GLM analysis, n = 4 subjects). Regions are shown at the same statistical threshold level ($p_{corr} < 0.001$, see color plot).

activated by stationary plaids after motion adaptation we computed a conjunction analysis (which means that only voxels that are significant for all contrasts will survive the statistical thresholding) including the contrast of post-adaptation stationary conditions vs. the fixation baseline and the contrasts of moving conditions vs. fixation baseline. The strict co-localization of all signals (including the MAE-related ones) to the same hMT^+ clusters suggests that the increased activity measured in area hMT^+ on stimulation with stationary plaids after adaptation to moving plaids is due to a specific net neural motion-related signal (**Figure 30b**).

Aside from the expected decay in activity both for post-adapting fixation and stationary stimuli (ANOVA, $p < 0.0001$, for hMT^+, bilaterally), there are subtle differences in the temporal pattern of decay (**Figure 30a**). Responses to stationary plaids were already higher early on if compared to activation induced by fixation stimuli, which do not induce MAE (ANOVA, Fisher PLSD, $p < 0.0001$, for hMT^+, bilaterally, already within the first 2 volumes, after correction for the hemodynamic delay), showing that high levels of MAE-related activity in the initial period were not signaling a simple decay from the previous period of moving stimulus presentation, but rather a genuine initial increase of activity. BOLD responses to real surface motion compared to fixation stimuli were also significantly higher already from the beginning of the period and increased thereafter significantly to a stable plateau.

The used attention tasks emphasized either the function of the ventral stream (color task) or the function of the dorsal stream (spatial angle task), but the measured activity upon motion adaptation was above baseline in hMT^+ irrespective of the task and regardless of the adaptation condition used (ANOVA, Fisher posthoc, $p << 0.01$ for all conditions), and there was no significant difference between the activation patterns observed with the two attentional tasks. It is also worth pointing out that these attentional tasks were present throughout both stationary and motion conditions, so no significant signal changes are expected to occur due to attentional fluctuations across conditions.

In summary, activity levels in these motion sensitive areas are increased upon plaid motion adaptation, even if disparate motion independent tasks keeping attention stably away from stationary plaid features (color task) or from moving plaid features

(spatial comparison task) are used to control for attention. The effect therefore appears to be general across motion independent tasks. Still, it remained an open question whether this would be the case in the presence of selective attention to concurrent orthogonal illusory/real motion features. Experiments 2a&b addressed this issue.

2.2.2. MAE-related motion signal is absent when attention is focused on concurrent independent motion features

In these experiments we have investigated neural responses to real motion and illusory MAEs when attention is controlled for by speed-tracking of apparent motion or real motion stimuli. The hypothesis was that if a MAE-related net motion signal exists and is masked by interference with concurrent motion task (as possibly in Huk et al.[75]), this masking should occur with motion-related tasks, regardless of whether motion is apparent or real. **Figure 9** illustrates the conditions tested in Experiments 2a&b.

Characterization of responses to superimposed AM

Before looking at the MAE-related neural singal we have characterized neural responses during the adaptation period, with and without superimposition of apparent or real concurrent motion (AM and RM). **Figure 31** shows the general BOLD-effect of superimposing AM on adapting or non-adapting plaid movement, and subsequent static plaids (yielding MAE for adapting conditions). As expected, global hMT^+ activity persisted at high levels when AM stimuli were superimposed to the static plaid period *after* the presentation of mixed (non-adapting) plaids (panel A, $p = 0.0024$ during the initial 8 second period, and $p < 0.0001$ thereafter), signifying a pure AM signal, since there can be no, and indeed were no, MAEs perceived after the presentation of mixed plaids. Moreover, a small but significant increase in activity was observed during the motion period compared to a pure plaid-motion activation when AM was overlayed on the moving plaid period (panel B, $p = 0.0294$, bottom white box highlights statistically significant blockwise difference). This shows that area hMT^+ was not reaching saturation with adapting plaid motion.

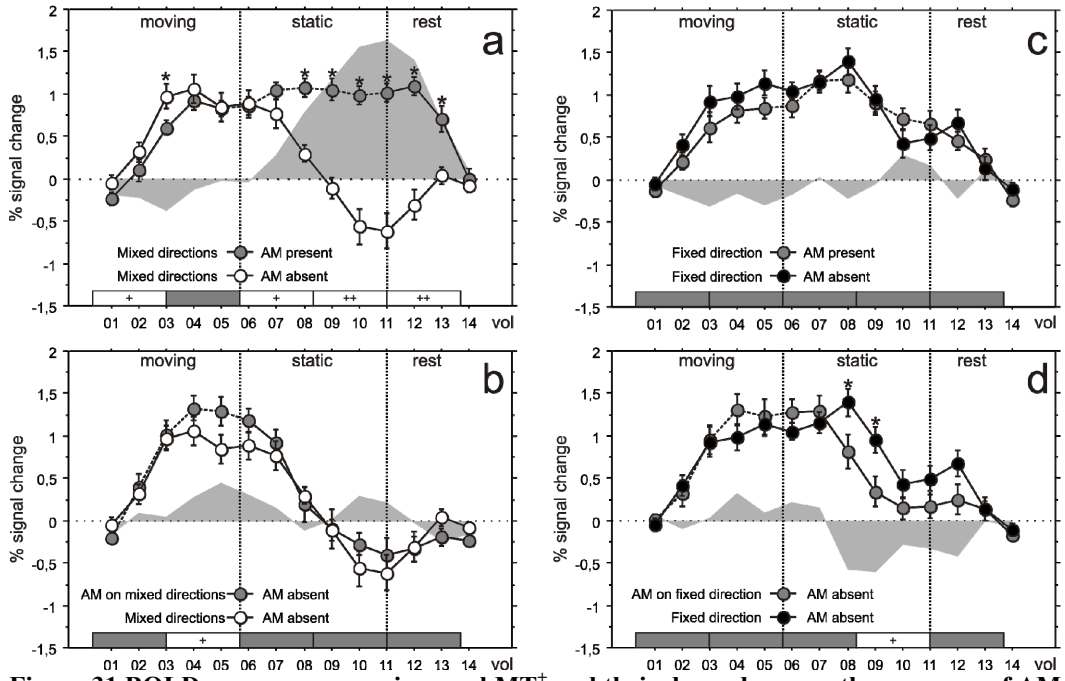

Figure 31 BOLD response curves in area hMT$^+$ and their dependence on the presence of AM. Data from individual ROIs averaged across subjects and hemispheres. **(a)** Mixed (non-adapting) motion vs. mixed motion with AM overlaid on static plaid. **(b)** Mixed motion vs. mixed motion with AM overlaid during plaid motion. **(c)** Fixed (adapting) motion vs. fixed motion with AM overlaid on static plaid. **(d)** Fixed motion vs. fixed motion with AM overlaid during plaid motion. Asterisks near the data points depict significance for volume-wise comparisons. Time points depict TRs (vol). Bars on the bottom of the graphs represent statistical comparisons for data pooled over 8-second blocks, dark bars: non-significant difference, white bars: significant difference (+: $p < 0.05$; ++: $p < 0.001$, ANOVA with Fisher's post hoc). Error bars on all plots represent 1 SEM.

The investigation of interaction between AM and MAE revealed a sort of cross-masking: superimposing AM stimuli after adaptation to fixed direction motion eliciting MAEs did not lead to any additive increase in activity (panel C, *ns*). This phenomenon was not due to putative saturation, because superimposing AM during the presentation of moving fixed plaids lead to a increase in activity during the movement period similar to the one observed with superimposed AM on mixed plaids. Furthermore, a subtle but interesting observation was that this prior superimposition of AM lead to a significant subsequent decay of hMT$^+$ activation during the static period in comparison to the presentation of fixed plaids alone (panel D, $p = 0.0018$). Since fixed plaid motion was always orthogonal to AM, this may have effectively acted as a mixed-like non-adapting situation ensuing quicker decline of hMT$^+$ activity and weaker MAEs.

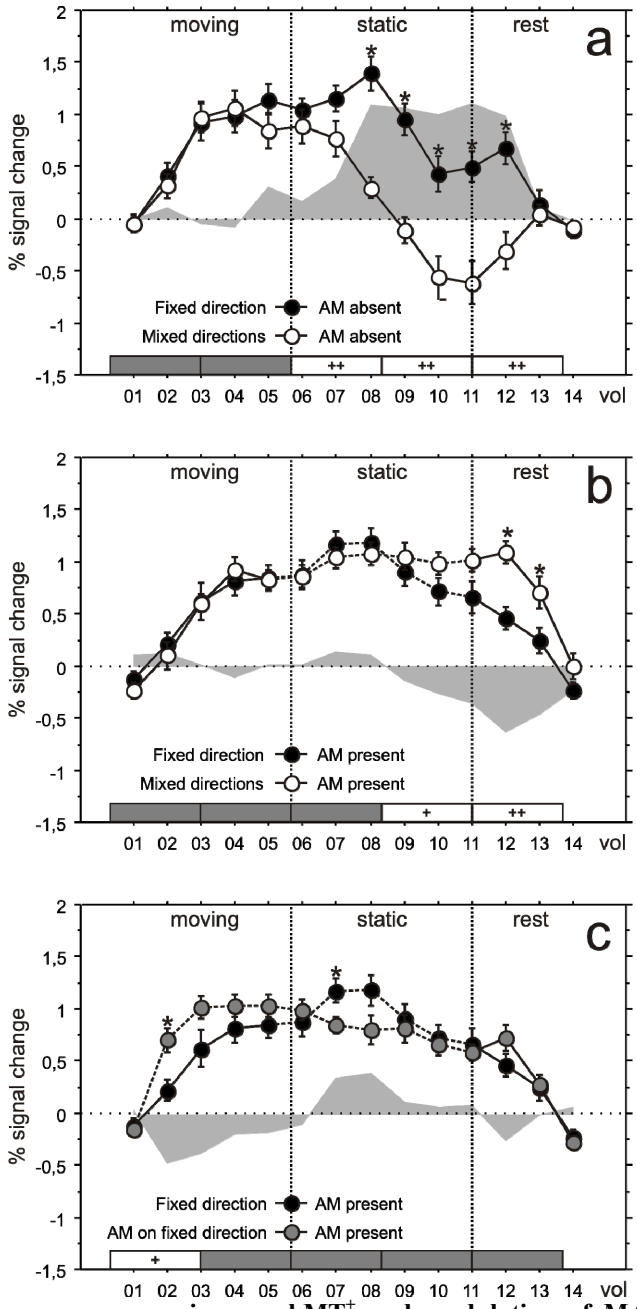

Figure 32 BOLD response curves in area hMT$^+$ and modulation of MAEs by presence or absence of AM

Data from individual ROIs averaged across subjects (n=4) and hemispheres (n = 8). **(a)** Fixed vs. mixed motion. **(b)** Fixed vs. mixed motion with AM overlaid during static plaid. **(c)** Fixed motion with AM overlaid on static plaid vs. fixed motion with AM overlaid on both plaid motion and static period. Asterisks near the data points depict significance for volume-wise comparisons. Time points depict TRs (vol). Bars on the bottom of the graphs represent statistical comparisons for data pooled over 8-second blocks, dark bars: non-significant difference, white bars: significant difference (+: $p < 0.05$; ++: $p < 0.001$, ANOVA with Fisher's post hoc). Error bars on all plots represent 1 SEM

Effects of selective attention to apparent motion on MAE-related motion signals

We have further focused on the observation that AM differentially modulates hMT^+ responses during (additive effect) and after (masking effect) plaid motion presentation.

If AM is absent during the static period (**Figure 32**), a significant difference in BOLD-response can be observed during the static and rest periods, corresponding to stronger responses (and presence of MAEs) after exposure to fixed-direction moving surfaces in comparison to mixed ones (panel A $p < 0.0001$ in first two blocks and $p = 0.0009$ in the last one). However, this difference disappears if AM has been overlaid during the static periods (panel B, see initial decrease of gray shaded area as compared to the panel A), showing the above-mentioned masking effect.

Interestingly, adding AM both during fixed motion and the ensuing static period did not change responses during the latter (panel C). Although there is a steeper initial increase in activity to significantly higher levels ($p = 0.025$) if AM was superimposed on fixed direction plaid motion (again proving that plaid motion does not saturate hMT^+ responses per se), the subsequent activation levels elicited by static displays overlaid with AM does not differ significantly. Nonetheless, there is a subtle but clear selective decrease of activation shortly after plaid motion was stopped in the condition where AM has already been present during plaid movement.

Comparison of the modulation effects caused by AM and RM tasks during the MAE test period

In this experiment, performed in 8 additional subjects at 3T, we have replicated the AM experiment and have concomitantly included a new condition, consisting overlaid real motion using similar stimuli as in the AM condition, on top of the MAE period, (for details see Methods). We have observed, as expected, a significant difference ($p < 0.05$) during the static test period after adaptation to fixed- vs. mixed-direction moving plaids (**Figure 33a**). However, this effect is abolished when subjects have to selectively attend either overlaid AM or RM during the test period (panels B and C, respectively).

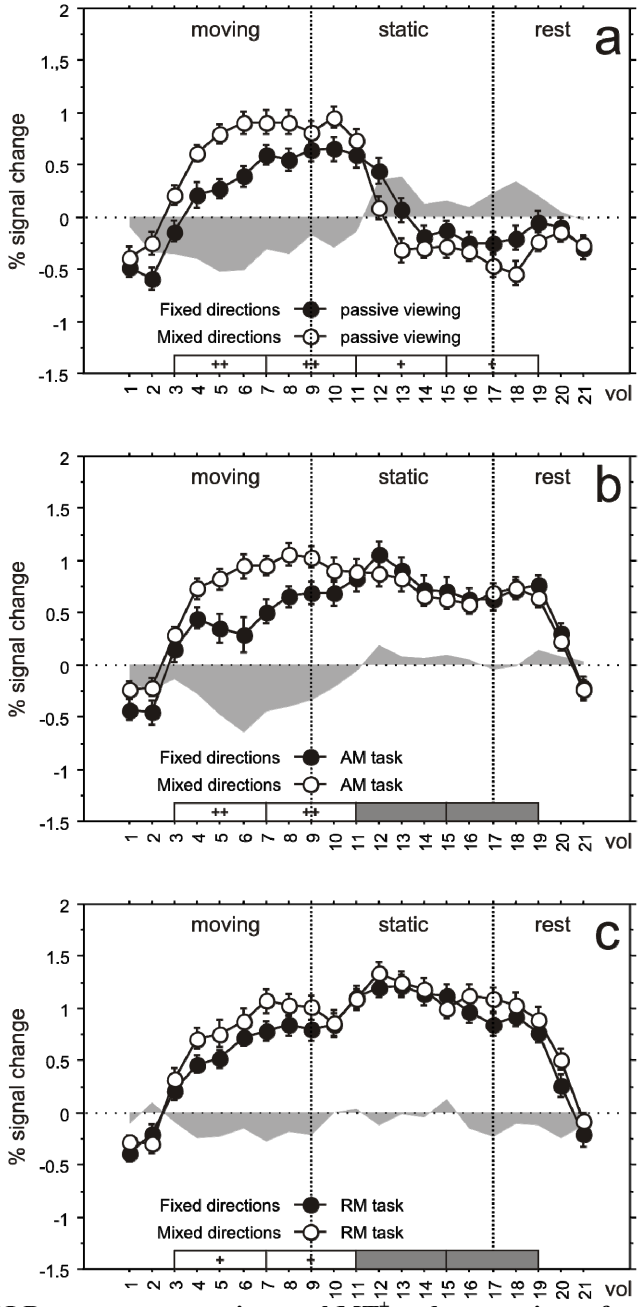

Figure 33 BOLD response curves in area hMT$^+$ and comparison of modulation of MAEs by the presence of selective attention to real (RM) or apparent motion (AM), as required by a speed judgment task

(a) Fixed vs. mixed direction adaptation, no attentional task during static plaids. **(b)** Fixed vs. mixed direction adaptation, AM task during static plaids. **(c)** Fixed vs. mixed direction adaptation, no attentional task during static plaids. Time points depict TRs (vol). Bars on the bottom of the graphs represent statistical comparisons for data pooled over 8-second blocks, dark bars: non-significant difference, white bars: significant difference (+: $p < 0.05$; ++: $p < 0.001$, ANOVA with Fisher's post hoc). Error bars on all plots represent 1 SEM.

2.3. Learning-induced changes in motion processing

During training, observers were presented with two fields of spatially superimposed moving dots (**Figure 10**); they had to discriminate the speed of dots moving in one direction while simultaneously ignoring dots that moved in an orthogonal direction (i.e. a task-irrelevant distractor). As shown in **Figure 34**, speed discrimination thresholds gradually improved as a result of training. Comparison of the performance during the first six blocks of training (speed discrimination threshold: 0.58 deg·s^{-1}) with the performance during the last six blocks of training (speed discrimination threshold: 0.49 deg·s^{-1}) revealed a significant learning effect ($p < 0.002$). These data demonstrate that the training sessions were sufficient to improve the efficiency of processing basic visual attributes such as stimulus speed.

2.3.1. Training decreased sensitivity to motion in task-irrelevant (distractor) direction

We next investigated how training on a speed discrimination task affects perceptual sensitivity to different motion directions by measuring motion detection thresholds for three different directions before and after training (i.e. the motion coherence required for threshold performance). The three tested directions included

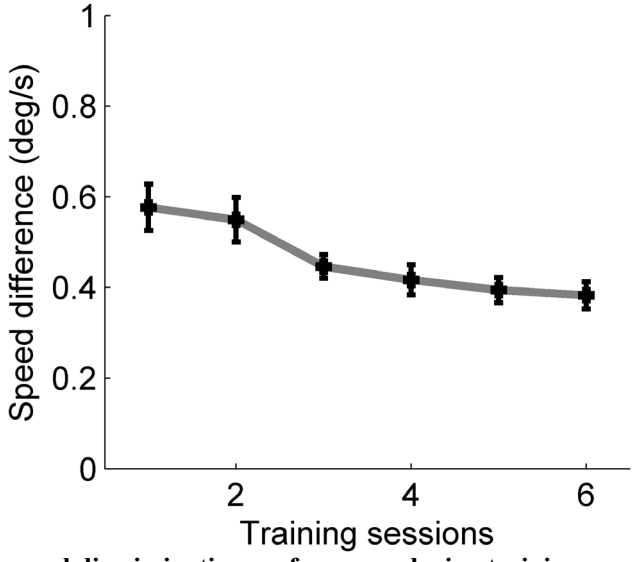

Figure 34 Motion speed discrimination performance during training.
Speed discrimination thresholds gradually improved as a result of training. Error bars indicate the SEM

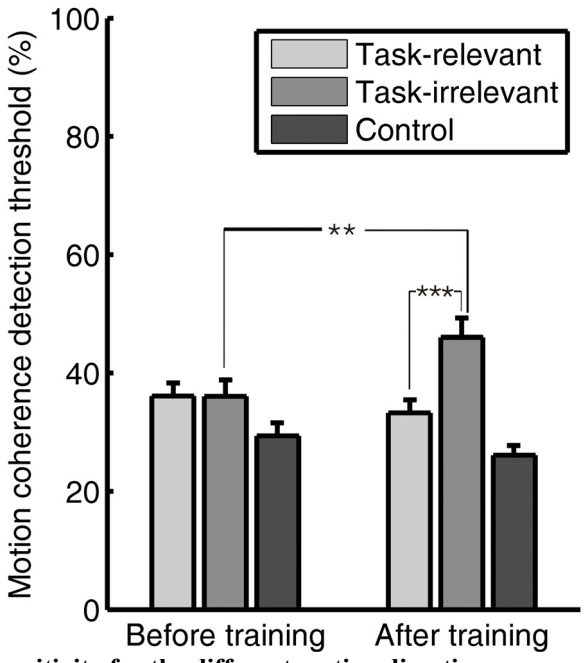

Figure 35 Perceptual sensitivity for the different motion directions.
Before training, there was no difference between the motion coherence detection thresholds for the directions that were task-relevant and task-irrelevant during training as well as for a control direction. After training, sensitivity for the direction that was task-irrelevant during training was strongly reduced. Error bars indicate the SEM

the two directions that were present during training (+45° and -45°) as well as a control direction that was equidistant from them (180°, downward). The results revealed that training had a strong effect on the observers' performance (**Figure 35**).

A repeated measures analysis of variance (ANOVA) showed no significant main effect of test session (before and after training, $p = 0.3$); however, there was a significant main effect of task relevance (task-relevant and task-irrelevant, $p < 0.001$) and a significant interaction between these variables ($p < 0.001$). Before training (**Figure 35**, left side), there was no difference in motion detection thresholds for the two directions that were present during training ($p = 0.966$); however, both of these directions had higher thresholds than the control direction. The increased sensitivity for the control direction might be explained by the fact that it was a cardinal direction (downward), for which transparent motion detection has been shown to be better than for non-cardinal motion directions.[253] However, the motion coherence threshold for the task-relevant direction was significantly lower than the threshold for the task-irrelevant direction (**Figure 35**, right side) after training ($p < 0.0001$).

Furthermore, a comparison of the motion coherence thresholds before and after training reveals that thresholds for the task-relevant direction decreased non-significantly ($p = 0.396$) whereas thresholds for the irrelevant direction significantly increased ($p < 0.001$). The threshold for the control direction also underwent a non-significant decrease ($p = 0.289$), further supporting the observation that training decreased sensitivity to motion in a direction that was continuously present as a task-irrelevant distractor during training.

Importantly, in our motion coherence detection experiment the three motion directions were presented randomly within a block and observers were required to indicate which of the two temporal intervals contained coherent motion. Thus, our design ensured that a possible learning-induced bias to choose the task-relevant rather than the task-irrelevant direction in case of uncertainty can be excluded as an explanation of the results of our motion coherence detection experiment.

For all experimental conditions subjects were instructed to maintain eye-gaze on the small fixation point at the center of the display. However, to verify that subjects were able to maintain fixation and that there was no differential pattern of fixations for different motion directions, we tracked the eye position of subjects while they were performing the motion coherence detection task. We did so for five randomly chosen subjects in the sessions before and after the training period. Trials were binned based on motion direction and we calculated the mean eye position (x and y values) for the period when the motion stimulus was present on each trial.

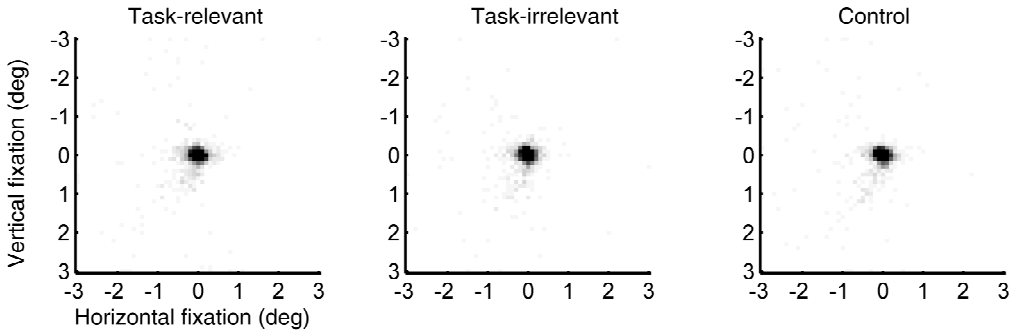

Figure 36 There was no difference between the fixation patterns for different motion directions. Representative fixation patterns of one of the subjects during the motion coherence detection threshold measurements after training in the case of the three different motion directions

We found no significant differences in the mean eye position for the three different motion directions (main effect of direction: before training $p = 0.221$; after training $p = 0.621$) indicating that there was no systematic bias in eye position induced by the direction of the motion stimulus (see **Figure 36**). Furthermore, additional analysis using ANOVA showed that there were no significant differences between the three motion directions in the saccadic frequency (main effect of direction before training $p = 0.255$ and after training $p = 0.259$) and in the cumulative saccadic amplitude (main effect of direction before training $p = 0.748$ and after training $p = 0.535$).

2.3.2. Training decreased fMRI responses to motion in task-irrelevant direction in extrastriate visual areas

Before and after training fMRI responses within visual cortex were measured to motion directions that were task-relevant and task-irrelevant during training. The two different directions were presented in separate blocks (i.e. no distractors were presented). Observers performed a two interval speed discrimination task during fMRI scanning. Speed discrimination performance before training was slightly better for the task-relevant direction compared to the task-irrelevant direction; this difference was magnified after training (**Figure 37**). However, ANOVA revealed no significant main effect of test session (before and after training, $p = 0.67$) and even though there was a significant main effect of task relevance (task-relevant and task-

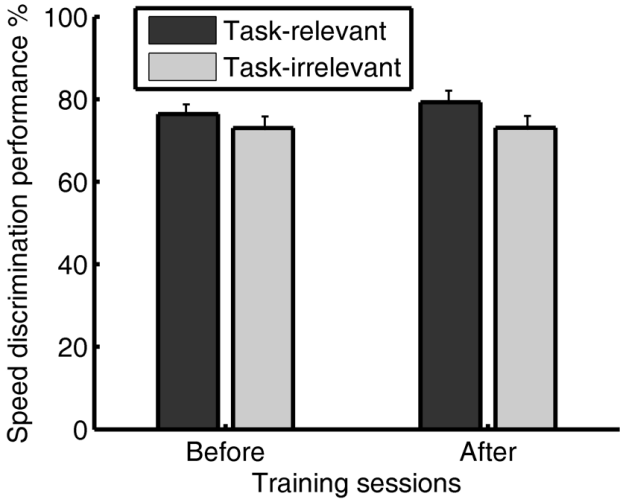

Figure 37 Motion speed discrimination performance during the fMRI scanning sessions. Error bars indicate the SEM.

irrelevant, $p < 0.003$) the interaction between these variables was not significant ($p = 0.265$). These data show that training did not significantly increase the difference in speed discrimination performance between the task-relevant and task-irrelevant directions during scanning. The apparent discrepancy between these results and the significant improvement of speed discrimination performance measured during training might be explained by the fact that during training the speed of the task-relevant motion direction had to be discriminated in the presence of a task-irrelevant distractor direction whereas during scanning only one motion direction was present during each trial.

In a separate scanning session carried out before training, we defined regions of interest (ROIs) in early retinotopic visual cortex as well as the human MT complex (hMT^+) using standard independent functional localizer tasks.[246-249, 254] We then performed a ROI-based analysis of the fMRI data obtained in the main experiment. The fMRI results reveal that before training, the magnitude of the fMRI responses evoked by the two motion directions were similar (**Figure 38**). However, after training, fMRI responses evoked by the task-irrelevant direction were smaller than responses evoked by the task-relevant direction. A repeated measures ANOVA revealed no significant main effect of test session (before and after training) ($p = 0.817$), no significant main effect of task relevance (task-relevant and irrelevant) ($p = 0.215$) but a significant interaction between these variables ($p = 0.016$). After training, a strong reduction of fMRI responses evoked by the task-irrelevant direction compared to responses evoked by the task-relevant direction (**Figure 38**) was observed in ROIs V2, V3, V3A, hMT^+ (for all ROIs $p < 0.023$; the significance threshold corrected for multiple comparison: $p = 0.033$ corresponding to FDR = 0.05) whereas in ROIs V1 and V4v the difference between the fMRI responses to task-relevant and task-irrelevant directions did not reach the significance level (V1 $p = 0.051$; V4v $p = 0.11$).

Although training did not significantly increase the difference in speed discrimination performance between the task-relevant and task-irrelevant directions during scanning it is possible that the difference between the fMRI responses to task-relevant and task-irrelevant directions might be the result of the small difference in speed discrimination performance. To exclude this possibility, an additional analysis

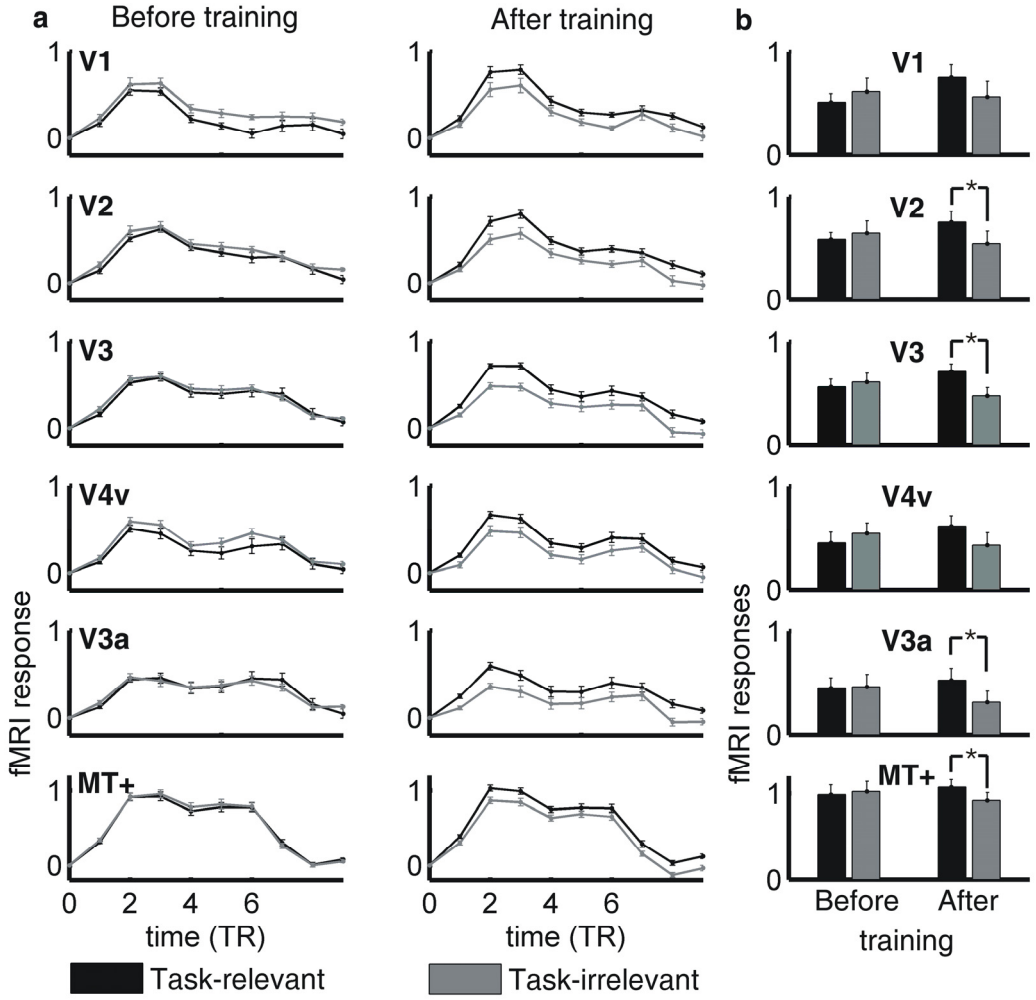

Figure 38 Effect of learning on the fMRI responses.
fMRI responses to the task-relevant and task-irrelevant directions before and after training. **(a)** Time courses and **(b)** response amplitudes of the fMRI responses in different visual cortical areas. Values on the ordinates represent: (a) percent BOLD signal change; and (b) calculated model fitting weights (in arbitrary units, see the Methods section). Error bars indicate the SEM

was performed to formally test the relationship between speed discrimination performance and fMRI responses. We divided the fMRI data from each subject into two median split subgroups based on speed discrimination performance. One subgroup contained the fMRI data from runs with the best speed discrimination performance and the other subgroup contained fMRI data from the runs where performance in the speed discrimination task was poor.

ANOVA revealed a significant difference in the speed discrimination performance between the these subgroups (good and poor, $p < 0.001$); no significant main effect of test session (before and after training, $p = 0.778$) and no significant

interaction between these variables ($p = 0.381$). Importantly, however, we found no significant differences in the fMRI responses between these two subgroups: no main effect of test session (before and after training, $p = 0.528$); no significant main effect of performance (good and poor, $p = 0.82$) and no significant interaction between these variables ($p = 0.522$). These results provide further support that the difference between the fMRI responses to task-relevant and task-irrelevant directions found after training are primarily due to a difference in the strength of neural responses to these two directions as a result of training and not due to the difference in the discrimination performance between the two directions during scanning.

Although, the present study was not designed to investigate across session effects, normalization of each cortical region's fMRI responses obtained in the main conditions with the magnitude of fMRI responses to the hMT^+ localizer provides an opportunity to compare the fMRI responses to the task-relevant and task-irrelevant directions before training to those obtained after training (see **Figure 39**). In the case of task-relevant direction normalized data showed a trend of increased neural responses in the early visual cortical areas after training compared to that before training, however, this difference was significant only in the primary visual cortex ($p = 0.0037$; the corrected significance level: $p = 0.0167$ corresponding to FDR = 0.05). On the other hand, a comparison of the fMRI responses to the task-irrelevant direction before and after training showed that learning resulted in a significant reduction of the fMRI responses in area hMT^+ and in area V4v ($p = 0.0025$ for hMT^+ and $p = 0.01$ for V4v; the corrected significance level: $p = 0.0167$ corresponding to FDR = 0.05).

Although we did not track eye position during scanning while the subjects performed a speed-discrimination task, the results of our control experiment speak against the possibility that the difference between the fMRI responses to the task-relevant and task-irrelevant directions could be explained by a difference in the pattern of fixations. The experimental procedure in the control experiment was the same as that in the main experiment with an exception that there were no fMRI scans before and after training. Instead, observers' eye position was recorded outside the scanner using the same stimuli and the same speed discrimination task, which were used during scanning in the main experiment.

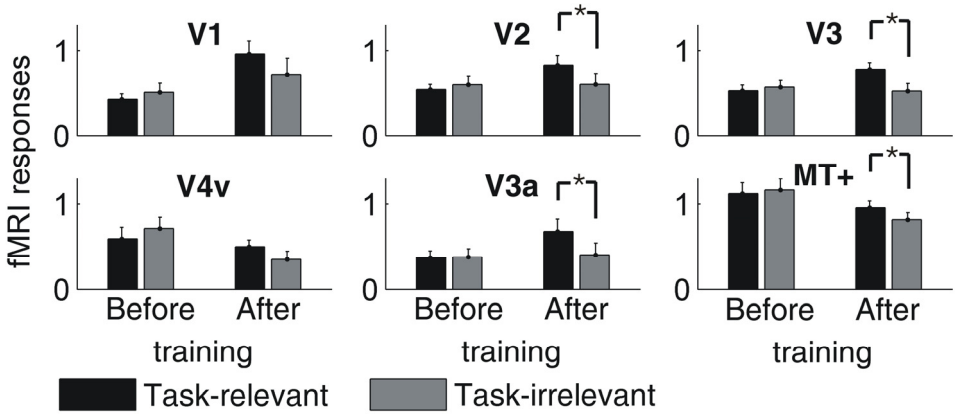

Figure 39 Effect of learning on the fMRI responses.
Normalized fMRI responses to the task-relevant and task-irrelevant directions before and after training. Values on the ordinates represent calculated model fitting weights (in arbitrary units, see the Methods section). Error bars indicate the SEM**.**

Eye position data from trials with task-relevant and task-irrelevant direction were separated and binned. We calculated the mean eye position (x and y values) for the period when the motion stimulus was present on each trial. We found no significant differences in the mean eye position for the two different motion directions (main effect of direction: before training $p = 0.533$; after training $p = 0.231$) indicating that there was no systematic bias in eye position induced by the direction of the motion stimulus. Furthermore, additional analysis showed that there were no significant differences between the three motion directions in the saccadic frequency (effect of direction before training $p = 0.121$ and after training $p = 0.35$) and in the cumulative saccadic amplitude (effect of direction before training $p = 0.13$ and after training $p = 0.67$).

Importantly, the motion coherence detection results obtained during the control experiment revealed that training led to similar learning effects as those in the main experiment: thresholds were slightly reduced for the task-relevant direction and increased for the task-irrelevant direction. ANOVA showed no significant main effect of test session (before and after training, $p = 0.659$); however, there was a significant main effect of task relevance (task-relevant and task-irrelevant, $p < 0.041$) and a significant interaction between these variables ($p < 0.032$). Thus, the results of our control experiment suggest that reduced fMRI responses to the task-irrelevant direction as compared to the task-relevant cannot be explained by a difference in the pattern of fixations between the two directions.

V. DISCUSSION

1. Disease-related changes in color vision

In the current studies, we adopted a novel methodological approach (testing with randomly interleaved multiple staircases with spatial and luminance noise) that allows independent assessment of the relative damage of blue-yellow and red-green pathways in a nonbiased way. In addition, we have searched for new psychophysical-clinical correlations, both in early and late disease stages. Appropriate spatial and temporal parameters of stimulation, that are not biased toward the function of a single stream, allowed investigation of whether the pathway that is affected earliest is also the most affected as the disease progresses.

1.1. Glaucoma study

The present study shows that a concomitant involvement of multiple chromatic pathways within the central retina is present in the natural history of glaucoma earlier than previously believed. This provides an advance over studies that did not include ocular hypertension,[140] or only described changes along the tritan axis in detail, or have included patients that were not age matched with control subjects.[125] One should, however, emphasize the merit of the work of Falcao-Reis et al.[123, 125]and Yu[126] who have championed the use of computerized color tests as advantageous over more traditional semi quantitative methods. Further, we found that progression of chromatic damage correlated significantly with clinical and perimetric measures.

It is worth emphasizing that our computerized approach provides more information than the usual evaluation with the Farnsworth-Munsell 100-hue test, which has been shown to be just a semi-quantitative test with bad reproducibility.[85] We used a strategy that allowed for the simultaneous comparison of relative damage of koniocellular and parvocellular systems, both in ocular hypertension and glaucoma, as measured by interleaved psychophysical staircase stimuli. These assessed function along the main confusion lines and along multiple color axes that

permitted the computation of discrimination ellipses. This strategy may help shed new light on the pathophysiology of glaucoma.

First, we found that significant central damage may have occurred early in a large subset of patients with hypertension, and such damage is not restricted to the blue-yellow pathway, but includes the red-green processing stream. Several reasons may help explain improved detection with our paradigm: size and luminance noise rendered the task particularly difficult and forced the subject to perform chromatic comparisons across multiple locations and between stimuli thus ensuring that the measurement conditions were not biased toward the activation of any functional stream.

It is noteworthy, however, that although early damage was already present in a significant number of patients with hypertension, we also found a subset with no measurable impairment. It is possible that the difference between these subsets is in the amount of time elapsed after diagnosis of ocular hypertension. Many of our patients had been observed for more than 5 years after diagnosis of hypertension, remaining in the preperimetric stage. In agreement with our hypothesis, elapsed time since diagnosis correlated significantly with chromatic performance (length of discrimination ellipses in our group of patients with hypertension). Although an age-related confound could be argued,[255] this effect was not significant in our patients with glaucoma.

Our findings of early dysfunction of both parvo- and koniocellular systems in glaucoma favor the functional-redundancy hypothesis[112, 128, 132, 139] in comparison to the preferential-loss model.[155-157] It is true that blue-yellow defects predominated in our patients and were actually significantly enhanced in comparison to the normal physiologic elongation, but this effect was of small magnitude. Our careful exclusion criteria avoided other possible causes of significant blue-yellow deficits in our population. That ellipse angle suggested this type of predominant loss should not obscure the significant early protan and deutan losses. It is even possible that such measures may be clinically as relevant as tritan loss. Indeed, they were significantly correlated with the C/D ratio. Furthermore, these measures proved to be significantly good predictors of perimetric damage (along with measures of ellipse length), which

is in agreement with a recent finding that development of glaucoma may actually be best predicted by a change in the length of the protan discrimination axis.[147]

We may indeed be facing the problem that a parameter that causes the severest damage does not imply that it is the most useful measure, because no significant correlation was found between tritan axis length and perimetric damage under the conditions of our measurements. Despite the prominent tritan loss, this measure correlated the least with progression of field loss once glaucoma was established. Further studies are necessary to clarify the relation between predominant damage and field loss (as considered in traditional assessment procedures)[145] and predominant progression and field loss.

Significant damage to the red-green chromatic pathway has only been associated with advanced glaucoma.[138, 150] Our data extend these results to ocular hypertension, and show that in a small subset of patients with advanced glaucoma, a predominant red-green loss may also be found.

We favor the view that assessing early macular involvement may provide clinically reliable and reproducible test measures, given that the amount of overlap across populations was much reduced in comparison with earlier studies.[125] This trend has been observed by some research groups: Adams et al.[114, 120] and Heron et al.[118, 119] using a flicker detection method, suggested that foveal chromatic function may be perturbed relatively early on in the disease process, although mostly through the short-wavelength sensitive pathway. This question was reexamined by Greenstein et al.[138] (discrimination of a 3° disc from a white background), who found losses among both opponent systems. Pacheco-Cutillas et al.[145] who also focused more on the fovea than on the whole of the macula (we prefer the latter approach), found similar results, although no significant conclusions are available so far on groups of patients with ocular hypertension.

Future studies should help define psychophysical conditions that help to improve the strategy used in this study for early detection of functional damage induced by high IOP. Taking advantage of static size and luminance noise helps the isolation of multiple chromatic pathways in an unbiased manner, but it remains to be clarified whether dynamic spatiotemporal noise will further improve this method.[256] We favor

static noise, because temporal changes may cause unpredictable activations in the magnocellular system.

In summary, our findings suggest that earlier detection of functional damage can be achieved in both the red-green and blue-yellow chromatic pathways than previously believed. Optimized psychophysical procedures based on luminance noise[86, 145, 256] may allow for the establishment of new clinical correlations that are useful to quantify disease progression and to define subpopulations of patients with ocular hypertension that may evolve into glaucoma.

1.2. Best disease study

The results of the present study provide new insights into the nature of the functional deficits in the neurosensory retina in VMD. In particular, they challenge the view that chromatic deficits in VMD are type I red-green (as is the current view in Stargardt disease as well).[85] That is true only for stage IV, and tritan deficits actually become statistically significant earlier than protan and deutan deficits, whereas the latter become more prominent only when the lesion size has increased or foveal involvement has emerged.

Computerized methods provide more information to study color vision than traditional tests, such as the FM-100 test,[86] whose semi quantitative scores have weak reproducibility.[85] Alternative approaches may, therefore, achieve better quantification of chromatic damage in macular disorders and may help validate traditional classifications,[85-88] which rely mostly on the FM-100 test and colorimetric equations.[85]

Psychophysical evidence is important in the context of VMD because ERG responses are often normal or supernormal, which renders interpretation difficult. Indeed, a recent ERG study[185] suggested that the M-cone response was normal and the L-cone response was supernormal and phase delayed. It is, however, difficult to conclude from this study whether one cone population is more affected than the other because it is unclear whether a supernormal response implies more or less damage of photoreceptor function.

Our study, which uses a highly sensitive quantitative method, shows that substantial damage occurs in all cone pathways in Best disease, even in a subset of patients with relatively preserved VA. These results are compatible with the now almost consensual postulate that the primary disturbance occurs in the RPE.[257]

Visual acuity has often been used as a clinical gold standard psychophysical measure, but options are needed to define better cutoff values between populations of controls and patients. All of our quantitative variables showed statistically significant correlations with VA, but most importantly, they proved to be more reliable in

quantifying relative damage and in predicting disease progression. Furthermore, they correlated significantly with staging and the size of the retinal lesion.

In summary, our quantitative phenotyping strategy proved to be adequate in defining cone dysfunction in different stages of Best disease. We suggest that this type of investigation, complemented with novel physiologic approaches to study cone function,[258, 259] should be applied in relatives of patients with Best disease who show no apparent phenotype.

2. Experiments on visual motion perception

2.1. Center-surround interactions in visual motion integration and segmentation

2.1.1. The role of ambiguity in center-surround interactions

We have investigated the influence of peripheral visual context on the perception of central motion. In Experiments 1-3 we found that contextual effects are strongly dependent on the presence of both local and global ambiguity. These findings have strong implications in the understanding of normal and impaired vision, because in the latter ambiguity is increased in general.

Natural scenes do present concomitant challenges to central and peripheral vision, and it is widely known that this is of particular relevance in normal vision, as well as in neurodevelopmental disorders, and diseases related to aging.[55, 194, 195, 260] Central-peripheral interactions, in particular those concerning magnocellular and motion processing, are of strong importance both in different eye diseases and aging, where temporal sensitivity is often decreased, and center-surround visual motion antagonism reduced.[206]

Our findings show that what subjects can perceive in the foveomacular regions is strongly influenced by the level of congruence/incongruence of peripheral visual information. These results extend previous findings in patients,[55, 195] showing that contextual information may be integrated over space to solve for local ambiguity even in normal vision.

We found that the dynamics of central motion integration significantly depended both on the type of motion perception in the contextual peripheral surround and on the presence of central local motion disambiguation cues. Transparently perceived surrounds (two perceived peripheral moving surfaces) evoked more consistent effects (enhancement of congruent percepts and suppression of incongruent percepts) as compared to non-transparent (just one perceived peripheral surface) surrounds (which only showed a clear enhancement effect of congruent percepts, at the level of

single percept duration). This influence was stronger using textured surrounds, in line with the fact that they are inherently unambiguous. Indeed, unambiguous feature motion provided by overlaid random dots completely determined the perceived direction of local contours, and thereby provided a solution to the aperture problem.[243] This rendered textured peripheries to have a powerful contextual influence.

A remarkable property of central textured stimuli was their own resistance to contextual modulation. This is probably due to the fact that their unambiguity renders them less susceptible to be influenced by the surround. We were however surprised to find that even when central textured stimuli were designed to be globally ambiguous, e.g. containing bimodally disambiguated local motion (50% of the dots providing bias towards one percept type, and 50% towards the other), surround modulation was not effective. This surprising effect is explained by the absence of local ambiguity in spite of the presence of global ambiguity. Indeed, whenever local motion became unambiguous, the effect of surround modulation diminished regardless of the overall luminance/contrast.

These observations have strong basic and clinical research implications. First, they suggest that the shifting balance between the coherent and transparent (two-surface) percepts are attributed to processing stages before any integration or combination of local motion signals, in agreement with previous work.[261] Second, these findings are also clinically relevant because motion may often become ambiguous in different visual disorders. Furthermore, in patients with macular diseases central ambiguity occurs more frequently, which implies that the surround has a more powerful effect, which may be used clinically in rehabilitation approaches.

Contextual effects were similar both for short (10 sec) and long (60 sec) stimulus presentations, which shows that they generalized across levels of motion adaptation, and were independent of pattern motion directions.

A possible locus of the described contextual modulation effects would be MT, a pattern selective region playing a key role in surface motion integration,[41] with well described center-surround modulation properties.[47, 208] However, an earlier point of

interaction could be potentially attained via an MT-V1 feedback analogous to the one suggested by the model of Bayerl and Neumann,[262] in which localized V1 motion signals are the target of feedback modulation by means of velocity matching operations. Since component (local) motion selective neurons represent the overwhelming majority in V1 and V2,[22, 43, 263-265] the proposed feedback route would produce an imbalance of early response distributions producing more robust shifts towards transparent than coherent interpretations on the population level. This model would thus explain the differential contextual modulation of surface integration processes for pattern (non-transparent) and component (transparent) motion conditions.

This notion is consistent with previous work[266] emphasizing that integration of local motion signals across space is a relevant mechanism in vision that might be implemented by the existence of a co-operative network linking neurons sensitive to different directions/speeds and different spatial locations. This view is, however, not inconsistent with the issue of spatial integration/separation within a visual area (in fact pattern and component neurons also co-exist in MT).

As stated above, the fact that locally disambiguated[243] but globally ambiguous (due to local bimodal motion distributions) textured stimuli could escape surround influences, – possibly posed either by top-down feedback[62, 267] or by collinear facilitation mechanisms,[205] that were likely enabled by our experimental conditions – does in any case provide strong evidence for an early neural locus underlying surround modulation.

Given the notion that contextual effects may occur even if the experimental subject is not aware of the presence of the modulatory stimulus,[200] which is also the case when stimuli are placed peripherally, future studies should determine the role of high level top down mechanisms in modulating such peripheral effects.

We were also able to measure how congruent and incongruent context influences central visual dominance and suppression durations.[268, 269] In this way we have found further evidence for distinct mechanisms underlying pattern and component surround modulation. Component surrounds lead to a higher frequency of perceptual switches (indicating higher perceptual instability, with consequentially shorter single percept

durations), enhanced dominance of congruent stimuli, and enhanced suppression of incongruent stimuli. Pattern surrounds are associated with fewer switches (i.e. increased percept stability) and although they enhance the individual duration of congruent stimuli, they are less effective in suppressing incongruent percepts (possibly because their main effect is to increase stability of all percept types). We conclude that context may distinctly influence both dominance and suppression of single percept durations, in parallel or not with percept stability, depending on the type of surround. Moreover, we found that the switch dynamics in our center-surround plaid displays were different than those found without contextual modulation[251] (in particular, the first percept was not always pattern.)

This notion of percept stability is also relevant for future studies seeking clinical applications for patients with scotomas. These studies should also elucidate how surround effects can be integrated into reciprocal inhibition based perceptual switch models similar to the ones suggested for binocular rivalry,[270, 271] which are relevant in strabismus and amblyopia research. Such a unified framework might also be useful to explain why non-transparent surrounds (resulting from perceptual integration) show such different dynamics as compared to transparent surrounds (resulting from perceptual segmentation).

We do believe that these results will help develop new rehabilitation strategies that take advantage of improved knowledge of the rules governing peripheral modulation of visual foveomacular signals. Center surround interactions may for example be stronger in diseases such as macular degenerations[192, 193] where central ambiguity is increased, but effective surrounds can still be processed in the visual periphery, and influence center processing.

Taken together, the presented work extends the knowledge on low-level contextual influences on the perception of local visual stimuli[63, 196-199] and integration of form and depth information in extracting surface representations in early visual areas[60] by demonstrating a role of peripheral perceptual bias in global surface segmentation/segregation processes and the role of enhancement/suppression mechanisms in this process. Finally, our study also clarifies the relative influence of local/global disambiguation, showing that peripheral influences on motion

integration in foveal vision are strongly modulated by local/global ambiguity, a fact that can be applied in novel low vision approaches to rehabilitation.

2.1.2. The role of local and global context in center-surround interactions

Our findings in Experiment 4 show that perceptual integration of center-surround congruent representations may be overcome by local conflicting contextual information provided by collinearity. Indeed, binding by collinearity and common fate mechanisms may simultaneously induce surface segmentation in the center and integration in the surround. This break-in center-surround coherence occurred specifically when one (not less and not more) set of the local moving grating contours of the coherent surrounds was collinear with one of the center component gratings and shared similar direction of motion. In other words, surrounds with opposite effects on the two center components (grouping vs. segmentation) lead to the two center motions being perceptually pulled in different directions by the surround motion. This unusual instance of the Gestalt *good continuation* rule shows that local cues can strongly influence perceptual decision towards center-surround incongruence based on the properties of the surround they are embedded in.

These results extend traditional Gestalt-based accounts that have postulated that cues such as collinearity provide a fixed criterion for surface binding.[59] These views were based on observations demonstrating that contour-integration mechanisms in early vision are sensitive to collinear configurations. It is indeed well-known that in locations where curves made of small line segments come in close proximity the assignment of contour segments to the different curves is, in general, based on local collinearity.[272]

However, our results do show that once an object is integrated (our coherent surrounds) its local properties can still induce distinct types of long range contextual effects based on collinearity and *common fate* mechanisms. In other words, local binding by collinearity and similarity of local motion cues can contribute both to perceptual integration and segmentation processes, simultaneously in surround and center regions. The balance between integration of component gratings and segmentation between transparent surfaces depends on the dynamics of the

interaction between competing local and global contexts. This notion of dynamic interplay between local and global factors is supported by the recent finding that transparency cues may paradoxically improve the pairing of color and motion of rapidly alternating surfaces.[273, 274]

Classical contextual effects have, in general, been studied in terms of threshold estimation of single grating or line stimuli features, near and supra-threshold perceptual figure-ground segmentation of static textures, and surface occlusion under different lighting conditions.[63, 198, 208] Whenever binding was addressed it was assumed to rely on low level local mechanisms that include lateral interactions in early visual cortex.[43, 61, 62] It is somewhat surprising, in light of conventional perceptual organization principles, that surround stimuli with matching collinearity can provide locally binding signals that lead to perceptual incongruency across space. This effect cannot be explained by models that postulate competition between segmentation processes based on surround suppression[206-208] or contour integration through long-range horizontal connections.[61, 63]

An explanation based on motion contrast accounts does not hold either, because if the observed incongruence could be explained by an increased motion contrast we would expect a significant difference between the *Surround-up* and *Surround-down* conditions (the *Surround-up* condition representing zero motion contrast with a complete alignment between moving center and surround contours, and the *Surround-down* condition representing maximum motion contrast with a complete misalignment of the moving contours on the center-surround border). However, these conditions yielded identical psychophysical results (see **Figure 27**).

If a low level explanation would explain the observed incongruence then a difference should have been observed between the modulation imposed by symmetrical and asymmetrical surrounds. Such a difference would suggest that plaid coherence could be affected by subtle changes in perceived relative contrast of its components[39] in spite of their physical identity. Indeed, surround patterns may reduce the apparent contrast of center patterns[275] in an orientation-tuned fashion.[276] However, the fact that we found no difference between symmetrical and asymmetrical surrounds and that subjects never reported any perceived changes in

relative component contrast on symmetrical surrounds further confirms that our observations reflect high-level feature binding processes that employ a set of hierarchical rules in interpreting the stimulus.

We therefore suggest that a causal contour capture mechanism[209] of collinearly moving grating elements at center-surround borders explains center surface segmentation. This represents an unusual instance of Gestalt *good continuation* and *common fate* rules, since it leads to center-surround perceptual incongruence. In other words, local motion signals at the figure-ground boundary can dynamically capture local contours in the center and help segment them into separate surfaces. The surrounding context remains unsegregated. This phenomenally striking effect is modulated by adaptation, since it is enhanced by prolonged stimulus exposure even after motion aftereffects have decayed, suggesting the presence of a storage mechanism.[277]

In conclusion, we have shown here that collinear facilitation does not necessarily result in motion integration but may even cause segmentation, thereby leading to center-surround perceptual incongruence. This work sheds new light on how the analysis of contextual information and surface perception in the human brain can be influenced by the nature of local information and common fate mechanisms in adjacent regions of the visual field. Accordingly, the brain uses a hierarchy of precedence rules in attributing motion to different segments of the visual scene[278] and in this case being *local* confers a high rank in the scheme of priorities. We suggest that adaptive interactions between surface parsing mechanisms and local contour capture by collinearity contribute to a break-in integration in the center in spite of its preservation in the surround. Contextual collinearity plays an important role in this process by inducing contour binding, which, if associated with local motion perceptual capture, may lead to dissociation of center-surround percepts. Thus, global surface perception is not merely a by-product of local binding by collinearity, as classically believed, but it also involves dynamical interactions between local and global context.

2.2. Neural correlates of real and illusory motion perception

Although the main goal of this study was to investigate how selective attention processes modulate hMT^+ processing evoked by motion aftereffects, we have also analysed the differential type of interaction between illusory (AM) and real motion signals prior to the adaptation phase. We could show that net MAE-related activity can be identified in area hMT^+ under sustained selective attention unrelated to motion perception, regardless whether we used a color task or a spatial angle comparison task. When selective attention was focused on a real or apparent motion task, the MAE-related processing, as probed by fMRI, was masked, even if subjects reported perceiving MAEs. Moreover, we identified additive interactions between plaid movement and AM/RM during the adaptation phase, and non-additive (masking) interactions during the MAE test period.

We do believe that our results do reconcile the apparently contradictory results of Tootell et al.[70] and Huk et al.[75] by showing that selective attention can suppress motion-adaptation related activity in area hMT^+, if and only if it is focused on concomitant motion features, regardless of whether they are apparent or real. In other words, perceptual interference/masking does occur if another motion task or stimulus is added, even if it is illusory.

Although our results replicate the findings of Huk et al.,[75] they also provide evidence for the existence of a genuine motion signal in area hMT^+, related to MAE, which is distinctly modulated by the type of difficulty-matched attention task used. The genuine MAE-related signal in hMT^+ can therefore be separated from the attentional mechanisms by which it is modulated.[279-283]

We have proved that distinct types of selective featural attention mechanisms differentially modulate motion aftereffect evoked activity in hMT^+, by showing that motion-unrelated tasks did not cancel MAE-related activations, regardless whether attention was focused on something other than the moving stimulus (color task), or when its static features still had to be attended to (angle comparison task). It is worth pointing out that the locus of spatial attention is distinct in these tasks. However,

results were similar for the color and angle tasks which shows that these results generalize across distinct conditions.

On the other hand, the net increase of activity in area hMT^+ that is evoked by motion adaptation underlying MAEs[69-72] was masked when we imposed selective attention to AM or RM. These findings suggest that selective attention to concurrent motion features leads to interference that masks the MAE-evoked signal. These results are consistent with and extend the findings of Huk et al.[75] using a task in which a slight physical motion was added to half of the MAE test stimulus and requiring the subjects to perform a speed comparison task. Under these conditions, they found no net increase in hMT^+ activity in the presence of a MAE condition (adaptation under constant direction of motion), as compared to the no-MAE condition (adaptation under mixed directions, which in general does not elicit a MAE).

The discrepancy between the activation patterns observed with different attention tasks further emphasize the special case of selective attention tasks that focus directly on motion perception and is in agreement with the previous literature.[214, 284-288]

Even though specific superposition of the AM/RM speed tracking tasks during the static test phase substantially reduced the BOLD difference between adapting fixed and non-adapting mixed conditions, a finding that was not observed with the motion -unrelated tasks, our participants reported MAEs only upon fixed conditions. This finding suggests that interaction across attentional networks is distinct within (all motion-related) and across (motion vs. non motion-related) feature domains.

Since color-matching is associated with ventral-stream function one cannot expect a very strong interaction within common processing pathways, but interestingly, angle-matching does not either cause interference, although it is related to dorsal-stream function, just like the motion tasks that shows marked interaction with MAE (see Castelo-Branco et al.[195, 289] for evidence that these types of tasks are specific to the dorsal stream). Our observations finding suppression of MAE-evoked increase of activity using attention to AM/RM motion stimuli showed that the specific type of featural attention is critically involved in the modulation of net activity in hMT^+. In other words, attention to motion provides a qualitatively distinct masking effect,

while task difficulty is not a relevant explanatory variable since we found distinct modulation patterns even though difficulty levels were adjusted across our temporally sustained tasks.

We were able to generate control conditions for selective attention without disrupting motion adaptation phenomena per se. Superposition of orthogonal AM during plaid motion produced a clear-cut increase in the BOLD response of area hMT^+ comparable to a modulation pattern of an additional moving surface,[41] and showing that hMT^+ responses were not saturated by the motion conditions.

We conclude that the neural substrate of illusory motion aftereffect perception can be identified in conditions requiring selective attention to concomitant non-motion features and is masked by concurrent apparent/real motion tasks. In other words, hMT^+ sensitivity to MAE can be differentially modulated by selective attention to various non-motion and motion features. Finally, superimposed real and apparent motion may lead to additive adaptation effects without saturation of hMT^+ responses, while the interaction of apparent motion and MAE reflects interference effects.

2.3. Learning-induced changes in motion processing

Our findings provide evidence that learning results in increased detection thresholds for task-irrelevant features during training. This learning-induced sensitivity decrease was specific for the feature that served as a distractor during training since the detection threshold for a control direction that was not present during training slightly decreased (rather than increased) after training. The observation of a small non-significant increase in sensitivity to task-relevant motion in the present task is consistent with previous reports showing improved perceptual performance for visual features that were task relevant during training[290-293] (for review see Fahle and Poggio[294]).

On the other hand, recent studies also suggest that learning results in increased sensitivity for subthreshold task-irrelevant visual features presented concurrently with the task-relevant information during training[236-238] whereas suprathreshold task-irrelevant features are not affected by training.[295] These findings apparently conflict with our observation of reduced sensitivity for task-irrelevant information.

However, several key differences between the studies might explain this discrepancy. First, the task-irrelevant stimulus used by Watanabe et al. was spatially separated from the task-relevant stimulus during training. Second, the target and distractor stimuli were very different - alphanumerical characters and moving dots respectively - suggesting that task-relevant and task-irrelevant stimuli were processed by at least partially distinct regions of visual cortex: one region specialized for processing shape/letter information and the other for processing visual motion. Due to distinctiveness of the relevant and irrelevant stimuli, it seems likely that the irrelevant stimulus did not strongly interact or interfere with target processing.

In the present study, however, task-relevant and task-irrelevant stimuli were spatially overlapping and structurally similar (i.e. both were moving dot patterns). Therefore, the stimuli were likely competing for access to the same neural processing mechanisms, which would be expected to drastically increase the amount of competition. We therefore posit that the learning-induced suppression of distractors – as opposed to enhancement as reported by Watanabe et al. – may only be observed

when the task-irrelevant information strongly interferes with the processing of task-relevant information and thus must be suppressed by attention during training.

The possibility that the strength of distractor suppression during training might affect learning has also been invoked[295] to explain why learning leads to increased sensitivity for subthreshold but not for suprathreshold task-irrelevant information. For example, attentional suppression of task-irrelevant information is less pronounced when the distractor is a very weak subthreshold signal as compared to when it is suprathreshold.[296] Thus, learning may result in increased sensitivity for subthreshold distractors but not for suprathreshold distractors because only the latter must be suppressed during training (and this suppression should attenuate any positive consequences of learning[295]). The results of the present study take this logic one step further and show that in cases when there is direct interference between task-relevant and task-irrelevant information that requires strong attentional suppression, training will actually produce *decreased* sensitivity for the task-irrelevant information.

We also found that learning results in decreased fMRI responses evoked by the task-irrelevant motion direction compared to the task-relevant motion direction throughout visual cortex. The strongest learning effects were observed in extrastriate visual cortical areas V2, V3, V3a and hMT^{+}, the latter two of which are known to be involved in visual motion processing.[54, 297-300] An important question is whether the observed reduction in fMRI responses associated with task-irrelevant stimuli can be explained by learning-induced changes in performance in the speed discrimination task that was performed during scanning (even though statistical analyses revealed no significant learning effects on performance in the speed discrimination task in the absence of distractors during scanning). To test this possibility, we investigated the relationship between speed discrimination performance and fMRI responses.

We found no significant differences in the fMRI responses between runs with the best speed discrimination performance and runs where performance in the speed discrimination task was poor. These findings suggest that the difference between the fMRI responses to task-relevant and task-irrelevant directions found after training in

the present study cannot be explained by the difference in the speed discrimination performance between the two directions during scanning.

Therefore, we propose that the learning-induced modulation of fMRI responses might be a combined effect of increased neural responses to the task-relevant direction and decreased neural responses to the task-irrelevant direction after training. Importantly, we also suggest that learning-induced modulation of neural responses to task-relevant and task-irrelevant directions is not restricted to the trained task condition, but affects processing of these directions generally, in a task independent manner.

Previous research has shown that the effect of perceptual learning on fMRI responses depends on several factors, including task and testing conditions as well as the time during learning when fMRI responses are measured.[224, 301, 302] These results imply that there are multiple mechanisms by which learning can modulate fMRI responses. In accordance with this, comparing fMRI responses after training to that before training suggest that the site and mechanisms of learning-induced facilitation of the task-relevant and suppression of the task-irrelevant information might be different. In particular, we found that fMRI responses to the motion direction that was task-relevant during training are enhanced in the primary visual cortex. On the other hand, learning-induced suppression of fMRI responses to the motion direction that was present as a distractor during training was most pronounced in the motion selective area hMT^+ and was absent in earlier cortical areas, such as the primary visual cortex.

We propose that the observed reductions of fMRI responses in hMT^+ might reflect suppressed neural responses to the task-irrelevant direction, which is supported by recent findings, showing that decreases in BOLD activity in early visual cortex are associated with decreased neural activity.[303] Importantly, previous research provided evidence that neural responses in area hMT^+ are sensitive to motion coherence and are associated with the perceived strength of the global coherent motion signal (for review see Serences and Boynton[300]).

Based on this, it is tempting to suggest that decreased neural responses in area hMT^+ to the motion direction that was task-irrelevant during training might underlay

learning-induced suppression of perceptual sensitivity for this direction found in our psychophysical experiments. In the same time, it is important to point out that in addition to the learning-induced modulation of the strength of direction selective neuronal responses, changes either in the receptive field tuning properties of direction selective neurons or in the readout of the visual cortical neuronal responses could also contribute to the observed behavioral learning effects. For example, previous neurophysiological studies provided evidence for sharpening of neuronal responses to the trained feature with learning in the macaque visual cortex (for recent review see Hoffman and Logothetis.)[304] Narrowing of the tuning curves, however, leads to a smaller fraction of cells being active for any given stimulus and thus would lead to a decreased BOLD signal.[302, 304] Therefore, in case of the present study, an explanation based on sharpening of neuronal responses would predict decreased fMRI responses to the task-relevant direction, which is not supported by the results of our fMRI experiment.

Unfortunately, to our knowledge the possibility that learning might also modulate the receptive field tuning properties of neurons responsible to features that present as distractors during training or might modify the readout of their responses at the higher stages of perceptual decision level processing has not been investigated before. Therefore, further research is required to explore whether these neural mechanisms might also contribute to learning-induced suppression of perceptual sensitivity to the task-irrelevant direction found in the present study.

It has been proposed that increasing the efficacy of noise exclusion might be a crucial component of perceptual learning and that it is achieved by improving the extraction of the visual information that is relevant for the trained task via reweighting or retuning of the perceptual template that is used to arrive at a decision.[230, 231, 233, 234] Our findings suggest that learning-induced decreases in neural responses to a competing task-irrelevant feature represents one of the mechanisms underlying such reweighting of the perceptual templates due to learning. To explain the effect of training on the task-irrelevant information, Seitz and Watanabe[239] proposed a model suggesting that perceptual learning involves a diffuse reinforcement signal that leads to long-lasting improvement of information processing for all stimuli presented concurrently with the task-relevant information

during training, even if the stimulus is a task-irrelevant distractor. This model, however, fails to account for the present observation of a learning-induced suppression of distractor information. We suggest that learning-induced suppression represents an important mechanism underlying more efficient distractor exclusion after training, and should be incorporated into models of perceptual learning.

VI. CONCLUSIONS

1. Disease-related changes in color vision

1.1. Glaucoma study

The present study shows that a concomitant involvement of multiple chromatic pathways within the central retina is present in the natural history of glaucoma earlier than previously believed. This provides an advance over studies that did not include ocular hypertension,[140] or only detailed changes along the tritan axis, or have included patients that were not age matched with control subjects.[125]

We found that progression of chromatic damage proved to be significantly good predictor of clinical and perimetric changes, which is in agreement with a recent finding that development of glaucoma may actually be best predicted by a change in the length of the protan discrimination axis.[147]

Our findings of early dysfunction of both parvo- and koniocellular systems in glaucoma favor the functional-redundancy hypothesis[112, 128, 132, 139] in comparison to the preferential-loss model.[155-157]

Taken together, our findings suggest that earlier detection of functional damage can be achieved in both the red-green and blue-yellow chromatic pathways than previously believed. Optimized psychophysical procedures based on luminance noise[86, 145, 256] may allow for the establishment of new clinical correlations that are useful to quantify disease progression and to define subpopulations of patients with ocular hypertension that may evolve into glaucoma.

1.2. Best disease study

We found that substantial damage occurs in all cone pathways in Best disease, even in a subset of patients with relatively preserved VA. These results are compatible with the now almost consensual postulate that the primary disturbance occurs in the RPE.[257]

Our findings challenge the view that chromatic deficits in VMD are type I red-green (as is the current view in Stargardt disease, as well).[85] This is true only for stage IV, and tritan deficits actually become statistically significant earlier than protan and deutan deficits, whereas the latter become more prominent only when the lesion size has increased or foveal involvement has emerged.

As all of our quantitative variables showed statistically significant correlations with VA, proved to be reliable in quantifying relative damage and in predicting disease progression, and correlated significantly with staging and the size of the retinal lesion, we can conclude that psychophysical color testing provides a safe, efficient, and non-invasive means for Best disease patient follow-up.

2. Experiments on visual motion perception

2.1. Center-surround interactions in visual motion integration and segmentation

We showed that the dynamics of central motion integration significantly depended both on the type of motion perception in the contextual peripheral surround and on the presence of local motion disambiguation cues. Transparently perceived surrounds evoked more consistent effects as compared to non-transparent surrounds.

The modulation was stronger using textured surrounds, in line with the fact that they are inherently unambiguous. Indeed, unambiguous feature motion provided by overlaid random dots completely determines the perceived direction of local contours, and thereby provides a solution to the aperture problem.[243] This rendered textured peripheries to have a powerful contextual influence. On the same token, textured centers escaped from modulation regardless of their inherent perceptual bias or the surrounds used.

Potential MT-V1 feedback analogous the model of Bayerl and Neumann[262] might explain the observed effect, producing an imbalance of early response distributions leading to more robust shifts towards transparent (component) than coherent interpretations on the population level. A model like this would explain the

differential contextual modulation of surface integration processes for pattern (non-transparent) and component (transparent) motion conditions.

Using surround with pattern motion direction orthogonal to that of the centers we showed that collinear facilitation does not necessarily result in motion integration but may even cause segmentation. This represents an unusual instance of Gestalt *good continuation* and *common fate* rules, since it leads to center-surround perceptual incongruence. This phenomenally striking effect can be explained by causal contour capture[209] mechanisms, where collinearly moving grating elements at center-surround borders dynamically capture local contours in the center thus helping to segment it into separate surfaces while the surrounding context remains unsegregated.

The presented study extends the knowledge on low-level contextual influences on the perception of local visual stimuli[63, 196-199] and integration of form and depth information in extracting surface representations in early visual areas,[60] by demonstrating a role of peripheral perceptual bias in global surface segmentation/segregation processes and the role of enhancement/suppression mechanisms in this process. Moreover, we showed that these processes can be differentially influenced by local information and common fate mechanisms in adjacent regions of the visual field. Our findings support the notion that the brain uses a hierarchy of precedence rules in attributing motion to different segments of the visual scene[278] and in this case being "local" confers a high rank in the scheme of priorities.

These observations have strong basic and clinical research implications. First, they suggest that the shifting balance between the coherent and transparent (two-surface) percepts are attributed to processing stages before any integration or combination of local motion signals occurs, in agreement with previous work.[261] Second, these findings are also clinically relevant because motion may often become ambiguous in different visual disorders, e.g. central ambiguity occurs more frequently in patients with macular diseases, implying that the surround might have a more powerful effect, which may be used clinically in rehabilitation approaches.

2.2. Neural correlates of real and illusory motion perception

We conclude that the neural substrates of illusory motion aftereffect perception can be identified in conditions requiring selective attention to concomitant non-motion features and is masked by concurrent apparent/real motion tasks. In other words, hMT^+ sensitivity to MAE can be differentially modulated by selective attention to various non-motion and motion features. Finally, superimposed real and apparent motion may lead to additive adaptation effects without saturation of area hMT^+ responses, while the interaction of apparent motion and MAE reflects interference effects.

We do believe that our results do reconcile the apparently contradictory results of Tootell et al.[70] and Huk et al.[75] by showing that selective attention can suppress motion-adaptation related activity in area hMT^+, if and only if it is focused on concomitant motion features, regardless of whether they are apparent or real. In other words, perceptual interference/masking does occur if another motion task or stimulus is added, even if it is illusory.

2.3. Learning-induced changes in motion processing

Our findings provide evidence that learning results in increased detection thresholds for task-irrelevant features during training. This learning-induced sensitivity decrease was specific for the feature that served as a distractor during training since the detection threshold for a control direction that was not present during training slightly decreased (rather than increased) after training.

We also found that learning results in decreased fMRI responses evoked by the task-irrelevant motion direction compared to the task-relevant motion direction throughout visual cortex. The strongest learning effects were observed in extrastriate visual cortical areas V2, V3, V3a and hMT^+, the latter two of which are known to be involved in visual motion processing,

We propose that the learning-induced modulation of fMRI responses might be a combined effect of increased neural responses to the task-relevant direction and decreased neural responses to the task-irrelevant direction after training. Importantly,

we also suggest that learning-induced modulation of neural responses to task-relevant and task-irrelevant directions is not restricted to the trained task condition, but affects processing of these directions generally, in a task independent manner.

Taken together, learning-induced suppression represents an important mechanism underlying more efficient distractor exclusion after training, and should be incorporated into models of perceptual learning.

VII. SUMMARY

Among our sensory modalities the visual modality is the one providing the highest information load. We live in an extremely rich visual environment; in general, one has to deal with constantly moving colored surface patches during visual information processing. In the present thesis I describe our work done on color vision, and visual motion processing.

We used computer-based psychophysics to test color vision in glaucoma and Best's vitelliform macular dystrophy. We found that color vision deficiencies are present in all cone pathways in both diseases despite the common views that associate glaucoma with selective blue-yellow deficits, and Best disease with selective red-green deficits. We also found that color vision deficits correlate well with standard clinical parameters used for staging in both pathologies.

We used psychophysics and/or functional magnetic resonance imaging (fMRI) to study center-surround interactions in surface integration, the interference between different observed motion types, and the effect of learning on surface segmentation.

By using psychophysics to study how moving surfaces are integrated we found strong surround influences on central ambiguous percepts. This effect depended on the inherent integration/segmentation bias of the surrounds, the presence/absence of local cues providing disambiguation, and the presence/absence of global context interfering with selected elements of the central moving surfaces.

We showed using fMRI that the interaction of real and apparent motion may lead to additive adaptation without saturation of hMT^+ responses, while the interaction of motion aftereffects and apparent motion reflects interference. Moreover, neural substrates of illusory motion aftereffects can be identified when selective attention is directed to concomitant non-motion features and are masked by concurrent apparent/real motion tasks.

We found that learning results in increased detection thresholds and decreased fMRI responses for task-irrelevant motion direction compared to the task-relevant motion direction throughout the visual cortex.

VIII. ÖSSZEFOGLALÁS

Érzékszervi modalitásaink közül a vizuális modalitás nyújtja a legmagasabb információ-sűrűséget. A körülöttünk levő vizuális környezet rendkívül gazdag; a látott információ feldolgozása során jellemzően folyamatosan mozgó színes felületekből kell rekonstruálnunk környezetünket. Dolgozatomban színlátással és mozgáslátással kapcsolatos eredményeinket mutatom be.

A színlátás változásait glaucoma (zöldhályog) és Best-féle vitelliform maculadystrophia esetében számítógép-alapú pszichofizikai módszerrel vizsgálva megállapítottuk, hogy mindkét betegség esetén érintett mindhárom csapból származó információ, annak ellenére, hogy a glaucomát jellemzően kék-sárga, a Best-féle sárgatest-elfajulást pedig vörös-zöld kiesésnek tartják. Ezen túlmenően azt találtuk, hogy a színlátás zavarai mindkét esetben jól korreláltak a stádiumbeosztásra használt klinikai paraméterekkel.

A mozgáslátás központ-környezet kölcsönhatásait a felületek szegmentációjára, a különféle észlelt mozgástípusok interakcióját, valamint a tanulás hatását a felületek szegmentációjára pszichofizika és funkcionális MR (fMR) segítségével vizsgáltuk.

Pszichofizika segítségével erőteljes környezeti hatást sikerült kimutatnunk a központi kétértelmű mozgó felületek integrációjára. Ez a hatás függött a környezet saját szegmentációs/integrációs alapállapotától az esetleges kétértelműséget feloldó lokális információ meglététől, illetve a központi mozgó felületek egyes elemeivel interferáló globális kontextustól.

Funkcionális MR segítségével megmutattuk, hogy a valós és látszólagos (apparens) mozgások együttesen additív adaptációhoz vezetnek a hMT^+-válaszok telítődése nélkül, míg a mozgási utóhatások és a látszólagos mozgások egymással interferálnak. Ráadásul a mozgási utóhatásra jellemző neurális választ más mozgásformákra irányuló figyelem kioltja, míg a nem mozgó sajátságokra való figyelem nem érinti.

Pszichofizika és fMR segítségével megállapítottuk, hogy tanulás során a feladat szempontjából irreleváns mozgásirányok érzékelési küszöbe emelkedik, míg a rájuk adott fMR-válasz az egész látókéregben csökken.

IX. SUMÁRIO

Das diversas modalidades sensoriais, a visão compreende uma proporção considerável da informação processada pelo ser humano. Vivemos num ambiente visual extraordinariamente rico, tendo que lidar com superfícies e objectos em constante movimento durante o processamento da informação visual. Na presente tese é descrito trabalho relativo a processamento de cor e movimento.

Usámos técnicas de psicofísicas computorizadas para avaliar a função cromática no glaucoma e distrofia viteliforme de Best. Verificámos que anomalias da visão cromática estão presentes nas três vias de cones em ambas as doenças, apesar da perspectiva tradicional que associa o glaucoma a défices selectivos da via azul-amarelo (koniocelular) e o doença de Best a défices selectivos da via verde-vermelho (parvocelular). Verificámos que os défices das vias cromáticas se correlacionam bem com parâmetros clínicos padrão de estadiamento destas patologias.

Usámos psicofísica e ressonância magnética funcional (RMf) para estudar a influência do contexto na integração de superfícies perceptuais, a interacção entre a percepção entre diferentes formas de movimento, e o papel da aprendizagem na segmentação de superfícies perceptuais.

O estudo psicofísico mostrou que a influência do contexto na integração de superfícies é fundamental quando a percepção em regiões centrais é ambígua. Este efeito dependeu do viés de base na integração/segmentação do contexto periférico, da presença/ausência de pistas locais, e na presença/ausência de um contexto global interferindo com elementos particulares das superfícies centrais em movimento.

Mostrámos, usando RMf que a interacção entre movimento real e aparente leva a adaptação aditiva enquanto que a interacção em a percepção de pós-imagens do movimento e o movimento aparente revela interferência. Além do mais, os substratos neurais das pós-imagens do movimento podem ser identificados quando a atenção selectiva é dirigida para aspectos concomitantes não relacionados com o movimento e são mascarados por tarefas exigindo processamento concomitante de movimento real/aparente.

Por fim, descobrimos efeitos de aprendizagem em termos de aumento dos limiares de detecção e respostas RMf reduzidas no córtex visual para movimento não relacionado com a tarefa relativamente a movimento relacionado com a tarefa.

REFERENCES

1. Sekuler R, Blake R. *Perception*. 3rd ed. New York: McGraw-Hill, Inc.; 1994.
2. Bear MF, Connors BW, Paradiso MA. The Eye. *Neuroscience - Exploring the brain.* Baltimore, MD: Lippincott Williams & Wilkins; 2007:277-308.
3. Sterling P. Retina. In: Shepherd GM (ed), *The synaptic organization of the brain.* New York: Oxford University Press; 1998:205-253.
4. Rockhill RL, Daly FJ, MacNeil MA, Brown SP, Masland RH. The diversity of ganglion cells in a mammalian retina. *J Neurosci* 2002; 22:3831-3843.
5. Roska B, Werblin F. Vertical interactions across ten parallel, stacked representations in the mammalian retina. *Nature* 2001; 410:583-587.
6. Wassle H, Boycott BB. Functional architecture of the mammalian retina. *Physiol Rev* 1991; 71:447-480.
7. Dacey DM. Origins of perception: retinal ganglion cell diversity and the creation of parallel visual pathways. In: Gazzanigga MS (ed), *The Cognitive Neurosciences III.* Cambridge, MA: MIT Press; 2004:281-301.
8. Frishman LJ. Basic visual processes. In: Goldstein EB (ed), *Blackwell handbook of perception.* Malden, MA: Blackwell Publishers, Ltd.; 2001:55-91.
9. Ahmad KM, Klug K, Herr S, Sterling P, Schein S. Cell density ratios in a foveal patch in macaque retina. *Vis Neurosci* 2003; 20:189-209.
10. Wassle H, Grunert U, Rohrenbeck J, Boycott BB. Retinal ganglion cell density and cortical magnification factor in the primate. *Vision Res* 1990; 30:1897-1911.
11. Derrington AM, Krauskopf J, Lennie P. Chromatic mechanisms in lateral geniculate nucleus of macaque. *J Physiol* 1984; 357:241-265.
12. Chichilnisky EJ, Kalmar RS. Temporal resolution of ensemble visual motion signals in primate retina. *J Neurosci* 2003; 23:6681-6689.
13. Dacey DM, Lee BB. The 'blue-on' opponent pathway in primate retina originates from a distinct bistratified ganglion cell type. *Nature* 1994; 367:731-735.
14. Bear MF, Connors BW, Paradiso MA. The Central Visual System. *Neuroscience - Exploring the brain.* Baltimore, MD: Lippincott Williams & Wilkins; 2007:309-341.
15. Van Essen DC, Anderson CH. Information processing strategies and pathways in the primate visual system. In: Zornetzer S, Davis JL, Lau C, McKenna T (eds), *An Introduction to Neural and Electronic Networks.* San Diego, CA: Academic Press; 1995:45-76.
16. Horton JC, Sincich LC. A new foundation for the visual cortical hierarchy. In: Gazzanigga MS (ed), *The Cognitive Neurosciences III.* Cambridge, MA: MIT Press; 2004:233-243.
17. LeVay S, Wiesel TN, Hubel DH. The development of ocular dominance columns in normal and visually deprived monkeys. *J Comp Neurol* 1980; 191:1-51.
18. Ts'o DY, Frostig RD, Lieke EE, Grinvald A. Functional organization of primate visual cortex revealed by high resolution optical imaging. *Science* 1990; 249:417-420.
19. Felleman DJ, Van Essen DC. Distributed hierarchical processing in the primate cerebral cortex. *Cereb Cortex* 1991; 1:1-47.
20. Clarke S, Walsh V, Schoppig A, Assal G, Cowey A. Colour constancy impairments in patients with lesions of the prestriate cortex. *Exp Brain Res* 1998; 123:154-158.
21. Rizzo M, Nawrot M, Blake R, Damasio A. A human visual disorder resembling area V4 dysfunction in the monkey. *Neurology* 1992; 42:1175-1180.
22. Movshon JA, Adelson EH, Gizzi MS, Newsome WT. The analysis of moving visual patterns. In: Chagas C, Gattass R, Gross C (eds), *Pattern Recognition Mechanisms.* Rome: Vatican Press; 1985:117-151.
23. Zihl J, von Cramon D, Mai N. Selective disturbance of movement vision after bilateral brain damage. *Brain* 1983; 106 (Pt 2):313-340.

24. Verdon WA, Adams AJ. Color vision. In: Norton TT, Corliss DA, Bailey JE (eds), *The psychophysical measurement of visual function.* Woburn, MA: Butterworth-Heinemann; 2002:217-288.
25. MacAdam DL. Visual sensitivities to color differences in daylight. *J Opt Soc Am* 1942; 32:247-274.
26. Dougherty RF, Wade AR. *Vischeck*. http://www.vischeck.com/ 2008-Nov-11:Colorblind vision simulation.
27. Dantes E. *Stock photo: flowers*. http://www.sxc.hu/photo/1101982.
28. Watson JD, Myers R, Frackowiak RS, Hajnal JV, Woods RP, Mazziotta JC, Shipp S, Zeki S. Area V5 of the human brain: evidence from a combined study using positron emission tomography and magnetic resonance imaging. *Cereb Cortex* 1993; 3:79-94.
29. Tootell RB, Reppas JB, Kwong KK, Malach R, Born RT, Brady TJ, Rosen BR, Belliveau JW. Functional analysis of human MT and related visual cortical areas using magnetic resonance imaging. *J Neurosci* 1995; 15:3215-3230.
30. Tootell RB, Taylor JB. Anatomical evidence for MT and additional cortical visual areas in humans. *Cereb Cortex* 1995; 5:39-55.
31. Ffytche DH, Guy CN, Zeki S. The parallel visual motion inputs into areas V1 and V5 of human cerebral cortex. *Brain* 1995; 118 (Pt 6):1375-1394.
32. Dupont P, De Bruyn B, Vandenberghe R, Rosier AM, Michiels J, Marchal G, Mortelmans L, Orban GA. The kinetic occipital region in human visual cortex. *Cereb Cortex* 1997; 7:283-292.
33. Van Oostende S, Sunaert S, Van Hecke P, Marchal G, Orban GA. The kinetic occipital (KO) region in man: an fMRI study. *Cereb Cortex* 1997; 7:690-701.
34. Reppas JB, Niyogi S, Dale AM, Sereno MI, Tootell RB. Representation of motion boundaries in retinotopic human visual cortical areas. *Nature* 1997; 388:175-179.
35. Goebel R, Khorram-Sefat D, Muckli L, Hacker H, Singer W. The constructive nature of vision: direct evidence from functional magnetic resonance imaging studies of apparent motion and motion imagery. *Eur J Neurosci* 1998; 10:1563-1573.
36. Braddick OJ, O'Brien JM, Wattam-Bell J, Atkinson J, Turner R. Form and motion coherence activate independent, but not dorsal/ventral segregated, networks in the human brain. *Curr Biol* 2000; 10:731-734.
37. Braddick OJ, O'Brien JM, Wattam-Bell J, Atkinson J, Hartley T, Turner R. Brain areas sensitive to coherent visual motion. *Perception* 2001; 30:61-72.
38. Newsome WT, Pare EB. A selective impairment of motion perception following lesions of the middle temporal visual area (MT). *J Neurosci* 1988; 8:2201-2211.
39. Adelson EH, Movshon JA. Phenomenal coherence of moving visual patterns. *Nature* 1982; 300:523-525.
40. Stoner GR, Albright TD, Ramachandran VS. Transparency and coherence in human motion perception. *Nature* 1990; 344:153-155.
41. Castelo-Branco M, Formisano E, Backes W, Zanella F, Neuenschwander S, Singer W, Goebel R. Activity patterns in human motion-sensitive areas depend on the interpretation of global motion. *Proc Natl Acad Sci U S A* 2002; 99:13914-13919.
42. Braddick O. Segmentation versus integration in visual motion processing. *Trends Neurosci* 1993; 16:263-268.
43. Castelo-Branco M, Goebel R, Neuenschwander S, Singer W. Neural synchrony correlates with surface segregation rules. *Nature* 2000; 405:685-689.
44. Albright TD, Stoner GR. Visual motion perception. *Proc Natl Acad Sci U S A* 1995; 92:2433-2440.
45. Albright TD, Desimone R, Gross CG. Columnar organization of directionally selective cells in visual area MT of the macaque. *J Neurophysiol* 1984; 51:16-31.
46. Geesaman BJ, Born RT, Andersen RA, Tootell RB. Maps of complex motion selectivity in the superior temporal cortex of the alert macaque monkey: a double-label 2-deoxyglucose study. *Cereb Cortex* 1997; 7:749-757.

47. Born RT, Tootell RB. Segregation of global and local motion processing in primate middle temporal visual area. *Nature* 1992; 357:497-499.
48. Malach R, Schirman TD, Harel M, Tootell RB, Malonek D. Organization of intrinsic connections in owl monkey area MT. *Cereb Cortex* 1997; 7:386-393.
49. Malonek D, Tootell RB, Grinvald A. Optical imaging reveals the functional architecture of neurons processing shape and motion in owl monkey area MT. *Proc Biol Sci* 1994; 258:109-119.
50. Groh JM. Predicting perception from population codes. *Nat Neurosci* 2000; 3:201-202.
51. Groh JM. Reading neural representations. *Neuron* 1998; 21:661-664.
52. Treue S, Hol K, Rauber HJ. Seeing multiple directions of motion-physiology and psychophysics. *Nat Neurosci* 2000; 3:270-276.
53. Sunaert S, Van Hecke P, Marchal G, Orban GA. Motion-responsive regions of the human brain. *Exp Brain Res* 1999; 127:355-370.
54. Huk AC, Heeger DJ. Pattern-motion responses in human visual cortex. *Nat Neurosci* 2002; 5:72-75.
55. Castelo-Branco M, Mendes M, Silva MF, Januario C, Machado E, Pinto A, Figueiredo P, Freire A. Specific retinotopically based magnocellular impairment in a patient with medial visual dorsal stream damage. *Neuropsychologia* 2006; 44:238-253.
56. Groh JM, Born RT, Newsome WT. How is a sensory map read Out? Effects of microstimulation in visual area MT on saccades and smooth pursuit eye movements. *J Neurosci* 1997; 17:4312-4330.
57. Salzman CD, Newsome WT. Neural mechanisms for forming a perceptual decision. *Science* 1994; 264:231-237.
58. Recanzone GH, Wurtz RH. Shift in smooth pursuit initiation and MT and MST neuronal activity under different stimulus conditions. *J Neurophysiol* 1999; 82:1710-1727.
59. Koffka K. *Principles of Gestalt psychology*. New York: Harcourt, Brace & World; 1935.
60. Bakin JS, Nakayama K, Gilbert CD. Visual responses in monkey areas V1 and V2 to three-dimensional surface configurations. *J Neurosci* 2000; 20:8188-8198.
61. Li W, Gilbert CD. Global contour saliency and local colinear interactions. *J Neurophysiol* 2002; 88:2846-2856.
62. Stettler DD, Das A, Bennett J, Gilbert CD. Lateral connectivity and contextual interactions in macaque primary visual cortex. *Neuron* 2002; 36:739-750.
63. Lorenceau J, Giersch A, Series P. Dynamic competition between contour integration and contour segmentation probed with moving stimuli. *Vision Res* 2005; 45:103-116.
64. Anstis S, Verstraten FAJ, Mather G. The motion aftereffect. *Trends in Cognitive Sciences* 1998; 2:111-117.
65. Verstraten FA, van der Smagt MJ, van de Grind WA. Aftereffect of high-speed motion. *Perception* 1998; 27:1055-1066.
66. Grunewald A. A model of transparent motion and non-transparent motion-aftereffects. In: Touretzky DS, Mozer MC, Hasselmo ME (eds), *NIPS*: MIT Press; 1995:837-843.
67. Kozak LR, Castelo-Branco M, Karmos G, Read JCA. A computational model of the motion aftereffect. *Invest Ophthalmol Vis Sci* 2004; 45:4336.
68. Kozak LR, Castelo-Branco M, Read JCA. Physiologically-realistic circuitry underlying the motion aftereffect. *J Vis* 2004; 4:846a.
69. Corbetta M, Miezin FM, Dobmeyer S, Shulman GL, Petersen SE. Attentional modulation of neural processing of shape, color, and velocity in humans. *Science* 1990; 248:1556-1559.
70. Tootell RB, Reppas JB, Dale AM, Look RB, Sereno MI, Malach R, Brady TJ, Rosen BR. Visual motion aftereffect in human cortical area MT revealed by functional magnetic resonance imaging. *Nature* 1995; 375:139-141.
71. He S, Cohen ER, Hu X. Close correlation between activity in brain area MT/V5 and the perception of a visual motion aftereffect. *Curr Biol* 1998; 8:1215-1218.
72. Culham JC, Dukelow SP, Vilis T, Hassard FA, Gati JS, Menon RS, Goodale MA. Recovery of fMRI activation in motion area MT following storage of the motion aftereffect. *J Neurophysiol* 1999; 81:388-393.

73. Taylor JG, Schmitz N, Ziemons K, Grosse-Ruyken ML, Gruber O, Mueller-Gaertner HW, Shah NJ. The network of brain areas involved in the motion aftereffect. *Neuroimage* 2000; 11:257-270.
74. Hautzel H, Taylor JG, Krause BJ, Schmitz N, Tellmann L, Ziemons K, Shah NJ, Herzog H, Muller-Gartner HW. The motion aftereffect: more than area V5/MT? Evidence from 15O-butanol PET studies. *Brain Res* 2001; 892:281-292.
75. Huk AC, Ress D, Heeger DJ. Neuronal basis of the motion aftereffect reconsidered. *Neuron* 2001; 32:161-172.
76. Mikami A, Newsome WT, Wurtz RH. Motion selectivity in macaque visual cortex. II. Spatiotemporal range of directional interactions in MT and V1. *J Neurophysiol* 1986; 55:1328-1339.
77. Mikami A, Newsome WT, Wurtz RH. Motion selectivity in macaque visual cortex. I. Mechanisms of direction and speed selectivity in extrastriate area MT. *J Neurophysiol* 1986; 55:1308-1327.
78. Newsome WT, Mikami A, Wurtz RH. Motion selectivity in macaque visual cortex. III. Psychophysics and physiology of apparent motion. *J Neurophysiol* 1986; 55:1340-1351.
79. Muckli L, Kriegeskorte N, Lanfermann H, Zanella FE, Singer W, Goebel R. Apparent motion: event-related functional magnetic resonance imaging of perceptual switches and States. *J Neurosci* 2002; 22:RC219.
80. Liu T, Slotnick SD, Yantis S. Human MT+ mediates perceptual filling-in during apparent motion. *Neuroimage* 2004; 21:1772-1780.
81. Coletta NJ. Temporal Factors in Vision. In: Norton TT, Corliss DA, Bailey JE (eds), *The psychophysical measurement of visual function.* Woburn, MA: Butterworth-Heinemann; 2002:177-215.
82. Fechner GT. *Elemente der Psychophysik*. Leipzig: Breitkopf und Härtel; 1860.
83. Corliss DA, Norton TT. Principles of psychophysical measurement. In: Norton TT, Corliss DA, Bailey JE (eds), *The psychophysical measurement of visual function.* Woburn, MA: Butterworth-Heinemann; 2002:1-34.
84. Watson AB, Pelli DG. QUEST: a Bayesian adaptive psychometric method. *Percept Psychophys* 1983; 33:113-120.
85. Roth A, Lanthony P. Vision des couleurs. In: Risse JF (ed), *Exploration de la Fonction Visuelle.* Paris: Masson; 1999:129-151.
86. Regan BC, Reffin JP, Mollon JD. Luminance noise and the rapid determination of discrimination ellipses in colour deficiency. *Vision Res* 1994; 34:1279-1299.
87. Pokorny J, Smith VC, Ernest JT. Macular color vision defects: specialized psychophysical testing in acquired and hereditary chorioretinal diseases. *Int Ophthalmol Clin* 1980; 20:53-81.
88. Pokorny J, Smith VC, Verriest G, Pinckers A. *Congenital and Acquired Color Vision Deficits*. New York, NY: Grune & Stratton; 1979.
89. Logothetis NK, Pauls J, Augath M, Trinath T, Oeltermann A. Neurophysiological investigation of the basis of the fMRI signal. *Nature* 2001; 412:150-157.
90. Ogawa S, Tank DW, Menon R, Ellermann JM, Kim SG, Merkle H, Ugurbil K. Intrinsic signal changes accompanying sensory stimulation: functional brain mapping with magnetic resonance imaging. *Proc Natl Acad Sci U S A* 1992; 89:5951-5955.
91. Kwong KK, Belliveau JW, Chesler DA, Goldberg IE, Weisskoff RM, Poncelet BP, Kennedy DN, Hoppel BE, Cohen MS, Turner R, et al. Dynamic magnetic resonance imaging of human brain activity during primary sensory stimulation. *Proc Natl Acad Sci U S A* 1992; 89:5675-5679.
92. Friston KJ, Holmes AP, Worsley KJ, Poline J-B, Frith CD, Frackowiak RSJ. Statistical parametric maps in functional imaging: A general linear approach. *Hum Brain Mapp* 1995; 2:189-210.
93. Friston KJ, Holmes AP, Poline JB, Grasby PJ, Williams SC, Frackowiak RS, Turner R. Analysis of fMRI time-series revisited. *Neuroimage* 1995; 2:45-53.
94. Worsley KJ, Friston KJ. Analysis of fMRI time-series revisited--again. *Neuroimage* 1995; 2:173-181.

95. Holmes AP. Statistical Issues in Functional Brain Mapping (PhD thesis). Glasgow: University of Glasgow; 1994.
96. De Martino F, Gentile F, Esposito F, Balsi M, Di Salle F, Goebel R, Formisano E. Classification of fMRI independent components using IC-fingerprints and support vector machine classifiers. *Neuroimage* 2007; 34:177-194.
97. Esposito F, Formisano E, Seifritz E, Goebel R, Morrone R, Tedeschi G, Di Salle F. Spatial independent component analysis of functional MRI time-series: to what extent do results depend on the algorithm used? *Hum Brain Mapp* 2002; 16:146-157.
98. Esposito F, Seifritz E, Formisano E, Morrone R, Scarabino T, Tedeschi G, Cirillo S, Goebel R, Di Salle F. Real-time independent component analysis of fMRI time-series. *Neuroimage* 2003; 20:2209-2224.
99. Formisano E, Esposito F, Di Salle F, Goebel R. Cortex-based independent component analysis of fMRI time series. *Magn Reson Imaging* 2004; 22:1493-1504.
100. Hollo G, Szabo A, Vargha P. Scanning laser polarimetry versus frequency-doubling perimetry and conventional threshold perimetry: changes during a 12-month follow-up in preperimetric glaucoma. A pilot study. *Acta Ophthalmol Scand* 2001; 79:403-407.
101. Katsanos A, Kothy P, Konstas AG, Vargha P, Hollo G. Correlation between polarimetric retinal nerve fiber layer thickness and retinal sensitivity determined with frequency-doubling technology. *Ophthalmic Surg Lasers Imaging* 2005; 36:394-400.
102. Toth M, Kothy P, Hollo G. Accuracy of scanning laser polarimetry, scanning laser tomography, and their combination in a glaucoma screening trial. *J Glaucoma* 2008; 17:639-646.
103. Toth M, Kothy P, Vargha P, Hollo G. Accuracy of combined GDx-VCC and matrix FDT in a glaucoma screening trial. *J Glaucoma* 2007; 16:462-470.
104. Kuehn MH, Fingert JH, Kwon YH. Retinal ganglion cell death in glaucoma: mechanisms and neuroprotective strategies. *Ophthalmol Clin North Am* 2005; 18:383-395, vi.
105. Kwon YH, Fingert JH, Kuehn MH, Alward WL. Primary open-angle glaucoma. *N Engl J Med* 2009; 360:1113-1124.
106. Khaw PT, Shah P, Elkington AR. Glaucoma--2: treatment. *BMJ* 2004; 328:156-158.
107. Khaw PT, Shah P, Elkington AR. Glaucoma--1: diagnosis. *BMJ* 2004; 328:97-99.
108. Harwerth RS, Carter-Dawson L, Shen F, Smith EL, 3rd, Crawford ML. Ganglion cell losses underlying visual field defects from experimental glaucoma. *Invest Ophthalmol Vis Sci* 1999; 40:2242-2250.
109. Vickers JC, Schumer RA, Podos SM, Wang RF, Riederer BM, Morrison JH. Differential vulnerability of neurochemically identified subpopulations of retinal neurons in a monkey model of glaucoma. *Brain Res* 1995; 680:23-35.
110. Yucel YH, Zhang Q, Weinreb RN, Kaufman PL, Gupta N. Effects of retinal ganglion cell loss on magno-, parvo-, koniocellular pathways in the lateral geniculate nucleus and visual cortex in glaucoma. *Prog Retin Eye Res* 2003; 22:465-481.
111. Martin PR, White AJ, Goodchild AK, Wilder HD, Sefton AE. Evidence that blue-on cells are part of the third geniculocortical pathway in primates. *Eur J Neurosci* 1997; 9:1536-1541.
112. Pearson P, Swanson WH, Fellman RL. Chromatic and achromatic defects in patients with progressing glaucoma. *Vision Res* 2001; 41:1215-1227.
113. Drance SM, Lakowski R, Schulzer M, Douglas GR. Acquired color vision changes in glaucoma. Use of 100-hue test and Pickford anomaloscope as predictors of glaucomatous field change. *Arch Ophthalmol* 1981; 99:829-831.
114. Adams AJ, Rodic R, Husted R, Stamper R. Spectral sensitivity and color discrimination changes in glaucoma and glaucoma-suspect patients. *Invest Ophthalmol Vis Sci* 1982; 23:516-524.
115. Hamill TR, Post RB, Johnson CA, Keltner JL. Correlation of color vision deficits and observable changes in the optic disc in a population of ocular hypertensives. *Arch Ophthalmol* 1984; 102:1637-1639.
116. Flammer J, Drance SM. Correlation between color vision scores and quantitative perimetry in suspected glaucoma. *Arch Ophthalmol* 1984; 102:38-39.

117. Airaksinen PJ, Lakowski R, Drance SM, Price M. Color vision and retinal nerve fiber layer in early glaucoma. *Am J Ophthalmol* 1986; 101:208-213.
118. Heron G, Adams AJ, Husted R. Central visual fields for short wavelength sensitive pathways in glaucoma and ocular hypertension. *Invest Ophthalmol Vis Sci* 1988; 29:64-72.
119. Heron G, Adams AJ, Husted R. Foveal and non-foveal measures of short wavelength sensitive pathways in glaucoma and ocular hypertension. *Ophthalmic Physiol Opt* 1987; 7:403-404.
120. Adams AJ, Heron G, Husted R. Clinical measures of central vision function in glaucoma and ocular hypertension. *Arch Ophthalmol* 1987; 105:782-787.
121. Sample PA, Weinreb RN. Color perimetry for assessment of primary open-angle glaucoma. *Invest Ophthalmol Vis Sci* 1990; 31:1869-1875.
122. Hart WM, Jr., Silverman SE, Trick GL, Nesher R, Gordon MO. Glaucomatous visual field damage. Luminance and color-contrast sensitivities. *Invest Ophthalmol Vis Sci* 1990; 31:359-367.
123. Falcao-Reis F, O'Donoghue E, Buceti R, Hitchings RA, Arden GB. Peripheral contrast sensitivity in glaucoma and ocular hypertension. *Br J Ophthalmol* 1990; 74:712-716.
124. Bassi CJ, Galanis JC. Binocular visual impairment in glaucoma. *Ophthalmology* 1991; 98:1406-1411.
125. Falcao-Reis FM, O'Sullivan F, Spileers W, Hogg C, Arden GB. Macular colour contrast sensitivity in ocular hypertension and glaucoma: evidence for two types of defect. *Br J Ophthalmol* 1991; 75:598-602.
126. Yu TC, Falcao-Reis F, Spileers W, Arden GB. Peripheral color contrast. A new screening test for preglaucomatous visual loss. *Invest Ophthalmol Vis Sci* 1991; 32:2779-2789.
127. Johnson CA, Adams AJ, Casson EJ, Brandt JD. Blue-on-yellow perimetry can predict the development of glaucomatous visual field loss. *Arch Ophthalmol* 1993; 111:645-650.
128. Johnson CA, Adams AJ, Casson EJ, Brandt JD. Progression of early glaucomatous visual field loss as detected by blue-on-yellow and standard white-on-white automated perimetry. *Arch Ophthalmol* 1993; 111:651-656.
129. Casson EJ, Johnson CA, Shapiro LR. Longitudinal comparison of temporal-modulation perimetry with white-on-white and blue-on-yellow perimetry in ocular hypertension and early glaucoma. *J Opt Soc Am A Opt Image Sci Vis* 1993; 10:1792-1806.
130. Greenstein VC, Shapiro A, Hood DC, Zaidi Q. Chromatic and luminance sensitivity in diabetes and glaucoma. *J Opt Soc Am A Opt Image Sci Vis* 1993; 10:1785-1791.
131. Heron G, Erskine NA, Farquharson E, Moore AT, White H. Colour vision screening in glaucoma: the Tritan Album and other simple tests. *Ophthalmic Physiol Opt* 1994; 14:233-238.
132. Johnson CA. The Glenn A. Fry Award Lecture. Early losses of visual function in glaucoma. *Optom Vis Sci* 1995; 72:359-370.
133. Felius J, de Jong LA, van den Berg TJ, Greve EL. Functional characteristics of blue-on-yellow perimetric thresholds in glaucoma. *Invest Ophthalmol Vis Sci* 1995; 36:1665-1674.
134. Felius J, van den Berg TJ, Spekreijse H. Peripheral cone contrast sensitivity in glaucoma. *Vision Res* 1995; 35:1791-1797.
135. Sample PA, Madrid ME, Weinreb RN. Evidence for A Variety of Functional Defects in Glaucoma-Suspect Eyes. *J Glaucoma* 1994; 3:S5-S18.
136. Sample PA, Martinez GA, Weinreb RN. Short-wavelength automated perimetry without lens density testing. *Am J Ophthalmol* 1994; 118:632-641.
137. Gray LS, Heron G, Cassidy D, Clark GM, Cowley GR, Gourlay DM, Ross FM. Comparison of age-related changes in short-wavelength-sensitive cone thresholds between normals and patients with primary open-angle glaucoma. *Optom Vis Sci* 1995; 72:205-209.
138. Greenstein VC, Halevy D, Zaidi Q, Koenig KL, Ritch RH. Chromatic and luminance systems deficits in glaucoma. *Vision Res* 1996; 36:621-629.
139. Johnson CA. Diagnostic value of short-wavelength automated perimetry. *Curr Opin Ophthalmol* 1996; 7:54-58.

140. Alvarez SL, Pierce GE, Vingrys AJ, Benes SC, Weber PA, King-Smith PE. Comparison of red-green, blue-yellow and achromatic losses in glaucoma. *Vision Res* 1997; 37:2295-2301.
141. Fristrom B. Peripheral colour contrast thresholds in ocular hypertension and glaucoma. *Acta Ophthalmol Scand* 1997; 75:376-382.
142. Sample PA, Bosworth CF, Weinreb RN. Short-wavelength automated perimetry and motion automated perimetry in patients with glaucoma. *Arch Ophthalmol* 1997; 115:1129-1133.
143. Porciatti V, Di Bartolo E, Nardi N, Fiorentini A. Responses to chromatic and luminance contrast in glaucoma: a psychophysical and electrophysiological study. *Vision Res* 1997; 37:1975-1987.
144. Sample PA, Bosworth CF, Weinreb RN. Selectivity in glaucoma injury. *Arch Ophthalmol* 1998; 116:396-398.
145. Pacheco-Cutillas M, Edgar DF, Sahraie A. Acquired colour vision defects in glaucoma-their detection and clinical significance. *Br J Ophthalmol* 1999; 83:1396-1402.
146. Horn FK, Jonas JB, Budde WM, Junemann AM, Mardin CY, Korth M. Monitoring glaucoma progression with visual evoked potentials of the blue-sensitive pathway. *Invest Ophthalmol Vis Sci* 2002; 43:1828-1834.
147. Fristrom B. Colour contrast sensitivity in ocular hypertension. A five-year prospective study. *Acta Ophthalmol Scand* 2002; 80:155-162.
148. Racette L, Sample PA. Short-wavelength automated perimetry. *Ophthalmol Clin North Am* 2003; 16:227-236, vi-vii.
149. Holopigian K, Greenstein VC, Seiple W, Hood DC, Ritch R. Electrophysiologic assessment of photoreceptor function in patients with primary open-angle glaucoma. *J Glaucoma* 2000; 9:163-168.
150. Kalloniatis M, Harwerth RS, Smith EL, 3rd, DeSantis L. Colour vision anomalies following experimental glaucoma in monkeys. *Ophthalmic Physiol Opt* 1993; 13:56-67.
151. Merigan WH, Maunsell JH. How parallel are the primate visual pathways? *Annu Rev Neurosci* 1993; 16:369-402.
152. Maddess T, Henry GH. Performance of nonlinear visual units in ocular hypertension and glaucoma. *Clin Vision Sci* 1992; 7:371-383.
153. Maddess T, Goldberg I, Dobinson J, Wine S, Welsh AH, James AC. Testing for glaucoma with the spatial frequency doubling illusion. *Vision Res* 1999; 39:4258-4273.
154. Shabana N, Cornilleau Peres V, Carkeet A, Chew PT. Motion perception in glaucoma patients: a review. *Surv Ophthalmol* 2003; 48:92-106.
155. Quigley HA, Dunkelberger GR, Green WR. Chronic human glaucoma causing selectively greater loss of large optic nerve fibers. *Ophthalmology* 1988; 95:357-363.
156. Quigley HA, Sanchez RM, Dunkelberger GR, L'Hernault NL, Baginski TA. Chronic glaucoma selectively damages large optic nerve fibers. *Invest Ophthalmol Vis Sci* 1987; 28:913-920.
157. Glovinsky Y, Quigley HA, Pease ME. Foveal ganglion cell loss is size dependent in experimental glaucoma. *Invest Ophthalmol Vis Sci* 1993; 34:395-400.
158. Harwerth RS, Smith EL, 3rd, Chandler M. Progressive visual field defects from experimental glaucoma: measurements with white and colored stimuli. *Optom Vis Sci* 1999; 76:558-570.
159. Harwerth RS, Crawford ML, Frishman LJ, Viswanathan S, Smith EL, 3rd, Carter-Dawson L. Visual field defects and neural losses from experimental glaucoma. *Prog Retin Eye Res* 2002; 21:91-125.
160. Brecher R, Bird AC. Adult vitelliform macular dystrophy. *Eye* 1990; 4 (Pt 1):210-215.
161. Best F. Über eine hereditäre Maculaaffektion: Beiträge zur Vererbungslehre. *Z Augenheilkd* 1905; 13:199-212.
162. Deutman AF. Electro-oculography in families with vitelliform dystrophy of the fovea. Detection of the carrier state. *Arch Ophthalmol* 1969; 81:305-316.
163. Krill AE, Morse PA, Potts AM, Klien BA. Hereditary vitelliruptive macular degeneration. *Am J Ophthalmol* 1966; 61:1405-1415.
164. Bard LA, Cross HE. Genetic counseling of families with Best macular dystrophy. *Trans Sect Ophthalmol Am Acad Ophthalmol Otolaryngol* 1975; 79:OP865-873.

165. Gass JD. A clinicopathologic study of a peculiar foveomacular dystrophy. *Trans Am Ophthalmol Soc* 1974; 72:139-156.
166. Mohler CW, Fine SL. Long-term evaluation of patients with Best's vitelliform dystrophy. *Ophthalmology* 1981; 88:688-692.
167. Godel V, Chaine G, Regenbogen L, Coscas G. Best's vitelliform macular dystrophy. *Acta Ophthalmol Suppl* 1986; 175:1-31.
168. Clemett R. Vitelliform dystrophy: long-term observations on New Zealand pedigrees. *Aust N Z J Ophthalmol* 1991; 19:221-227.
169. Weingeist TA, Kobrin JL, Watzke RC. Histopathology of Best's macular dystrophy. *Arch Ophthalmol* 1982; 100:1108-1114.
170. O'Gorman S, Flaherty WA, Fishman GA, Berson EL. Histopathologic findings in Best's vitelliform macular dystrophy. *Arch Ophthalmol* 1988; 106:1261-1268.
171. Frangieh GT, Green WR, Fine SL. A histopathologic study of Best's macular dystrophy. *Arch Ophthalmol* 1982; 100:1115-1121.
172. Patrinely JR, Lewis RA, Font RL. Foveomacular vitelliform dystrophy, adult type. A clinicopathologic study including electron microscopic observations. *Ophthalmology* 1985; 92:1712-1718.
173. Miller SA. Multifocal Best's vitelliform dystrophy. *Arch Ophthalmol* 1977; 95:984-990.
174. Marquardt A, Stohr H, Passmore LA, Kramer F, Rivera A, Weber BH. Mutations in a novel gene, VMD2, encoding a protein of unknown properties cause juvenile-onset vitelliform macular dystrophy (Best's disease). *Hum Mol Genet* 1998; 7:1517-1525.
175. Petrukhin K, Koisti MJ, Bakall B, Li W, Xie G, Marknell T, Sandgren O, Forsman K, Holmgren G, Andreasson S, Vujic M, Bergen AA, McGarty-Dugan V, Figueroa D, Austin CP, Metzker ML, Caskey CT, Wadelius C. Identification of the gene responsible for Best macular dystrophy. *Nat Genet* 1998; 19:241-247.
176. Lotery AJ, Munier FL, Fishman GA, Weleber RG, Jacobson SG, Affatigato LM, Nichols BE, Schorderet DF, Sheffield VC, Stone EM. Allelic variation in the VMD2 gene in Best disease and age-related macular degeneration. *Invest Ophthalmol Vis Sci* 2000; 41:1291-1296.
177. Eksandh L, Bakall B, Bauer B, Wadelius C, Andreasson S. Best's vitelliform macular dystrophy caused by a new mutation (Val89Ala) in the VMD2 gene. *Ophthalmic Genet* 2001; 22:107-115.
178. Palomba G, Rozzo C, Angius A, Pierrottet CO, Orzalesi N, Pirastu M. A novel spontaneous missense mutation in VMD2 gene is a cause of a Best macular dystrophy sporadic case. *Am J Ophthalmol* 2000; 129:260-262.
179. Bakall B, Marknell T, Ingvast S, Koisti MJ, Sandgren O, Li W, Bergen AA, Andreasson S, Rosenberg T, Petrukhin K, Wadelius C. The mutation spectrum of the bestrophin protein--functional implications. *Hum Genet* 1999; 104:383-389.
180. Kramer F, White K, Pauleikhoff D, Gehrig A, Passmore L, Rivera A, Rudolph G, Kellner U, Andrassi M, Lorenz B, Rohrschneider K, Blankenagel A, Jurklies B, Schilling H, Schutt F, Holz FG, Weber BH. Mutations in the VMD2 gene are associated with juvenile-onset vitelliform macular dystrophy (Best disease) and adult vitelliform macular dystrophy but not age-related macular degeneration. *Eur J Hum Genet* 2000; 8:286-292.
181. Sun H, Tsunenari T, Yau KW, Nathans J. The vitelliform macular dystrophy protein defines a new family of chloride channels. *Proc Natl Acad Sci U S A* 2002; 99:4008-4013.
182. Marmorstein LY, McLaughlin PJ, Stanton JB, Yan L, Crabb JW, Marmorstein AD. Bestrophin interacts physically and functionally with protein phosphatase 2A. *J Biol Chem* 2002; 277:30591-30597.
183. Francois J, De Rouck A, Fernandez-Sasso D. Electro-oculography in vitelliform degeneration of the macula. *Arch Ophthalmol* 1967; 77:726-733.
184. Palmowski AM, Allgayer R, Heinemann-Vernaleken B, Scherer V, Ruprecht KW. Detection of retinal dysfunction in vitelliform macular dystrophy using the multifocal ERG (MF-ERG). *Doc Ophthalmol* 2003; 106:145-152.
185. Scholl HP, Kremers J, Apfelstedt-Sylla E, Zrenner E. L- and M-cone driven ERGs are differently altered in Best's macular dystrophy. *Vision Res* 2000; 40:3159-3168.

186. Falsini B, Porciatti V, Porrello G, Merendino E, Minnella A, Cermola S, Buzzonetti L. Macular flicker electroretinograms in Best vitelliform dystrophy. *Curr Eye Res* 1996; 15:638-646.

187. Wajima R, Chater SB, Katsumi O, Mehta MC, Hirose T. Correlating visual acuity and electrooculogram recordings in Best's disease. *Ophthalmologica* 1993; 207:174-181.

188. Massof RW, Fleischman JA, Fine SL, Yoder F. Flicker fusion thresholds in Best macular dystrophy. *Arch Ophthalmol* 1977; 95:991-994.

189. DeLint PJ, Berendschot TT, van Norren D. A comparison of the optical Stiles-Crawford effect and retinal densitometry in a clinical setting. *Invest Ophthalmol Vis Sci* 1998; 39:1519-1523.

190. Burns SA, Elsner AE. Localizing color vision deficiencies in eye disease. In: Drum B, Verriest G (eds), *Colour Vision Deficiencies*. The Hague, the Netherlands: Dr W Junk Publishers; 1988:167-180.

191. Scullica L, Falsini B. Diagnosis and classification of macular degenerations: an approach based on retinal function testing. *Doc Ophthalmol* 2001; 102:237-250.

192. Campos SH, Forjaz V, Kozak LR, Silva E, Castelo-Branco M. Quantitative phenotyping of chromatic dysfunction in Best macular dystrophy. *Arch Ophthalmol* 2005; 123:944-949.

193. Maia-Lopes S, Silva ED, Silva MF, Reis A, Faria P, Castelo-Branco M. Evidence of widespread retinal dysfunction in patients with stargardt disease and morphologically unaffected carrier relatives. *Invest Ophthalmol Vis Sci* 2008; 49:1191-1199.

194. Silva MF, Faria P, Regateiro FS, Forjaz V, Januario C, Freire A, Castelo-Branco M. Independent patterns of damage within magno-, parvo- and koniocellular pathways in Parkinson's disease. *Brain* 2005; 128:2260-2271.

195. Castelo-Branco M, Mendes M, Sebastiao AR, Reis A, Soares M, Saraiva J, Bernardes R, Flores R, Perez-Jurado L, Silva E. Visual phenotype in Williams-Beuren syndrome challenges magnocellular theories explaining human neurodevelopmental visual cortical disorders. *J Clin Invest* 2007; 117:3720-3729.

196. Albright TD, Stoner GR. Contextual influences on visual processing. *Annu Rev Neurosci* 2002; 25:339-379.

197. Ben-Av MB, Shiffrar M. Disambiguating velocity estimates across image space. *Vision Res* 1995; 35:2889-2895.

198. Bonneh Y, Sagi D. Effects of spatial configuration on contrast detection. *Vision Res* 1998; 38:3541-3553.

199. Westheimer G, Ley EJ. Spatial and temporal integration of signals in foveal line orientation. *J Neurophysiol* 1997; 77:2677-2684.

200. Clifford CW, Harris JA. Contextual modulation outside of awareness. *Curr Biol* 2005; 15:574-578.

201. Kapadia MK, Ito M, Gilbert CD, Westheimer G. Improvement in visual sensitivity by changes in local context: parallel studies in human observers and in V1 of alert monkeys. *Neuron* 1995; 15:843-856.

202. Allman J, Miezin F, McGuinness E. Stimulus specific responses from beyond the classical receptive field: neurophysiological mechanisms for local-global comparisons in visual neurons. *Annu Rev Neurosci* 1985; 8:407-430.

203. Levitt JB, Lund JS. Contrast dependence of contextual effects in primate visual cortex. *Nature* 1997; 387:73-76.

204. Tanaka K, Hikosaka K, Saito H, Yukie M, Fukada Y, Iwai E. Analysis of local and wide-field movements in the superior temporal visual areas of the macaque monkey. *J Neurosci* 1986; 6:134-144.

205. Loffler G, Orbach HS. Modeling the integration of motion signals across space. *J Opt Soc Am A Opt Image Sci Vis* 2003; 20:1472-1489.

206. Betts LR, Taylor CP, Sekuler AB, Bennett PJ. Aging reduces center-surround antagonism in visual motion processing. *Neuron* 2005; 45:361-366.

207. Paffen CL, Tadin D, te Pas SF, Blake R, Verstraten FA. Adaptive center-surround interactions in human vision revealed during binocular rivalry. *Vision Res* 2006; 46:599-604.

208. Tadin D, Lappin JS, Gilroy LA, Blake R. Perceptual consequences of centre-surround antagonism in visual motion processing. *Nature* 2003; 424:312-315.
209. Scholl BJ, Nakayama K. Causal capture: contextual effects on the perception of collision events. *Psychol Sci* 2002; 13:493-498.
210. Beauchamp MS, Cox RW, DeYoe EA. Graded effects of spatial and featural attention on human area MT and associated motion processing areas. *J Neurophysiol* 1997; 78:516-520.
211. O'Craven KM, Rosen BR, Kwong KK, Treisman A, Savoy RL. Voluntary attention modulates fMRI activity in human MT-MST. *Neuron* 1997; 18:591-598.
212. Buchel C, Josephs O, Rees G, Turner R, Frith CD, Friston KJ. The functional anatomy of attention to visual motion. A functional MRI study. *Brain* 1998; 121 (Pt 7):1281-1294.
213. Kastner S, Pinsk MA, De Weerd P, Desimone R, Ungerleider LG. Increased activity in human visual cortex during directed attention in the absence of visual stimulation. *Neuron* 1999; 22:751-761.
214. Alais D, Blake R. Neural strength of visual attention gauged by motion adaptation. *Nat Neurosci* 1999; 2:1015-1018.
215. Treue S, Martinez Trujillo JC. Feature-based attention influences motion processing gain in macaque visual cortex. *Nature* 1999; 399:575-579.
216. Seidemann E, Newsome WT. Effect of spatial attention on the responses of area MT neurons. *J Neurophysiol* 1999; 81:1783-1794.
217. Kozak LR, Castelo-Branco M. Peripheral influences on motion integration in foveal vision are modulated by central local ambiguity and center-surround congruence. *Invest Ophthalmol Vis Sci* 2008; 50:980-988.
218. Dolan RJ, Fink GR, Rolls E, Booth M, Holmes A, Frackowiak RS, Friston KJ. How the brain learns to see objects and faces in an impoverished context. *Nature* 1997; 389:596-599.
219. Vaina LM, Belliveau JW, des Roziers EB, Zeffiro TA. Neural systems underlying learning and representation of global motion. *Proc Natl Acad Sci U S A* 1998; 95:12657-12662.
220. Gauthier I, Tarr MJ, Anderson AW, Skudlarski P, Gore JC. Activation of the middle fusiform 'face area' increases with expertise in recognizing novel objects. *Nat Neurosci* 1999; 2:568-573.
221. Schiltz C, Bodart JM, Dubois S, Dejardin S, Michel C, Roucoux A, Crommelinck M, Orban GA. Neuronal mechanisms of perceptual learning: changes in human brain activity with training in orientation discrimination. *Neuroimage* 1999; 9:46-62.
222. Schwartz S, Maquet P, Frith C. Neural correlates of perceptual learning: a functional MRI study of visual texture discrimination. *Proc Natl Acad Sci U S A* 2002; 99:17137-17142.
223. Furmanski CS, Schluppeck D, Engel SA. Learning strengthens the response of primary visual cortex to simple patterns. *Curr Biol* 2004; 14:573-578.
224. Kourtzi Z, Betts LR, Sarkheil P, Welchman AE. Distributed neural plasticity for shape learning in the human visual cortex. *PLoS Biol* 2005; 3:e204.
225. Sigman M, Pan H, Yang Y, Stern E, Silbersweig D, Gilbert CD. Top-down reorganization of activity in the visual pathway after learning a shape identification task. *Neuron* 2005; 46:823-835.
226. Op de Beeck HP, Baker CI, DiCarlo JJ, Kanwisher NG. Discrimination training alters object representations in human extrastriate cortex. *J Neurosci* 2006; 26:13025-13036.
227. Mukai I, Kim D, Fukunaga M, Japee S, Marrett S, Ungerleider LG. Activations in visual and attention-related areas predict and correlate with the degree of perceptual learning. *J Neurosci* 2007; 27:11401-11411.
228. Ghose GM. Learning in mammalian sensory cortex. *Curr Opin Neurobiol* 2004; 14:513-518.
229. Vidnyanszky Z, Sohn W. Learning to suppress task-irrelevant visual stimuli with attention. *Vision Res* 2005; 45:677-685.
230. Dosher BA, Lu ZL. Perceptual learning reflects external noise filtering and internal noise reduction through channel reweighting. *Proc Natl Acad Sci U S A* 1998; 95:13988-13993.
231. Dosher BA, Lu ZL. Mechanisms of perceptual learning. *Vision Res* 1999; 39:3197-3221.
232. Gold J, Bennett PJ, Sekuler AB. Signal but not noise changes with perceptual learning. *Nature* 1999; 402:176-178.

233. Li RW, Levi DM, Klein SA. Perceptual learning improves efficiency by re-tuning the decision 'template' for position discrimination. *Nat Neurosci* 2004; 7:178-183.
234. Lu ZL, Dosher BA. Perceptual learning retunes the perceptual template in foveal orientation identification. *J Vis* 2004; 4:44-56.
235. Fine I, Jacobs RA. Comparing perceptual learning tasks: a review. *J Vis* 2002; 2:190-203.
236. Watanabe T, Nanez JE, Sasaki Y. Perceptual learning without perception. *Nature* 2001; 413:844-848.
237. Watanabe T, Nanez JE, Sr., Koyama S, Mukai I, Liederman J, Sasaki Y. Greater plasticity in lower-level than higher-level visual motion processing in a passive perceptual learning task. *Nat Neurosci* 2002; 5:1003-1009.
238. Seitz AR, Watanabe T. Psychophysics: Is subliminal learning really passive? *Nature* 2003; 422:36.
239. Seitz A, Watanabe T. A unified model for perceptual learning. *Trends Cogn Sci* 2005; 9:329-334.
240. Paffen CL, Verstraten FA, Vidnyanszky Z. Attention-based perceptual learning increases binocular rivalry suppression of irrelevant visual features. *J Vis* 2008; 8:25 21-11.
241. Op de Beeck HP, Wagemans J, Vogels R. Effects of perceptual learning in visual backward masking on the responses of macaque inferior temporal neurons. *Neuroscience* 2007; 145:775-789.
242. Fishman GA, Baca W, Alexander KR, Derlacki DJ, Glenn AM, Viana M. Visual acuity in patients with Best vitelliform macular dystrophy. *Ophthalmology* 1993; 100:1665-1670.
243. Alais D, van der Smagt MJ, Verstraten FA, van de Grind WA. The perceived direction of textured gratings and their motion aftereffects. *Perception* 1995; 24:1383-1396.
244. Leopold DA, Wilke M, Maier A, Logothetis NK. Stable perception of visually ambiguous patterns. *Nat Neurosci* 2002; 5:605-609.
245. Boynton GM, Engel SA, Glover GH, Heeger DJ. Linear systems analysis of functional magnetic resonance imaging in human V1. *J Neurosci* 1996; 16:4207-4221.
246. Engel SA, Rumelhart DE, Wandell BA, Lee AT, Glover GH, Chichilnisky EJ, Shadlen MN. fMRI of human visual cortex. *Nature* 1994; 369:525.
247. Sereno MI, Dale AM, Reppas JB, Kwong KK, Belliveau JW, Brady TJ, Rosen BR, Tootell RB. Borders of multiple visual areas in humans revealed by functional magnetic resonance imaging. *Science* 1995; 268:889-893.
248. DeYoe EA, Carman GJ, Bandettini P, Glickman S, Wieser J, Cox R, Miller D, Neitz J. Mapping striate and extrastriate visual areas in human cerebral cortex. *Proc Natl Acad Sci U S A* 1996; 93:2382-2386.
249. Várallyay G, Kozák LR. Neuroradiológia. In: Somlai J (ed), *Neuroophthalmologia.* Budapest: PressCon; 2007:17-22.
250. Kimmig H, Ohlendorf S, Speck O, Sprenger A, Rutschmann RM, Haller S, Greenlee MW. fMRI evidence for sensorimotor transformations in human cortex during smooth pursuit eye movements. *Neuropsychologia* 2008; 46:2203-2213.
251. Hupe JM, Rubin N. The dynamics of bi-stable alternation in ambiguous motion displays: a fresh look at plaids. *Vision Res* 2003; 43:531-548.
252. Alais D, Wenderoth P, Burke D. The size and number of plaid blobs mediate the misperception of type-II plaid direction. *Vision Res* 1997; 37:143-150.
253. Greenwood JA, Edwards M. An oblique effect for transparent-motion detection caused by variation in global-motion direction-tuning bandwidths. *Vision Res* 2007; 47:1411-1423.
254. Tootell RB, Mendola JD, Hadjikhani NK, Ledden PJ, Liu AK, Reppas JB, Sereno MI, Dale AM. Functional analysis of V3A and related areas in human visual cortex. *J Neurosci* 1997; 17:7060-7078.
255. Breton ME, Krupin T. Age covariance between 100-Hue color scores and quantitative perimetry in primary open angle glaucoma. *Arch Ophthalmol* 1987; 105:642-645.
256. Barbur JL, Harlow AJ, Plant GT. Insights into the different exploits of colour in the visual cortex. *Proc Biol Sci* 1994; 258:327-334.

257. Marmorstein AD, Marmorstein LY, Rayborn M, Wang X, Hollyfield JG, Petrukhin K. Bestrophin, the product of the Best vitelliform macular dystrophy gene (VMD2), localizes to the basolateral plasma membrane of the retinal pigment epithelium. *Proc Natl Acad Sci U S A* 2000; 97:12758-12763.

258. Cideciyan AV, Jacobson SG. An alternative phototransduction model for human rod and cone ERG a-waves: normal parameters and variation with age. *Vision Res* 1996; 36:2609-2621.

259. Hood BC, Birch DG, Pepperberg DR. The trailing edge of the photoreceptor response from human cones derived using a two-flash ERGparadigm. *Visual Science and Its Applications.* Washington, DC: Optical Society of America; 1996:64-67.

260. Silva MF, Maia-Lopes S, Mateus C, Guerreiro M, Sampaio J, Faria P, Castelo-Branco M. Retinal and cortical patterns of spatial anisotropy in contrast sensitivity tasks. *Vision Res* 2008; 48:127-135.

261. Noest AJ, van den Berg AV. The role of early mechanisms in motion transparency and coherence. *Spat Vis* 1993; 7:125-147.

262. Bayerl P, Neumann H. Disambiguating visual motion through contextual feedback modulation. *Neural Comput* 2004; 16:2041-2066.

263. Gizzi MS, Katz E, Schumer RA, Movshon JA. Selectivity for orientation and direction of motion of single neurons in cat striate and extrastriate visual cortex. *J Neurophysiol* 1990; 63:1529-1543.

264. Guo K, Benson PJ, Blakemore C. Pattern motion is present in V1 of awake but not anaesthetized monkeys. *Eur J Neurosci* 2004; 19:1055-1066.

265. Schmidt KE, Castelo-Branco M, Goebel R, Payne BR, Lomber SG, Galuske RA. Pattern motion selectivity in population responses of area 18. *Eur J Neurosci* 2006; 24:2363-2374.

266. Smith AT, Snowden RJ, Milne AB. Is global motion really based on spatial integration of local motion signals? *Vision Res* 1994; 34:2425-2430.

267. Pack CC, Gartland AJ, Born RT. Integration of Contour and Terminator Signals in Visual Area MT of Alert Macaque. *J Neurosci* 2004; 24:3268-3280.

268. Alais D, Blake R. Grouping visual features during binocular rivalry. *Vision Res* 1999; 39:4341-4353.

269. Blake R, Logothetis NK. Visual competition. *Nat Rev Neurosci* 2002; 3:13-21.

270. Blake R. A neural theory of binocular rivalry. *Psychol Rev* 1989; 96:145-167.

271. Laing CR, Chow CC. A spiking neuron model for binocular rivalry. *J Comput Neurosci* 2002; 12:39-53.

272. Kovacs I, Julesz B. Perceptual sensitivity maps within globally defined visual shapes. *Nature* 1994; 370:644-646.

273. Moradi F, Shimojo S. Perceptual-binding and persistent surface segregation. *Vision Res* 2004; 44:2885-2899.

274. Clifford CW, Spehar B, Pearson J. Motion transparency promotes synchronous perceptual binding. *Vision Res* 2004; 44:3073-3080.

275. Chubb C, Sperling G, Solomon JA. Texture interactions determine perceived contrast. *Proc Natl Acad Sci U S A* 1989; 86:9631-9635.

276. Cannon MW, Fullenkamp SC. Spatial interactions in apparent contrast: inhibitory effects among grating patterns of different spatial frequencies, spatial positions and orientations. *Vision Res* 1991; 31:1985-1998.

277. Verstraten FA, Fredericksen RE, Grusser OJ, van de Grind WA. Recovery from motion adaptation is delayed by successively presented orthogonal motion. *Vision Res* 1994; 34:1149-1155.

278. Ramachandran VS, Anstis S. Figure-ground segregation modulates apparent motion. *Vision Res* 1986; 26:1969-1975.

279. Berman RA, Colby CL. Auditory and visual attention modulate motion processing in area MT+. *Brain Res Cogn Brain Res* 2002; 14:64-74.

280. Chaudhuri A. Modulation of the motion aftereffect by selective attention. *Nature* 1990; 344:60-62.

281. Georgiades MS, Harris JP. The spatial spread of attentional modulation of the motion aftereffect. *Perception* 2000; 29:1185-1201.
282. Georgiades MS, Harris JP. Effects of attentional modulation of a stationary surround in adaptation to motion. *Perception* 2002; 31:393-408.
283. Rees G, Frith CD, Lavie N. Modulating irrelevant motion perception by varying attentional load in an unrelated task. *Science* 1997; 278:1616-1619.
284. Culham JC, Verstraten FA, Ashida H, Cavanagh P. Independent aftereffects of attention and motion. *Neuron* 2000; 28:607-615.
285. Lankheet MJ, Verstraten FA. Attentional modulation of adaptation to two-component transparent motion. *Vision Res* 1995; 35:1401-1412.
286. Mukai I, Watanabe T. Differential effect of attention to translation and expansion on motion aftereffects (MAE). *Vision Res* 2001; 41:1107-1117.
287. Shulman GL. Attentional effects of adaptation of rotary motion in the plane. *Perception* 1993; 22:947-961.
288. Sohn, Vidnyanszky, Blaser, Papathomas. Attention to one component of bivectorial transparent motion strongly inhibits the processing of the unattended component. *J Vis* 2001; 1:85-85.
289. Castelo-Branco M, Mendes M, Silva F, Massano J, Januario G, Januario C, Freire A. Motion integration deficits are independent of magnocellular impairment in Parkinson's disease. *Neuropsychologia* 2008; IN PRESS.
290. Ramachandran VS, Braddick O. Orientation-specific learning in stereopsis. *Perception* 1973; 2:371-376.
291. Fiorentini A, Berardi N. Perceptual learning specific for orientation and spatial frequency. *Nature* 1980; 287:43-44.
292. Ball K, Sekuler R. A specific and enduring improvement in visual motion discrimination. *Science* 1982; 218:697-698.
293. Karni A, Sagi D. Where practice makes perfect in texture discrimination: evidence for primary visual cortex plasticity. *Proc Natl Acad Sci U S A* 1991; 88:4966-4970.
294. Fahle M, Poggio T. *Perceptual Learning*. Cambridge, Massachussetts: MIT Press; 2002.
295. Tsushima Y, Seitz AR, Watanabe T. Task-irrelevant learning occurs only when the irrelevant feature is weak. *Curr Biol* 2008; 18:R516-517.
296. Tsushima Y, Sasaki Y, Watanabe T. Greater disruption due to failure of inhibitory control on an ambiguous distractor. *Science* 2006; 314:1786-1788.
297. Nishida S, Sasaki Y, Murakami I, Watanabe T, Tootell RB. Neuroimaging of direction-selective mechanisms for second-order motion. *J Neurophysiol* 2003; 90:3242-3254.
298. Kamitani Y, Tong F. Decoding seen and attended motion directions from activity in the human visual cortex. *Curr Biol* 2006; 16:1096-1102.
299. Serences JT, Boynton GM. Feature-based attentional modulations in the absence of direct visual stimulation. *Neuron* 2007; 55:301-312.
300. Serences JT, Boynton GM. The representation of behavioral choice for motion in human visual cortex. *J Neurosci* 2007; 27:12893-12899.
301. Yotsumoto Y, Watanabe T, Sasaki Y. Different dynamics of performance and brain activation in the time course of perceptual learning. *Neuron* 2008; 57:827-833.
302. Carmel D, Carrasco M. Perceptual learning and dynamic changes in primary visual cortex. *Neuron* 2008; 57:799-801.
303. Shmuel A, Augath M, Oeltermann A, Logothetis NK. Negative functional MRI response correlates with decreases in neuronal activity in monkey visual area V1. *Nat Neurosci* 2006; 9:569-577.
304. Hoffman KL, Logothetis NK. Cortical mechanisms of sensory learning and object recognition. *Philos Trans R Soc Lond B Biol Sci* 2009; 364:321-329.

THE BIBLIOGRAPHY OF THE CANDIDATE'S PUBLICATIONS

Publications related to the thesis

2009 *IF: 3.673* Gál V, **Kozák LR**, Kóbor I, Bankó ÉM, Serences JT, Vidnyánszky Z: Learning to filter out visual distractors **Eur J Neurosci 29**(8):1723-1731

2009 *IF: 3.528* **Kozak LR** and Castelo-Branco M: Peripheral influences on motion integration in foveal vision are modulated by central local ambiguity and center-surround congruence, ***Invest Ophthalmol Vis Sci*** **50**(2):980-988. DOI:10.1167/iovs.08-2094

2005 *IF: 3.274* Campos SH, Forjaz V, **Kozak LR**, Silva E and Castelo-Branco M: Quantitative phenotyping of chromatic dysfunction in Best macular dystrophy, ***Arch Ophthalmol*** **123**(7):944-949.

Cited: 6 times

2004 *IF:3.577* Castelo-Branco M, Faria P, Forjaz V, **Kozak LR** and Azevedo H: Simultaneous comparison of relative damage of chromatic pathways in ocular hypertension and glaucoma: correlation with clinical measures, ***Invest Ophthalmol Vis Sci*** **45**(2):499-505.

Cited: 14 times

Under revision ***Castelo-Branco M *, Kozak LR ****, *Formisano E, Backes WH, Teixeira J, Xavier J, Goebel R: The type of featural attention differentially modulates hMT$^+$ responses to illusory motion aftereffects under revision at* ***J Neurophysiol*** *(* shared first authorship)*

Under revision ***Kozak LR****, Lima B, Neuenschwander S, Muckli L, Castelo-Branco M: Motion coherence is differentially affected by local-global common fate between center and surround components, under revision in* ***Percept Psychophys***

Publications unrelated to the thesis

2009 **Kozák LR**, Hegyi M, Barsi P, Rudas G: Clonazepam can facilitate sensorimotor functional MRI examinations in status epilepticus during sleep, (in Hungarian), ***Ideggyogy Sz 62****(3-4):130-135*

2009 Hegyi M, Siegler Z, Barsi P, Rudas G, Lengyel Z, Szakáll S, Bognar L, **Kozak LR**, Neuwirth M, Fogarasi A: Surgically cured resistant epilepsy--caused by hemispherical dysgenesis--case report, (in Hungarian), ***Ideggyogy Sz 62****(5-6):185-189*

2002 *IF: 1.160* Eke A, Hermán P, Kocsis L, **Kozak LR**: The fractal characterization of complexity in temporal physiological signals, ***Physiol Meas***, **23**(1): R1-R38.

Cited: 53 times

Citable abstracts related to the thesis

2007 Castelo-Branco M, **Kozak LR**, Teixeira J, Xavier J: The role of visual area hMT/V5 in dissociating perceptual decision from veridical stimulus properties, ECVPerception, Arezzo, Italy, *Perception* 2007; 36:135-135.

2007 Gál V, **Kozák LR**, Kóbor I, Bankó E, Serences J, Vidnyánszky Z: Perceptual and neural mechanisms of visual attentional suppression, ECVP, Arezzo, Italy, *Perception* 2007; 36:115-115.

2005 **Kozak LR**, Lima B, Neuenschwander S, Muckli L, Castelo-Branco M: Contextual modulation of bistable plaid motion perception, ECVP, A Coruña, Spain, *Perception* 2005; 34: 163-163 Suppl. S,

2005 **Kozak LR**, Formisano E, Backes W, Teixeira J, Xavier J, Goebel R, Castelo-Branco M: Neural correlates of illusory motion perception: the influence of apparent motion on plaid motion aftereffects, VSS, Sarasota, FL, USA, *J Vis* 5(8):666a. doi:10.1167/5.8.666

2005 **Kozak LR**, Formisano E, Backes W, Teixeira J, Xavier J, Goebel R, M Castelo-Branco: Human neural responses to overlaid real and apparent motion: implications for mechanisms of illusory motion perception, ARVO, Fort Lauderdale, Fl, USA, *Invest Ophthalmol Vis Sci* 2005; 46: E-Abstract 5657.

2004 **Kozak LR**, Formisano E, Goebel R, Castelo-Branco M: Interactions between visual attention and illusory motion perception, EVER, Vilamoura, Portugal; *Ophthal Res **36** (S1):168 [abstract No: 2421]*

2004 Castelo-Branco M, Forjaz V, Campos SH, **Kozak LR**, Silva E: Chromatic adaptation in Best's macular dystrophy: implications for quantitative phenotyping and clinical staging, ARVO, Fort Lauderdale, FL, USA; *Invest Ophthalmol Vis Sci* 2004;45: E- 4334.

2003 Castelo-Branco M, Faria P, Forjaz V, Campos Sh, **Kozak LR**: Quantification of relative damage of chromatic pathways in diseases involving the central or peripheral retina, EVER, Alicante, Spain, *Ophthal Res **35** (S1):195 [abstract No: 2363]*

2003 Faria P, Castelo-Branco M, Forjaz V, **Kozak LR**, Azevedo H: Early and late damage of parvo and koniocellular function in ocular hypertension and glaucoma: correlation with clinical markers of disease progression, EVER, Alicante, Spain, *Ophthal Res **35** (S1):204 [abstract No: 2444]*

2003 Forjaz V, Campos Sh, **Kozak LR**, Silva E, Castelo-Branco M: Chromatic deficits in Best's macular dystrophy: insights for the development of new clinical tools, EVER, Alicante, Spain, *Ophthal Res **35** (S1):43 [abstract No: 261]*

2003 Castelo-Branco M, Faria P, Forjaz V, Campos S, **Kozak LR**: Early quantification of chromatic pathway involvement in central and peripheral retinal disorders (Quantificação precoce do envolvimento relativo das vias cromáticas em doenças da retina central ou periférica), SPO, Vilamoura, Portugal, *Oftalmologia* **27**(4):5.

Citable abstracts unrelated to the thesis

2009 **Kozak LR**, Rudas G, Vidnyanszky Z, Nagy Z: Pulse triggering can improve the quality of diffusion tensor imaging data in neonatal subjects, ESNR, Athens, Greece*, to appear in Neuroradiology*

2009 **Kozak LR**, Gyuricza I, Gyorke T, Szidonya L, Gyebnar J, Kovacs T, Rudas G, Barsi P: Medial temporal lobe atrophy score: a locally derived measure with strong global implications, ESNR, Athens, Greece*, to appear in Neuroradiology*

2009 **Kozak LR**, Hegyi M, Barsi P, Rudas G: Clonazepam can assist performing sensorimotor functional MRI examinations in status epilepticus during sleep, ESNR, Athens, Greece*, to appear in Neuroradiology*

2009 Gyuricza I, **Kozak LR**, Gyorke T, Szidonya L, Gyebnar J, Kovacs T, Rudas G, Barsi P: Cerebral MR-volumetric examinations in the diagnosis of Alzheimer disease, ESNR, Athens, Greece*, to appear in Neuroradiology*

2009 **Kozák LR**, Rudas G, Vidnyánszky Z, Nagy Z: Examining the Need for Pulse Triggering When Collecting Diffusion Tensor Imaging Data from Neonatal Subjects, PAS 2009, Baltimore, MD, USA*, E-PAS2009:3868.277*

2008 **Kozák LR**, Barsi P, Erőss L, Vidnyánszky Z, Rudas G: Optimization of clinical functional MRI protocols at 3 Tesla, ESNR, Krakow, Poland, *Neuroradiology, 2008, 50 Suppl1: A2:2:2*

2008 Bangó M, Kelen D, **Kozák LR**, Róka A, Szabó M, Rudas G: Serial proton MR spectroscopy measurement of cerebral metabolites in asphyxiated infants during the first week of life, International Congress of UENPS, Rome, Italy, *Early Hum Dev, 2008;84:S57-S57.*

2007 Nagy Z, **Kozák LR**, Bangó M, Szabó M, Rudas G, Vidnyánszky Z: Measuring the CSF temperature using diffusion MRI: a possible method to monitor the brain temperature of cooled babies, ESPR, Prague, Czech Republic, *Acta Paediatr* 2007;96:47-47.

2007 Castelo-Branco M, **Kozak LR**, Teixeira J, Xavier J: The role of visual area hMT/V5 in dissociating perceptual decision from veridical stimulus properties, ECVP, Arezzo, Italy, *Perception* 2007;36:135-135.

2007 Kóbor I, Gál V, Bankó E, Körtvélyes J, **Kozák LR**, Vidnyánszky Z: ERP correlates of decision making in a motion direction discrimination task, ECVP, Arezzo, Italy, *Perception* 2007;36:142-142.

2007 Vidnyánszky Z, Gál V, Kóbor I, **Kozák L**, Serences J: Attentional suppression spreads throughout the visual field, VSS, Sarasota, FL, USA, *J Vis*, 7(9):787a,

2004 **Kozak LR**, Castelo-Branco M, Read JCA: Physiologically-realistic circuitry underlying the motion aftereffect, VSS, Sarasota, FL, USA, *J Vis* 4(8):486a,

2004 **Kozak LR**, Castelo-Branco M, Karmos G, Read JCA: A computational model of the motion aftereffect, **poster**, ARVO, Fort Lauderdale, FL, USA; *Invest Ophthalmol Vis Sci* 2004;45: E-4366.

ACKNOWLEDGEMENTS

The first and warmest thanks go to my family: my mother Éva Honti Kiss, my wife Mónika Popper, my fathers Lajos Kozák and Aladár Kiss, and my in-laws, György Popper and Andrea Kerek. My mother's perseverance and love helped me through the most difficult times of my life, she's always been there for me and she never gave up on me. Móni is my wife, my love, my partner, my colleague. We've been taking our journey together since her first day at medical school, and what a journey! She's been there for me through ups and downs, always supporting me, and always telling me her opinion frankly, without sugar-coating, which helped us through difficult times. My father Lajos died too early, to see me grow up, but I always felt his presence through my mother. Aladár was the real father for me: a former teacher, always being strict, but righteous; his determination lead me to study medicine. My in-laws are great people. I have to thank them for accepting me to their family: György, a mathematician soon became the third fatherly figure in my life, guiding me towards science through my interest in mathematics, and Andrea, a consultant ophthalmologist who has been giving all her support to us through these years. This thesis would have never been finished without the help of these people, without their unconditional love, patience and support; therefore I dedicate this work to them.

With similar importance: I would like to express my gratitude to my thesis supervisors György Karmos, and Miguel Castelo-Branco. This thesis would not have been born without their support, patience, and guidance.

György Karmos, or Gyurka as most of us know him, is my mentor. The most I've learned about conducting research and loving science, I've learned from him. He has always been there to listen to my most ridiculous questions, to give some very good advice, and to cover my back in some cases. Also, he supported my decision for leaving his lab for one of the biggest adventures in my life: those three years in Coimbra, and later guided me to the Szentágothai Knowledge Center – Semmelweis University MR Research Center after my return to Budapest.

Miguel Castelo-Branco gave me the opportunity to study human vision, and he guided me towards functional MRI. He was the one suggesting me to get involved in computational modeling, as well. Most of what I know about human motion perception and fMRI, I've learned from him. Those years in Coimbra were the defining years in my scientific career.

I would like to thank András Eke at the Institute of Human Physiology and Clinical Experimental Research of Semmelweis University, whose lab I started my scientific career

in as a research student; and Gábor Rudas the director and Zoltán Vidnyánszky the scientific director of the Szentágothai Knowledge Center – Semmelweis University MR Research Center, where I've been working in the last three years, for their support and advices. I'm especially grateful to Gábor for partly guiding me back to my original profession, and getting me involved in clinical fMRI investigations, and to Zoltán for letting me join his research group, thus continuing vision research, and also for a careful reading of the present thesis.

I would like to thank Péter Hermán (currently at Yale University) for teaching me programming in Matlab at the Eke lab, and guiding me through all the intricacies of fractal analysis methods, and also for his friendship and advices.

I would like to thank my friends and colleagues at the Institute for Psychology of the Hungarian Academy of Sciences: István Ulbert (for his advices during the time I've spent there), Csaba Rajkai (my roommate, for the long discussions), Péter Lakatos, Péter Kottra, János Horváth (for suggesting the EDCBS course), István Czigler (director, for his careful reading of the thesis, and for his suggestions), and all the others.

I would like to thank my friends and colleagues at the IBILI/AIBILI Coimbra: José G. Cunha-Vaz (the former head of the institute, for the opportunity to work in Coimbra), Fátima Silva and Vasco Forjaz (my roommates, for the long discussions and their friendship), Paulo Pereira (for his friendship and his tremendous work helping us settle in Coimbra), the other members of Miguel's lab (Susana Maia Lopes, Patrícia Figueiredo, Aldina Reis, Mafalda Mendes and Joana Costa), my co-authors (Pedro Faria, Helena Azevedo, Sónia Campos, Eduardo Silva), and those who helped in the investigations (Adozinda Simões and Rita Vaz), last but not least Alda Gonçalves (the secretary of IBILI, without her help nothing would have been done), and all the others I don't list here.

I would like to thank my friends and colleagues at the Szentágothai Knowledge Center – Semmelweis University MR Research Center: the members of the Vidnyánszky lab (Viktor Gál, István Kóbor, Éva Bankó, Judit Körtvélyes, for their friendship, and for sharing the great adventure of setting up the scanner for research), the members of the clinical core (Péter Barsi, György Várallyay, József Kenéz, for their friendship and support, and their guidance in my clinically-oriented research), Márta Bangó (PhD student, for the discussions), my MSc and MD thesis students (Dávid Póka and Vivien Tóth, for teaching me how to be a supervisor), the radiographers (Kinga Skultéty, László Bús, Gábor Lehel), our administrator Éva Varga, and the secretaries (Györgyi Podoletz, Tímea Ráczkevy, and Judit Rózsa, for their immense help in dealing with all the necessities).

I would like to thank my friends and colleagues in Maastricht, The Netherlands, Frankfurt am Main, Germany, and Glasgow, U.K. for their support, and advices (Rainer Goebel, Elia Formisano, Sergio Neuenschwander, Bruss Lima, Kerstin Schmidt, Lars Muckli).

I would like to thank the members of the Secretarial Office of the School of PhD Studies, Semmelweis University (especially Anita Marosfalvi and Anna Marádi) for their kind assistance during my PhD studies.

I would like to thank the organizers of the European Diploma in Cognitive and Brain Sciences program, and the students of the 2003/04 session, especially Jan Lammertyn, Roi Cohen-Kadosh, and Chiara della Libera for their friendship and the long discussions.

I would like to thank the organizers, teachers and students of the IBRO/FENS Advanced Course in Computational Neuroscience, especially Vasco Galhardo (the local organizer, for sharing his computational neuroscience library with me), and Jenny CA Read (my course project supervisor, for guiding me through this great experience, and for teaching me parts of Matlab that I've never known existed).

I would like to thank all my friends not listed here, for their friendship and support.

I would like to thank for the generous support of the Calouste Gulbenkian Foundation via their "Programa de Estimulo à Investigação" grant for me and Miguel Castelo-Branco that helped kick-start my research in Coimbra; the support of the School of PhD Studies of Semmelweis University (for providing my PhD scholarship while in Hungary); INFARMED, Portugal (for providing scholarship for my first year in Portugal); the Foundation for Science and Technology (FCT), Portugal (for their SFRH/BD/13344/2003 scholarship during my stay in Portugal); the Luso-American Foundation (for their travel grants).

The works presented in this thesis were also supported by the following grants: POCTI/NSE/35823/2000/FEDER, PTDC/PSI/67381/2006, POCI/SAU/NEU/60281/2004, Bial Foundation Grant 15/02, and RNIFC (the National Imaging Network of Portugal) for Miguel Castelo-Branco; POE 3.1/B1/03/109/2002 for Vasco Forjaz; Comissão de Fomento da Investigção em Cuidados de Saúde, Ministério da Saúde P.E. no. 120/01 for Pedro Faria; Hungarian Scientific Research Fund (T048949) and the Bólyai Fellowship for Zoltán Vidnyánszky.

The experiments dealing with motion processing were performed using Cogent 2000 developed by the Cogent 2000 team at the FIL and the ICN and Cogent Graphics developed by John Romaya at the LON at the Wellcome Department of Imaging Neuroscience.

REPRINTS OF PUBLICATIONS RELATED TO THE THESIS